# First-principles study of the exchange interactions and Curie temperature in Heusler alloys

**Dissertation**

zur Erlangung des akademischen Grades

doctor rerum naturalium (Dr. rer. nat.)

vorgelegt der

Mathematisch-Naturwissenschaftlich-Technischen Fakultät

(mathematisch-naturwissenschaftlicher Bereich)

der Martin-Luther-Universität Halle-Wittenberg

von Herrn Ersoy Şaşıoğlu

geb. am: 15 December 1975 in Antalya, Turkey

Gutachter:

1. PD. Dr. Leonid Sandratskii
2. Prof. Dr. Peter Dederichs
3. Prof. Dr. Olle Eriksson

Halle (Saale), 25. April 2006

# List of publications

*Papers included in the thesis*

- **First-principles calculation of the inter sublattice exchange interactions and Curie temperatures of the full Heusler alloys $Ni_2MnX$ (X=Ga, In, Sn, Sb)**
  *E. Şaşıoğlu, L. M. Sandratskii and P. Bruno*
  Phys. Rev. B **70** 024427 (2004)

- **First-principles study of exchange interactions and Curie temperatures of half-metallic ferrimagnetic full Heusler alloys $Mn_2VZ$ (Z=Al, Ge)**
  *E. Şaşıoğlu, L. M. Sandratskii and P. Bruno*
  J. Phys.: Condens. Matter **17** 995 (2005)

- **Pressure dependence of the Curie temperature in $Ni_2MnSn$ Heusler alloy: A first-principles study**
  *E. Şaşıoğlu, L. M. Sandratskii and P. Bruno*
  Phys. Rev. B **71** 214412 (2005)

- **Above-room-temperature ferromagnetism in half-metallic Heusler compounds NiCrP, NiCrSe, NiCrTe and NiVAs: A first-principles study**
  *E. Şaşıoğlu, L. M. Sandratskii and P. Bruno*
  J. Appl. Phys. **98** 063523 (2005)

- **Exchange interactions and temperature dependence of the magnetization in half-metallic Heusler alloys**
  *E. Şaşıoğlu, L. M. Sandratskii, P. Bruno and I. Galanakis*
  Phys. Rev. B **72** 184415 (2005)

- **Magnetic phase diagram of the semi-Heusler alloys from first principles**
  *E. Şaşıoğlu, L. M. Sandratskii and P. Bruno*
  Appl. Phys. Lett. **89** 222508 (2006)

- **Role of the conduction electrons in mediating exchange interactions in Heusler alloys**
  *E. Şaşıoğlu, L. M. Sandratskii and P. Bruno*
  In preparation to appear in Phys. Rev. B

*Papers not included in the thesis*

- **Magnetic exchange coupling and Curie temperature of Ni$_{(1+x)}$MnSb (x=0, 0.25, 0.5, 0.75, 1) from first principles**
  *E. Şaşıoğlu, L. M. Sandratskii and P. Bruno*
  J. Mag. Mag. Mater., **290-291** 385 (2005)

- **Stability of ferromagnetism in the half-metallic pnictides and similar compounds: A first-principles study**
  *E. Şaşıoğlu, I. Galanakis, L. M. Sandratskii and P. Bruno*
  J. Phys.: Condens. Matt. **17** 3915 (2005)

- **Exchange interactions and Néel temperature of a Fe monolayer on W(001): A first-principles study**
  *L. M. Sandratskii, E. Şaşıoğlu and P. Bruno*
  Phys. Rev. B **73** 014430 (2006)

- **First-principles investigation of magnetism of U films and U(001)$_1$/Fe(110)$_3$ multilayers**
  *A. Laref, E. Şaşıoğlu and L. M. Sandratskii*
  J. Phys.: Condens. Matt. **17** 4177 (2006)

- **Search for half-metallic ferrimagnetism in V-based Heusler alloys Mn$_2$VZ (Z=Al, Ga, In, Si, Ge, Sn)**
  *K. Özdoğan, I. Galanakis, E. Şaşıoğlu, and B. Aktaş*
  J. Phys.: Condens. Matt. **18** 2905 (2006)

- **Effect of doping disorder on the half metallicity of full Heusler alloys**
  *I. Galanakis, K. Özdoğan, B. Aktaş, and E. Şaşıoğlu*
  Appl. Phys. Lett. **89** 042502 (2006)

- **Defects in CrAs and related compounds as a route to half-metallic ferrimagnetism**
  *I. Galanakis, K. Özdoğan, E. Şaşıoğlu, and B. Aktaş*
  Phys. Rev. B **74** 140408(R) (2006)

- **Doping and disorder in the Co$_2$MnAl and Co$_2$MnGa half-metallic Heusler alloys**
  *K. Özdoğan, E. Şaşıoğlu, B. Aktaş, and I. Galanakis*
  Phys. Rev. B **74** 172412 (2006)

# Contents

# Acknowledgments

I am most grateful to my supervisor PD. Dr. Leonid Sandratskii, for giving me the opportunity to do this work, for his continuous guidance and encouragement throughout my studies. He was always very helpful and motivating.

I am very thankful to Prof. Dr. Patrick Bruno for his guidance through very useful discussions.

Moreover, I benefited from the collaboration with Dr. Iosif Galanakis and from useful discussions with Prof. Dr. Josef Kudrnovský during his stay in MPI-Halle.

I would gratefully acknowledge Mr. A. Akın Ünal and Dr. M. Perez Jigato for reading my thesis and offering helpful comments and advices.

I also would like to thank my colleagues in the Theory Department of the Max-Planck-Institute of Microstructure Physics for the pleasant atmosphere and a lot of friendly discussions during the seminars.


This work is dedicated to my family



Ersoy Şaşıoğlu

Halle (Saale), Germany

December 22, 2005

# Abstract

This work contains the theoretical investigations of the exchange interactions and Curie temperature in various Heusler alloys. The calculations are performed within the parameter-free density-functional theory with the state-of-the-art ASW-method. The calculation of the exchange parameters is based on the frozen-magnon approach. The Curie temperature is estimated within mean-field (MF) and random-phase-approximation (RPA) approaches. The obtained results are divided in three parts. In the first part, a systematic study of the both intra-sublattice and inter-sublattice exchange interactions as well as Curie temperatures for experimentally well-established Heusler alloys is presented. We focused on the microscopical mechanisms of the formation of the long range magnetic order. For Ni-based compounds $Ni_2MnZ$ (Z = Ga, In, Sn, Sb) we obtain a strong dependence of the exchange interactions on the Z constituent (*sp*-atom) despite the closeness of calculated and experimental Curie temperatures of all four compounds. The role of the *sp*-electrons in mediating exchange interactions between Mn atoms is further revealed by studying non-stoichiometric compositions of Pd- and Cu-based semi and full Heusler alloys. We found that an important factor strongly influencing the electronic properties of the Heusler alloys is the spin polarization of the *sp*-electrons. We obtained a clear relationship between the strength of the exchange interaction and the *sp*-electron spin polarization. In all considered systems the Mn-Mn exchange interaction is long-ranged and shows RKKY-type oscillations.

In the second part, a detailed study of magnetism of half-metallic Heusler compounds promising for magnetoelectronics applications is presented. We study both ferromagnetic and ferrimagnetic compounds. The role of the inter-sublattice exchange interactions in formation of the very high Curie temperature is revealed. We investigate the effect of the half-metallic gap on the stability of exchange interactions and Curie temperature. We study spin wave spectra and temperature dependence of the magnetization employing multi-sublattice Green function technique within Tyablikov decoupling scheme. We predicted new semi Heusler compounds with very high $T_C$ values.

In the last part, we study the pressure dependence of electronic structure, exchange interactions, and Curie temperature in the ferromagnetic Heusler alloy $Ni_2MnSn$. In agreement with the experiment we obtain an increase of Curie temperature from 362 K at ambient pressure to 396 K at 12 GPa. Extending the variation of the lattice parameter beyond the range studied experimentally, we obtained non-monotonic pressure dependence of the Curie

temperature and metamagnetic transition. We relate the theoretical dependence of $T_C$ on the lattice constant to the corresponding dependence predicted by the empirical interaction curve. The Mn-Ni atomic interchange observed experimentally is simulated to study its influence on the Curie temperature.

# Introduction

Heusler alloys are known for more than 100 years. They are named after Friedrich Heusler, a German mining engineer and chemist, who discovered in 1903 Cu-Mn-Al to be ferromagnetic, although the alloy consists of non-ferromagnetic elements. Today two classes of materials are called Heusler alloys: The semi-Heusler alloys with general formula XYZ and the full-Heusler alloys with $X_2YZ$. The X and Y elements come from the transition metal group, whereas the Z component is the element of the III-V group. The semi- and full-Heusler alloys are characterized by the $C1_b$ and $L2_1$ structures, respectively. These compounds exhibit very rich magnetic behavior. One finds in the same family of alloys diverse magnetic phenomena: itinerant and localized magnetism, antiferromagnetism, helimagnetism, or non-collinear magnetism. Recently, Heusler alloys have attracted considerable experimental and theoretical interest due to three unique properties that they exhibit: i) Half-metallic behavior, ii) magnetic shape memory effect and iii) inverse magnetocaloric effect.

The half-metallicity was first predicted by de Groot and collaborators in 1983 when studying the band structure of a half-Heusler alloy NiMnSb. Then the half-metallic ferromagnets have become one of the most studied classes of materials. The existence of a gap in the minority-spin band structure leads to 100% spin polarization of the electron states at the Fermi level and makes these systems attractive for applications in the emerging field of spintronics. In half-metals, the creation of a fully spin-polarized current should be possible that should maximize the efficiency of magnetoelectronics devices. Besides strong spin polarization of the charge carriers in the ground state, the half-metallic materials should have a compatible lattice structure with the industrially used zincblende semiconductors and possess a high Curie temperature to allow the applications in the devices operating at room temperature. Available experimental information shows that the Heusler alloys are promising systems also in this respect.

The other properties are related to the combination of magnetic and structural features of the Heusler alloys. At low temperatures several Heusler compounds, e.g. $Ni_2MnGa$, $Co_2NbSn$ etc., undergo a martensitic transition from a highly symmetric cubic austenitic to a low symmetry martensitic phase. In the case when the Heusler alloys are magnetic in the martensitic phase, they can exhibit the magnetic shape memory effect (MSM). In these alloys, an external magnetic field can induce large strains when applied in the martensitic state. Shape memory alloys are promising smart materials for future technological applications.

They can be used as sensors and actuators in different fields. The inverse magnetocaloric effect (MCE) has its origin in a martensitic phase transformation that modifies the exchange interactions due to the change in the lattice parameters. For samples with compositions close to $Ni_2MnZ$ (Z = Ga, Sn) stoichiometry an inverse MCE has been reported. At the martensitic phase, applying a magnetic field adiabatically causes the sample to cool. This feature is regarded promising for the development of economical and ecological refrigerants working near room temperature.

In addition to these three unique properties, Heusler alloys also provide fundamental aspects for magnetism in complex systems. This is due to their complex crystal structure and observed diverse magnetic behavior. Thus, these systems are of great interest for fundamental investigations concerning the understanding of microscopic physical mechanisms leading to complex magnetic phenomena.

Despite very strong interest to the structural and half-metallic properties of Heusler alloys and the fact that finite temperature magnetic behavior is governed by the exchange interactions the theoretical study of these quantities and the Curie temperature in these systems received less attention. The first contribution to the density functional theory (DFT) of the exchange interactions and Curie temperatures in Heusler alloys was made in an early paper by Kübler and collaborators where the microscopic mechanisms of the magnetism of these systems were discussed on the basis of the comparison of the ferromagnetic and antiferromagnetic configurations of the Mn moments. To our knowledge no further studies have been reported on this subject before the present work was started. The first-principles study of the exchange interactions is one of the major tasks of the thesis. To predict new Heusler compounds with desired properties, the theoretical understanding of the exchange interactions in these systems is essential.

The thesis is divided into two parts. The first part contains the discussion of computational methods and materials. In the second part calculational results are presented. The first part is organized as follows. In chapter 1, we discuss the main aspects of DFT with a special emphasis on non-collinear magnetism. A brief introduction to the augmented spherical wave (ASW) method used in the thesis is given. Chapter 2 is devoted to the brief discussion of different aspects of magnetism in condensed matter and main exchange mechanisms in local moment systems. First-principles approaches to the exchange interactions are introduced. The calculation of exchange interactions for a multi-sublattice material within the frozen-magnon method is discussed in detail. A brief introduction to the magnetism at finite temperatures and the discussion of magnetic excitations is given in chapter 3. To study the temperature dependence of magnetization in Heusler alloys we generalized the MF and RPA approximations to the multi-sublattice case. In the last chapter of the first part (chapter 4) we review previous experimental and theoretical studies on the structural and magnetic properties of Heusler alloys.

The results of our extensive investigations on various Heusler alloys are collected in the second part. The discussion of the results is split into three chapters. In chapter 5, we discuss

the main exchange mechanisms in Heusler alloys paying special attention to the role of the *sp*-electrons in establishing magnetic properties. We begin with well known stoichiometric Ni-based full Heusler compounds $Ni_2MnZ$ (Z=Ga, In, Sn, Sb) and report a systematic study of the exchange interaction between atoms of different sublattices and show that pattern of exchange interactions in these systems deviates strongly from the physical picture that can be expected on the basis of the experimental information. Indeed, despite the observed macroscopic similarities such as common crystal structure, similar chemical composition, and close experimental values of the Curie temperature the microscopic physical mechanisms of the ferromagnetism appeared to be different. We found that the exchange interactions of the compounds vary widely depending on the Z constituent. In particular, the intersublattice interactions change strongly from system to system. We show that, in agreement with experiment, different patterns of exchange interactions lead to similar values of the Curie temperatures. Then to gain further insight into the role of the *sp*-electrons in mediating exchange interactions between Mn atoms we extended the calculations to the non-stoichiometric compositions of Cu- and Pd-based semi- and full-Heusler alloys. In this case we find that an important factor strongly influencing the electronic properties of the Heusler alloys is the spin polarization of the *sp*-electrons. We obtain a clear relationship between the strength of the exchange interactions and the *sp*-electron polarization. The larger the *sp*-electron polarization, the stronger the exchange interactions and, as a result the higher the Curie temperature. In particular the systems with vanishing *sp*-electron spin polarization are characterized by the value of the Curie temperature that is also very close to zero. This property reveals the decisive role of the *sp*-electrons of the X and Z atoms in mediating the exchange interaction between the Mn spin moments.

Chapter 6 is devoted to the study of magnetism of half-metallic (HM) Heusler compounds that have potential for applications in the field of spintronics. We study both ferromagnetic and ferrimagnetic Heusler compounds. We revealed the role of the intersublattice exchange interactions in the formation of the very high Curie temperature in some full Heusler compounds such as $Co_2MnSi$ and $Mn_2VAl$. We investigate the effect of the half-metallic gap on the stability of exchange interactions and Curie temperatures. We study spin wave spectra and temperature dependence of the magnetization employing multi-sublattice Green function technique within Tyablikov decoupling scheme. We predicted new half-metallic semi Heusler compounds with very high $T_C$ values.

In chapter 7 we study the effect of pressure on magnetic properties of Heusler alloys by the example of $Ni_2MnSn$. In particular, we report the pressure dependence of electronic structure, exchange interactions and Curie temperature focusing on the low pressure region where the experimental information is available. We relate the theoretical dependence of $T_C$ on the lattice constant to the corresponding dependence predicted by the empirical interaction curve. The Mn-Ni atomic interchange observed experimentally is simulated to study its influence on the Curie temperature. Finally, our conclusions are summarized in chapter 8.

# Part I

# Methods and Materials

# Chapter 1

# Density Functional Theory of Magnetic Systems

## 1.1    Introduction

Density-functional theory (DFT) is one of the most popular and successful quantum mechanical approaches to the study of matter. It offers a powerful and elegant way for calculating the ground-state properties of interacting electrons. It is nowadays routinely applied for calculating, e.g., the band structure of solids in physics and the binding energy of molecules in chemistry. The systems may range in complexity from a single atom to a complex system such as as proteins and carbon nanotubes. DFT has been extensively applied to many areas of condensed matter physics. In particular, it has been remarkably successful in explaining the magnetic properties of transition metals and their alloys.

Traditional methods in electronic structure calculations, like Hartree-Fock theory are based on the complicated many-electron wavefunctions. The main idea of DFT is to replace the many-body electronic wavefunction with the electronic density $n(\mathbf{r})$ as the basic quantity. Whereas the many-body wavefunction is dependent on $3N$ (or $4N$ if spin is included) variables, the density $n(\mathbf{r})$ is only a function of three variables and is a simpler quantity to deal with both conceptually and practically. DFT reduces the calculations of the ground state properties of systems of interacting particles exactly to the solution of single-particle Hartree-type equations. This is why it has been most useful approach for many electron systems.

In many-body electronic structure calculations of solids and molecules the Born-Oppenheimer approximation provides the first simplification to the many body Hamiltonian. Due to their masses the nuclei move much slower than the electrons. This means that one can consider the electrons as moving in the field of fixed nuclei, i.e, the nuclear kinetic energy is zero and their potential energy is merely a constant. Thus, the electronic part of the Schrödinger equation

reduces to

$$
\begin{aligned}
H\Psi(\mathbf{r}_1, \mathbf{r}_2, \cdots \mathbf{r}_N) &= [T + V_{ext} + U_{ee}]\Psi(\mathbf{r}_1, \mathbf{r}_2, \cdots \mathbf{r}_N) \\
&= \left[ -\frac{\hbar^2}{2m} \sum_i^N \nabla_i^2 + \sum_i^N V(\mathbf{r}_i) + \sum_{i \neq j}^N U(\mathbf{r}_i, \mathbf{r}_j) \right] \Psi(\mathbf{r}_1, \mathbf{r}_2, \cdots \mathbf{r}_N) \\
&= E\Psi(\mathbf{r}_1, \mathbf{r}_2, \cdots \mathbf{r}_N)
\end{aligned}
\tag{1.1}
$$

where $\Psi(\mathbf{r}_1, \mathbf{r}_2, \cdots \mathbf{r}_N)$ is the wave function of stationary electronic state, $N$ is the number of electrons and $U_{ee}$ is the electron-electron interaction. The operators $T$ and $U_{ee}$ are the same for any system, while $V_{\text{ext}}$ is system dependent. As it is seen from Eq. (1.1) the actual difference between a single-particle problem and the much more complicated many-particle problem comes from the interaction term $U_{\text{ee}}$. In principle, the solution of many-body Schrödinger equation is possible with the sophisticated methods such as perturbation theory in physics or configuration interaction methods in quantum chemistry. However, the problem with these methods is the huge computational effort, which makes it practically impossible to apply them efficiently to larger complex systems.

DFT provides a way to systematically map the many-body problem, with $U_{\text{ee}}$, onto a single-body problem without $U_{ee}$. In DFT the key variable is the particle density $n(\mathbf{r})$ which is given by

$$
n(\mathbf{r}) = N \int d\mathbf{r}_2 \int d\mathbf{r}_3 \int d\mathbf{r}_4 \cdots \int d\mathbf{r}_N |\Psi(\mathbf{r}, \mathbf{r}_2, \cdots \mathbf{r}_N)|^2
\tag{1.2}
$$

## 1.2 Thomas-Fermi model

Historically, the density functional theory has its conceptual roots in the Thomas-Fermi model. In 1927 Thomas and Fermi [1] showed that for interacting electrons moving in an external potential $v_{\text{ext}}(\mathbf{r})$, the relation between $v_{ext}(\mathbf{r})$ and the density distribution $n(\mathbf{r})$ can be expressed as

$$
n(\mathbf{r}) = \gamma[\mu - v_{\text{eff}}(\mathbf{r})]^{3/2}
\tag{1.3}
$$

where $\gamma = \frac{1}{3\pi 2}\left(\frac{2m}{\hbar 2}\right)^{3/2}$ and $\mu$ is the $\mathbf{r}$ independent chemical potential and the second term in Eq. (1.3) is the classical electrostatic potential generated by the electron density $n(\mathbf{r})$.

$$
v_{\text{eff}}(\mathbf{r}) = v_{\text{ext}}(\mathbf{r}) + \int \frac{n(\mathbf{r}')}{|\mathbf{r} - \mathbf{r}'|} d\mathbf{r}'
\tag{1.4}
$$

Eq. (1.3) works well for systems with slowly varying density. Although this was an important first step, the Thomas-Fermi equation's accuracy is limited because it neglects exchange and correlation effects.

Hohenberg and Kohn started from Thomas-Fermi theory and established the connection between the electron density $n(\mathbf{r})$ and the many-electron Schrödinger equation [2]. Thus, the work of Hohenberg and Kohn is considered to be at the heart of the density functional theory.

## 1.3 Hohenberg-Kohn theorems

The first Hohenberg-Kohn theorem states that

- The ground state density $n_0(\mathbf{r})$ of the interacting electrons in some external potential $v_{\text{ext}}(\mathbf{r})$ determines this potential uniquely.

It follows from the first theorem that the ground state energy is a functional of $n_0(\mathbf{r})$

$$E_0 = E[n_0] = \langle \Psi_0 | T + V_{\text{ext}} + U_{\text{ee}} | \Psi_0 \rangle \tag{1.5}$$

where $\Psi_0 = \Psi_0[n_0]$ and contribution of the external potential $\langle \Psi_0 | V_{ext} | \Psi_0 \rangle$ can be written explicitly in terms of the density

$$V_{ext}[n_0] = \int v_{ext}(\mathbf{r}) n_0(\mathbf{r}) d\mathbf{r} \tag{1.6}$$

The functionals $T[n_0]$ and $U_{\text{ee}}[n_0]$ and are called universal functionals while $V_{\text{ext}}[n_0]$ is not universal and depends on the system under consideration. The second Hohenberg-Kohn theorem provides a variational principle

- For any given density $n(\mathbf{r})$ associated to an $N$ electron system with external potential $v_{\text{ext}}(\mathbf{r})$ the minimum of the energy functional is obtained with the ground state density.

$$E_0 \leq E[n] = T[n] + V_{\text{ext}}[n] + U_{\text{ee}}[n] \tag{1.7}$$

The ground state can be obtained by minimizing the functional $E[n]$ with respect to $n(\mathbf{r})$ if the functionals $T[n]$ and $U_{\text{ee}}[n]$ are known. A successful minimization of the energy functional will yield the ground state density $n_0(\mathbf{r})$ and thus all other ground state properties of interest.

## 1.4 Kohn-Sham equations

In 1965 Kohn and Sham showed that the variational problem of minimizing the energy functional can be solved by applying the Lagrangian method of undetermined multipliers [3]. In order to proceed we will write the total energy functional $E[n]$ as

$$E[n] = T[n] + \int v_{ext}(\mathbf{r}) n(\mathbf{r}) d\mathbf{r} + \frac{1}{2} \int d\mathbf{r} d\mathbf{r}' \frac{n(\mathbf{r}) n(\mathbf{r}')}{|\mathbf{r} - \mathbf{r}'|} + E_{xc}[n(\mathbf{r})] \tag{1.8}$$

Eq. (1.8) contains the kinetic energy, the energy because of the the external potential, the energy of the static electron-electron Coulomb repulsion (Hartree term) and the exchange correlation energy. The $E_{\text{xc}}$ includes all the many particle interactions.

The main problem is to find the expressions for $T[n]$ and $E_{xc}[n]$. An explicit forms of $T[n]$ and $E_{xc}$ are not known in general, we use the variational principle on the total energy functional to write

$$\frac{\delta E[n]}{\delta n(\mathbf{r})} + \mu \frac{\delta(N - \int n(\mathbf{r}) d\mathbf{r})}{\delta n(\mathbf{r})} = 0 \tag{1.9}$$

where $\mu$ is a Lagrange multiplier which guaranties the particle number conservation. As suggested by Kohn and Sham it is convenient to split up the kinetic energy term into two terms $T = T_0 + T_{xc}$, where $T_{xc}$ stands for the exchange-correlation part of the kinetic energy and $T_0$ is the the kinetic energy of non-interacting particles. The first assumption of the Kohn-Sham theory is that $\Psi(\mathbf{r}_1, \mathbf{r}_2, \cdots \mathbf{r}_N)$ many-body wave function is a Slater determinant($\Psi \approx \Phi^{SD}$). Then using the density $n(\mathbf{r}) = \sum_{i\,occ} |\psi_i(\mathbf{r})|^2$ and taking the functional derivative in Eq. (1.9) we arrive at a set of effective single-particle equations called the Kohn-Sham equations

$$\left[ -\frac{\hbar^2}{2m}\nabla^2 + v_{\text{eff}}(\mathbf{r}) \right]\psi_i(\mathbf{r}) = \varepsilon_i \psi_i(\mathbf{r}) \tag{1.10}$$

which are the single particle Schrodinger equations where the external potential has been replaced by an effective potential given by

$$v_{\text{eff}}(\mathbf{r}) = v_{ext}(\mathbf{r}) + e^2 \int \frac{n(\mathbf{r}')}{|\mathbf{r} - \mathbf{r}'|}d\mathbf{r}' + v_{xc}(\mathbf{r}) \tag{1.11}$$

where the exchange-correlation potential is given by

$$v_{xc}(\mathbf{r}) = \frac{\delta(E_{xc}[n])}{\delta n(\mathbf{r})} \tag{1.12}$$

Note that the exchange-correlation part of the kinetic energy $T_{xc}$ is included in $E_{xc}$ in Eq. (1.12) .

The Kohn-Sham equation has to be solved self-consistently. Usually one starts with an initial guess for the density $n(\mathbf{r})$ , then one calculates the corresponding effective potential $v_{\text{eff}}(\mathbf{r})$ and solves the Kohn-Sham equations for the $\psi_i$ . From these one calculates a new density and starts again. This procedure is then repeated until convergence is reached. Once this is done, the ground state energy can be expressed by the Kohn-Sham formula

$$E_0 = \sum_{i\,occ} \varepsilon_i - \frac{e^2}{2} \int d\mathbf{r}d\mathbf{r}' \frac{n(\mathbf{r})n(\mathbf{r}')}{|\mathbf{r} - \mathbf{r}'|} + E_{xc}[n(\mathbf{r})] - \int v_{xc}(\mathbf{r})n(\mathbf{r})d\mathbf{r} \tag{1.13}$$

## 1.5 Approximations for $E_{xc}[n]$

Although Kohn-Sham formalism reduces the many-particle interacting electron problem to an effective single particle Schrödinger equation, the solution of the Eq. (1.10) requires certain approximations. The major problem with DFT is that the exact functionals for exchange and correlation are not known except for the free electron gas. However, approximations exist which permit the calculation of certain physical quantities quite accurately.

### 1.5.1 The local density approximation (LDA)

The most commonly used and successful approximation is the Local Density Approximation (LDA), where the exchange correlation energy depends only on the density at the coordinate where the functional is evaluated

$$E_{xc}[n] = \int n(\mathbf{r})\epsilon_{xc}[n(\mathbf{r})]d\mathbf{r} \tag{1.14}$$

where $\epsilon_{xc}[n(\mathbf{r})]$ is the exchange and correlation energy per particle of a uniform electron gas of density $n(\mathbf{r})$. This quantity can be further split into two parts:

$$\epsilon_{xc}[n(\mathbf{r})] = \epsilon_x[n(\mathbf{r})] + \epsilon_c[n(\mathbf{r})] \tag{1.15}$$

The exchange part,$\epsilon_x[n(\mathbf{r})]$ which represents the exchange energy of an electron in a uniform electron gas of a particular density, was originally derived by Bloch in 1929 [4] which is given as

$$\epsilon_x[n(\mathbf{r})] = -\frac{3}{4}\left(\frac{3n(\mathbf{r})}{\pi}\right)^{1/3} \tag{1.16}$$

The correlation part cannot be derived analytically, but can be calculated numerically with high accuracy by means of Monte Carlo simulations.

Although LDA is a simple approximation, it is surprisingly accurate for solids and solid surfaces, including those with rapid density variations. However it tends to underestimate atomic ground state energies and ionization energies, while overestimating binding energies. The accuracy of LDA is certainly insufficient for most applications in chemistry. LDA also fails in strongly correlated systems like heavy fermions.

### 1.5.2 The generalized gradient approximation (GGA)

The first attempt to go beyond the LDA is the use of not only the information about the density $n(\mathbf{r})$ at a particular point $\mathbf{r}$ but also the information about the density gradient $\nabla n(\mathbf{r})$ in order to account for the non-homogeneity of the true electron density. The resulting approximation is so-called the generalized gradient approximation (GGA) which is given as

$$E_{xc}[n] = \int n(\mathbf{r})\epsilon_{xc}[n(\mathbf{r}), \nabla n(\mathbf{r})]d\mathbf{r} \tag{1.17}$$

For systems where the charge density is slowly varying, the GGA has proved to be an improvement over LDA. Using the GGA very good results for molecular geometries and ground state energies have been achieved.

## 1.6 Extension to spin-polarized systems

The initial formulation of Density functional theory dealt with non-spin polarized (non-magnetic) systems. In principle DFT can be applied to magnetic systems where the spin polarization leads to a magnetization density $\mathbf{m}(\mathbf{r})$, since the magnetization is a functional $\mathbf{m}[n(\mathbf{r})]$ of ground state charge density $n(\mathbf{r})$. In 1972 Barth and Hedin [5] extended the DFT to the spin polarized case. The authors formulated the functionals in terms of the spin density matrix $\rho_{\alpha\beta}(\mathbf{r})$ which is defined as

$$\rho_{\alpha\beta}(\mathbf{r}) = n(\mathbf{r})\delta_{\alpha\beta} + \mathbf{m}(\mathbf{r}) \cdot \sigma_{\alpha\beta} \tag{1.18}$$

where $\sigma \equiv (\sigma_x, \sigma_y, \sigma_z)$ are the Pauli matrices.

To introduce the vector field $\mathbf{m}(\mathbf{r})$ in the formulation of DFT we will generalize the notion of Kohn-Sham orbitals. In non-spin polarized case these orbitals are scalar functions. To describe a general magnetization density using single particle wave functions, one has to resort to a representation with two component spinors,

$$\psi_i(\mathbf{r}) = \left[ \begin{array}{c} \varphi_{i\alpha}(\mathbf{r}) \\ \varphi_{i\beta}(\mathbf{r}) \end{array} \right] \tag{1.19}$$

where $\varphi_{i\alpha}(\mathbf{r})$ and $\varphi_{i\beta}(\mathbf{r})$ corresponds to the two spin projections.

In terms of these two component spinors the density matrix can be represented in the form

$$\rho(\mathbf{r}) = \sum_{i \, occ} \left[ \begin{array}{c} \varphi_{i\alpha}(\mathbf{r}) \\ \varphi_{i\beta}(\mathbf{r}) \end{array} \right] [\varphi_{i\alpha}(\mathbf{r}) \; \varphi_{i\beta}(\mathbf{r})]^* = \sum_{i \, occ} \left[ \begin{array}{cc} \varphi_{i\alpha}(\mathbf{r})\varphi_{i\alpha}^*(\mathbf{r}) & \varphi_{i\alpha}(\mathbf{r})\varphi_{i\beta}^*(\mathbf{r}) \\ \varphi_{i\beta}(\mathbf{r})\varphi_{i\alpha}^*(\mathbf{r}) & \varphi_{i\beta}(\mathbf{r})\varphi_{i\beta}^*(\mathbf{r}) \end{array} \right] \tag{1.20}$$

For a collinear ferromagnet the non-diagonal part of the density matrix becomes zero. But this is not the case for non-collinear magnets as will be seen in the next section.

Using spinors the magnetization density $\mathbf{m}(\mathbf{r})$ and charge density $n(\mathbf{r})$ can be expressed as

$$\mathbf{m}(\mathbf{r}) = \mu_B \sum_{i \, occ} \psi_i^\dagger(\mathbf{r})\sigma\psi_i(\mathbf{r}) \tag{1.21}$$

$$n(\mathbf{r}) = \sum_{i \, occ} \psi_i^\dagger(\mathbf{r})\mathbf{I}\psi_i(\mathbf{r}) \tag{1.22}$$

where $\mu_B$ is the Bohr magneton and $\mathbf{I}$ is the unit matrix.

As it is shown in Ref. [5] the density matrix is a basic physical quantity which uniquely determines all ground-state properties of a magnetic electron system. In particular, the total energy is a functional of the density matrix and assumes its minimum for the ground-state value of the density matrix. In the first step, one determines the total energy as a functional of the density matrix and then applies the variation procedure to find the minimum of the functional. In spin polarized case a standard representation of the energy functional is given by

$$E[\rho] = T[\rho] + \frac{e^2}{2}\int d\mathbf{r}d\mathbf{r}' \frac{n(\mathbf{r})n(\mathbf{r}')}{|\mathbf{r} - \mathbf{r}'|} + \sum_{\alpha\beta}\int v_{\alpha\beta}^{ext}(\mathbf{r})\rho_{\alpha\beta}(\mathbf{r})d\mathbf{r} + E_{xc}[\rho] \tag{1.23}$$

Following the same way as in the non-polarized case the single particle Kohn-Sham equations can be given as

$$\sum_\beta \left[ -\delta_{\alpha\beta}\frac{\hbar^2}{2m}\nabla^2 + v_{\alpha\beta}^{eff}(\mathbf{r}) \right]\varphi_{i\beta}(r) = \delta_{\alpha\beta}\varepsilon_i\varphi_{i\beta}(\mathbf{r}) \tag{1.24}$$

where the effective potential matrix elements $v_{\alpha\beta}^{eff}(\mathbf{r})$ can be written as

$$v_{\alpha\beta}^{eff}(\mathbf{r}) = v_{\alpha\beta}^{ext}(\mathbf{r}) + \delta_{\alpha\beta}e^2\int \frac{n(\mathbf{r}')}{|\mathbf{r} - \mathbf{r}'|}d\mathbf{r}' + v_{\alpha\beta}^{xc}(\mathbf{r}) \tag{1.25}$$

with the exchange-correlation potential matrix elements

$$v_{\alpha\beta}^{xc}(\mathbf{r}) = \frac{\delta(E_{xc}[\rho])}{\delta\rho_{\alpha\beta}(\mathbf{r})} \tag{1.26}$$

## 1.7  Non-collinear magnetism

An essential difference between non-collinear and collinear magnets is the absence of a natural spin quantization axis common for the whole crystal in the non-collinear case. As a result, each one-electron state in a non-collinear magnet must be treated as a two-component spinor function (see Eq. (1.19)). Here we follow the formulation given in Ref.[6]

We define the standard spin-$\frac{1}{2}$ rotation matrix $U(\theta, \phi)$ as follows

$$U(\theta, \phi) = \begin{bmatrix} \cos(\theta/2)\exp(i\phi/2) & \sin(\theta/2)\exp(-i\phi/2) \\ -\sin(\theta/2)\exp(i\phi/2) & \cos(\theta/2)\exp(-i\phi/2) \end{bmatrix} \tag{1.27}$$

and the spinor wavefunction can be represented in the following form using Eq. (1.27)

$$\begin{bmatrix} \varphi_\alpha(\mathbf{r}) \\ \varphi_\beta(\mathbf{r}) \end{bmatrix} = U(\theta(\mathbf{r}), \phi(\mathbf{r})) \begin{bmatrix} 1 \\ 0 \end{bmatrix} \tag{1.28}$$

where the polar angles $\theta(\mathbf{r})$ and $\phi(\mathbf{r})$ determine the direction of the spin moment of the given state at point $\mathbf{r}$ . Correspondingly the density matrix of the crystal is not diagonal in the non-collinear case:

$$\rho(\mathbf{r}) = \begin{bmatrix} \rho_{\alpha\alpha}(\mathbf{r}) & \rho_{\alpha\beta}(\mathbf{r}) \\ \rho_{\beta\alpha}(\mathbf{r}) & \rho_{\beta\beta}(\mathbf{r}) \end{bmatrix} \tag{1.29}$$

The sum of the diagonal elements of $\rho(\mathbf{r})$ gives the charge density, while the difference of them gives the projection of the magnetization density on the global quantization axis. The non-diagonal elements of the matrix determine the component of the magnetization density perpendicular to the quantization axis and are responsible for the non-collinearity of the magnetic structure.

While deriving the Kohn-Sham equations in the previous section, we have not made any assumption of collinearity, i.e. all spin parallel or anti parallel to a global quantization axis. Therefore, for a non-collinear ferromagnet, the Kohn-Sham equations take the same form. Additionally in the local approximation the spatial variation in the magnetization direction does not influence the exchange correlation potential ( see Eq. (1.25)) at a given point. From this property it follows that for such a system it is convenient to choose the system with the $z$ axis parallel to the magnetization direction in the point. In this reference frame the non-diagonal elements of the density matrix becomes zero and the results of the theory of the ferromagnetic electron gas can be employed to determine the form of the exchange correlation potential.

With the help of the spin$-\frac{1}{2}$ rotation matrices (1.27) we can transform the density matrix from the global coordinates system to the local system as

$$\begin{bmatrix} \rho_{\alpha\alpha}(\mathbf{r}) & \rho_{\alpha\beta}(\mathbf{r}) \\ \rho_{\beta\alpha}(\mathbf{r}) & \rho_{\beta\beta}(\mathbf{r}) \end{bmatrix} = U(\theta(\mathbf{r}), \phi(\mathbf{r}))^\dagger \begin{bmatrix} \rho_+(\mathbf{r}) & 0 \\ 0 & \rho_-(\mathbf{r}) \end{bmatrix} U(\theta(\mathbf{r}), \phi(\mathbf{r})) \tag{1.30}$$

where the polar angles $\theta(\mathbf{r})$ and $\phi(\mathbf{r})$ determining the direction of the local magnetization in point $\mathbf{r}$ are defined by the components of the density matrix in the global system:

$$\tan \phi(\mathbf{r}) = -\frac{\text{Im}[\rho_{\alpha\beta}(\mathbf{r})]}{\text{Re}[\rho_{\alpha\beta}(\mathbf{r})]} \tag{1.31}$$

$$\tan \theta(\mathbf{r}) = \frac{2(\{\text{Re}[\rho_{\alpha\beta}(\mathbf{r})]\}^2 + \{\text{Im}[\rho_{\alpha\beta}(\mathbf{r})]\}^2)^{1/2}}{\rho_{\alpha\alpha}(\mathbf{r}) - \rho_{\beta\beta}(\mathbf{r})} \tag{1.32}$$

Finally, the effective potential $v^{\text{eff}}(\mathbf{r})$ can be written in the form.

$$v^{\text{eff}}(\mathbf{r}) = U(\theta(\mathbf{r}), \phi(\mathbf{r}))^\dagger \begin{bmatrix} v_+^{\text{eff}}(\mathbf{r}) & 0 \\ 0 & v_-^{\text{eff}}(\mathbf{r}) \end{bmatrix} U(\theta(\mathbf{r}), \phi(\mathbf{r})) \tag{1.33}$$

where

$$v_\sigma^{\text{eff}}(\mathbf{r}) = -e^2 \sum_{n\nu} \frac{Z_\nu}{|\mathbf{r} - (\mathbf{R}_n + \mathbf{a}_\nu)|} + e^2 \int \frac{n(\mathbf{r}')}{|\mathbf{r} - \mathbf{r}'|} d\mathbf{r}' + v_\sigma^{xc}[\rho_+(\mathbf{r}), \rho_-(\mathbf{r})], \quad \sigma = \pm 1 \tag{1.34}$$

In Eq. (1.34) $Z_\nu$ is the atomic number, $\mathbf{R}_n$ are the lattice vectors and $\mathbf{a}_\nu$ are the atomic positions within a unit cell.

As in the non-spin polarized case the Kohn-Sham equations has to be solved in a self-consistent way. Compared with the case of a collinear magnet the present problem is much more involved. This is because of the additional degrees of freedom connected with the spatial variation in the magnetization direction.

- **Atomic sphere approximation (ASA)**

In order to simplify the problem the atomic sphere approximation (ASA) is usually used. It is supposed that within the atomic sphere of a given atom the magnetization direction is constant and non-collinearity of the magnetic structure is reduced to the different directions of the magnetic moments of different atoms. In this case the angles $\theta$ and $\phi$ in Eq. (1.34) become $\mathbf{r}$ independent and can be determined through a formula similar to Eq. (1.31) but with the use of integrated density matrices:

$$\rho_{n\nu} = \int_{\Omega_{n\nu}} \rho(\mathbf{r}) d\mathbf{r} \tag{1.35}$$

where the integration is carried out over the $(n\nu)$th atomic sphere with radius $S_\nu$.

With the assumption of the spherical symmetry of the potential within the atomic spheres, we can rewrite the effective potential (1.34) in the final form

$$v^{\text{eff}}(\mathbf{r}) = U(\theta_{n\nu}, \phi_{n\nu})^\dagger \begin{bmatrix} v_{+,n\nu}^{\text{eff}}(|\mathbf{r}_{n\nu}|) & 0 \\ 0 & v_{-,n\nu}^{\text{eff}}(|\mathbf{r}_{n\nu}|) \end{bmatrix} U(\theta_{n\nu}, \phi_{n\nu}) \Theta_\nu(|\mathbf{r}_{n\nu}|) \tag{1.36}$$

where

$$\Theta_\nu(|\mathbf{r}_{n\nu}|) = \begin{cases} \Theta_\nu(r) = 1, & r < S_\nu \\ \Theta_\nu(r) = 0, & r > S_\nu \end{cases} \tag{1.37}$$

The implementation of the non-collinear magnetism in augmented spherical wave (ASW) method is discussed in detail in Refs.[6, 7, 8] and will not be presented here. A brief introduction to ASW method will be given in the last section of this chapter.
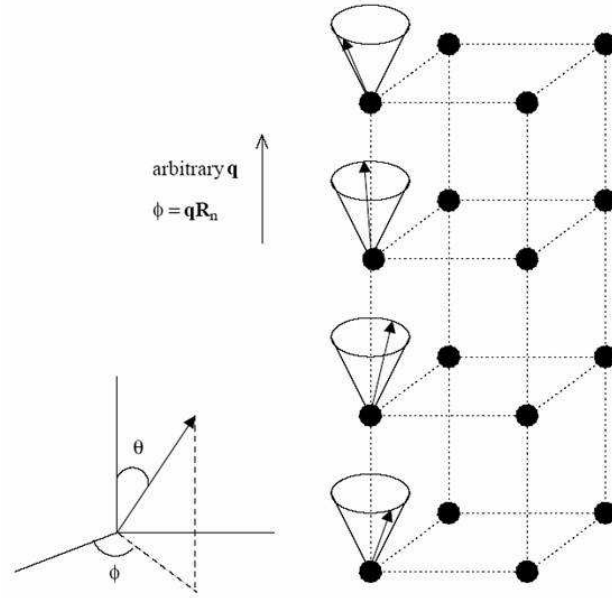
Figure 1.1: A spin spiral structure with vector $\mathbf{q}$ parallel to the $z$ axis.

### 1.7.1  Spin spirals

Spin spiral is a particular form of the non-collinear magnetic structure which is defined by giving the Cartesian coordinates of the magnetization vector as

$$\mathbf{m}_{n\nu} = m_\nu(\cos(\mathbf{q}\mathbf{R}_n + \phi_\nu)\sin\theta_\nu, \sin(\mathbf{q}\mathbf{R}_n + \phi_\nu)\sin\theta_\nu, \cos\theta_\nu) \qquad (1.38)$$

where $m_\nu$ is the magnitude of the magnetic moment of atom ($\nu$), $(\mathbf{q}\mathbf{R}_n + \phi_\nu)$ and $\theta_\nu$ are polar angles, $\mathbf{R}_n$ is a lattice vector and $\mathbf{q}$ is the wave vector that characterizes the spin spiral.

A schematic representation of the spin spiral structure with vector $\mathbf{q}$ parallel to the $z$ axis is shown in figure 1.7.1. An apparent difficulty for the first-principles calculation of a spiral structure is the lack of translational symmetry along the direction of the wave vector $\mathbf{q}$. In this case one has to resort to a large super-cell along this direction. Also the dimension of such a super-cell must be at least as large as the wavelength of the spiral. In this case the treatment of small-$\mathbf{q}$ excitations becomes impossible because of the extremely large super cells. However, one can show that spin spiral configurations can be described without resorting to super-cells [9, 10, 11]. This can be achieved with the help of generalized Bloch theorem which allows the DFT treatment of spin spirals in chemical unit cells.

### 1.7.2  Generalized Bloch theorem

As it is seen from the figure 1.7.1 and Eq. (1.38) all atoms of the spiral structure separated by a translation $\mathbf{R}_n$ posses magnetic moments of the same magnitude and hence they are equivalent. This equivalence leads to the generalization of the Bloch theorem. This is first

pointed out by Herring [9] and later by Sandratskii [10, 11]. Transformations combining a lattice translation $T_\mathbf{R}$ and a spin rotation about $z$ axis by an angle $\phi = \mathbf{q} \cdot \mathbf{R}_n$ leave the spiral structure invariant. The symmetry operators that describe these transformations belong to a spin-space group (SSG). The generalized translations has the following properties: i) the spinors transform according to

$$\{\mathbf{q}\mathbf{R}_n|T_\mathbf{R}\}\psi(\mathbf{r}) = \begin{pmatrix} \mathrm{e}^{-i\mathbf{q}\mathbf{R}/2} & 0 \\ 0 & \mathrm{e}^{i\mathbf{q}\mathbf{R}/2} \end{pmatrix} \psi(\mathbf{r} - \mathbf{R}) \tag{1.39}$$

ii) they commute with the Kohn-Sham Hamiltonian of a spin spiral structure, and iii) they form an Abelian group isomorphic to the group of ordinary space translations by vector $\mathbf{R}_n$. Isomorphism of two groups leads to coincidence of their irreducible representation. Therefore, they have the same irreducible representation, which constitutes the Bloch Theorem in the case of ordinary space translations. The generalized Bloch theorem is then given as

$$\{\mathbf{q}\mathbf{R}_n|T_\mathbf{R}\}\psi_\mathbf{k}(\mathbf{r}) = \mathrm{e}^{-i\mathbf{k}\cdot\mathbf{R}_n}\psi_\mathbf{k}(\mathbf{r}) \tag{1.40}$$

where the vectors $\mathbf{k}$ lie in the first Brillouin zone which is defined in the usual way by the vectors $\mathbf{R}_n$. Eq. (1.40) permits us to write any eigenfunction in the form

$$\psi_\mathbf{k}(\mathbf{r}) = \mathrm{e}^{-i\mathbf{k}\cdot\mathbf{R}_n}u_\mathbf{k}(\mathbf{r}) \tag{1.41}$$

where the spinors $u_\mathbf{k}(\mathbf{r})$ have the generalized periodicity of the Hamiltonian

$$\{\mathbf{q}\mathbf{R}_n|T_\mathbf{R}\}u_\mathbf{k}(\mathbf{r}) = u_\mathbf{k}(\mathbf{r}) \tag{1.42}$$

These properties allows us to solve the Kohn-Sham equations in the presence of spin spirals without using super-cells.

## 1.8 Augmented spherical wave (ASW) method

The Augmented Spherical Wave (ASW) was developed in the seventies by A. R. Williams, J. Kübler, and C. D. Gelatt for the purpose of the solution of the one-particle Kohn-Sham equations within DFT [12]. It is one of the most efficient methods for calculating electronic and magnetic properties of real solids. The method is based on the Born-Oppenheimer approximation and it makes use of crystalline periodicity and the Bloch theorem.

The ASW program package employs both the local density approximation (LDA) and the generalized gradient approximation (GGA) for the exchange correlation potential within the atomic sphere approximation (ASA). Full potential version is also developed [13, 14, 15]. Commercial version of the full-potential ASW package can be obtained from [15].

The ASW method fully includes both the core and the valence electrons in the self-consistent field calculations. For this reason, it allows the treatment of the whole periodic table including transition metal atoms as well as the lanthanides and actinides. Furthermore,

its minimal basis set makes it one of the fastest scheme among the modern electronic structure codes. For $3d$ elements it uses atomic-like $s$, $p$, $d$ orbitals and thus each atom contributes with 9 or 16 basis functions to the secular matrix, which is much less than the 100 functions necessary in plane wave based methods. Additional speed-up comes from the fact that the ASW method is a so-called linearized method.

Finally, ASW method allows non-relativistic as well as scalar-relativistic and full-relativistic calculations and it can handle both spin-restricted and spin-polarized calculations. Also, a distinct feature of the ASW method is that it allows the treatment of non-collinear magnetic systems.

# Chapter 2

# First-Principles Calculation of Exchange Interactions

Before introducing the first-principles methods for the calculation of exchange interactions in magnetic systems we will briefly review two different aspects of magnetism in solids and the main exchange mechanisms in local moment systems.

## 2.1 Models of magnetism

Magnetism has been a subject of great interest and intensive research in field of condensed matter physics over the last century. Two different physical models have been proposed to describe the magnetism in materials: one is localized and the other is the itinerant electron model. The former has been used successfully in magnetic insulators and rare earth (RE) elements and the latter for $3d$ transition metals and their alloys. These two models are opposed but complementary to each other and illustrate the intrinsic properties of magnetism of materials. However, they are still in the stage of development and in many cases they can not be separated from each other. For a deep understanding of magnetism in condensed matter there has been a trend to combine both models to develop a unified theory [16]. In this section we will briefly present these two models and introduce classical Heisenberg model for the treatment of the finite temperature magnetism in itinerant electron systems.

- **Localized electron model**

The modern theory of magnetism has started with the concept of a local magnetic moment of a fixed size. Within this concept Langevin gave an explanation for the Curie law of magnetic susceptibility [17]. Subsequently Weiss introduced the notion of an interaction (molecular field) between the atomic magnetic moments to explain the spontaneous magnetic order in solids. Combining this new concept with the studies of Langevin, Weiss was able to explain the finite temperature properties of ferromagnetic $3d$ transition metals [18].

Although Langevin-Weiss theory has explained quite successfully the essential properties of ferromagnets both below and above the Curie temperature, the magnitude of the molecular field which is responsible for magnetic order, could not be explained within the classical physics. Since the magnetic dipole-dipole interactions were known to give a value for the molecular field which is two or three orders of magnitude smaller than estimated from the observed value of $T_C$. This problem was resolved with the advent of quantum mechanics.

In 1928 Heisenberg attributed the origin of Weiss molecular field to the quantum mechanical exchange interaction between the magnetic moments and proposed a more general model [19]. If $\mathbf{S}_i$ is the atomic magnetic moment for a given site then the Heisenberg model is given by

$$H = -\sum_{i,j} J_{ij} \mathbf{S}_i \mathbf{S}_j \tag{2.1}$$

where $J_{ij}$ is the interatomic exchange interaction constant which is introduced phenomenologically and its physical origin will be discussed in the next section. $J_{ij} > 0$ for ferromagnets while it is negative for antiferromagnets. In principle, various magnetic orderings such as ferrimagnetism, helimagnetism can be derived from Heisenberg model by generalizing the sign and range of the exchange interactions. Moreover, Heisenberg model has led to discovery of spin waves as elementary excitations.

- **Itinerant electron model**

Magnetism in metals is usually explained on the basis of itinerant electron picture. One of the main reasons for this is that the saturation magnetization in $3d$ transition metals and their alloys is not integer.

Bloch first discussed the possibility of ferromagnetism in an electron gas on the basis of Hartree-Fock approximation [20]. Later Wigner pointed out the importance of electron-electron interactions on the suppression of the occurrence of ferromagnetism in electron gas [21]. Thus the occurrence of ferromagnetism in transition metals is considered to be connected with the atomic character of $3d$ electrons and mainly intra-atomic exchange interactions. Stoner developed an itinerant electron model to explain ferromagnetism in $3d$ transition metals [22]. In the Stoner model, magnetism in metals arises from a splitting between the up- and down-spin bands and it is favored when the density of states is high at the Fermi level. The instability of non-magnetic state with respect to formation of ferromagnetic order is given by the Stoner criterion which is define by

$$IN(E_F) > 1 \tag{2.2}$$

where $I$ is the intra-atomic exchange integral and $N(E_F)$ is the density of states at Fermi level. It can be seen from the Stoner criterion that whether there is ferromagnetism from itinerant electrons depends on the product of exchange integral and the DOS at the Fermi level. Stoner model explains very well why Fe, Co and Ni are ferromagnetic and several others are not. The calculated values of the $I$ and $N(E_F)$ for transition metals can be found

in [23]. It should be noted that the band structure calculations played a vitally important role in understanding itinerant electron magnetism [8]. The application of local spin density approximation (LSDA) in band theory has been remarkably successful in explaining ground state properties of transition metals and their alloys.

However, the Stoner model fails to reproduce the measured $T_C$ and the observed Curie-Weiss law above it. Calculated temperatures for $3d$ metals appeared to be too high compared with observations. Improvements to the Stoner model have been made that take into account the effect of spin fluctuations in a self consistent renormalized (SCR) way [16]. These studies built a bridge between two extreme limits of models (localized and itinerant) and unified them into one picture. In particular, these new theories have been very successful in describing several properties of weak itinerant ferromagnets.

### 2.1.1   Classical Heisenberg model for itinerant electrons

Although magnetic properties of $3d$ transition metals and their alloys are essentially defined by itinerant electrons, thermodynamic properties of such magnetic systems can quite often be quantitatively described by the Heisenberg model. This is because of the fact that in these systems the obtained Curie-Weiss susceptibility and observed temperature dependence of the magnetization show the main characteristics of local moment systems. Spin fluctuation theories show that only an effective classical Heisenberg model can be introduced for metals which provides a simple and accurate description of magnetism in these systems [16]. The procedure consists of mapping the complicated itinerant electron system onto an effective Heisenberg Hamiltonian with classical spins:

$$H_{\text{eff}} = -\sum_{i,j} J_{ij}\mathbf{e}_i\mathbf{e}_j \qquad (2.3)$$

where $J_{ij}$ is the effective exchange parameter and $\mathbf{e}_i$ is the unit vector pointing in the direction of the magnetic moment at site $i$. The values of magnetic moments are absorbed by the exchange parameter $J_{ij}$. The effective exchange interactions $J_{ij}$ between magnetic moments are determined from first-principles calculations.

Once the exchange parameters $J_{ij}$ are obtained, the spin dynamics and thermodynamic properties such as spin wave stiffness and Curie temperature can be determined from the effective Hamiltonian (2.3).

## 2.2   Origin of magnetism: Exchange interactions

In matter, magnetic moments are not usually free but interact with each other. These interactions result in a collective behavior of magnetic moments which manifest itself, below a critical temperature, by the onset of magnetic orders such as ferromagnetism or antiferromagnetism. Among the different interactions in magnetic systems only exchange interactions are

dominating and they are responsible for the microscopic magnetic behavior. It is thus of primary importance for determining the magnetic excitations and, hence, the Curie temperature of ferromagnetic systems.

The description of the fundamental features of the exchange interactions invokes a quantum mechanical approach, but their quantitative treatment is beyond the scope of this chapter. Loosely speaking, exchange is a combined effect of Pauli exclusion principle, electrostatic Coulomb repulsion and kinetic energy. Pauli exclusion principle keeps electrons with parallel spins apart, so reduces their Coulomb repulsion. The difference in energy between the parallel spin configuration and the antiparallel one is defined as the exchange energy. The magnetically ordered structures are the results of direct or indirect interactions between the local moments in sites or delocalized electronic moments in crystal. In the following we will briefly describe the three main exchange mechanisms which are most frequently observed in local moment systems.

- **Direct exchange**

This interaction is the direct consequence of the Pauli exclusion principle and depends strongly on the overlap of the participating wave functions (see Fig.). For small interatomic distances, antiferromagnetic coupling occurs (Cr and Mn). With increasing distance, ferromagnetic state becomes favorable (Fe, Co, Ni). For very large distances the coupling vanishes and paramagnetism is present [24].

- **RKKY exchange**

RKKY indirect exchange interaction (after Rudermann, Kittel, Kasuya and Yosida) takes over at distances beyond a few atomic spacings. It is mediated by the conduction electrons (s, p). A magnetic moment at site $i$ polarizes the s, p-electron gas and a second moment at site $j$ feels the induced polarization. This interaction starts out ferromagnetic at small distances and oscillates between negative and positive values with a period of $\lambda_F/2$, where $\lambda_F = 2\pi/k_F$ is the Fermi wavelength and $k_F$ is the Fermi wave-vector. In general the RKKY interaction gives rise to ferromagnetism if $k_F$ is small (nearly empty bands) and to antiferromagnetism when $k_F \sim \pi/a$ (half-filled band). This interaction can lead to long period magnetic structures (helimagnets, etc), that can be incommensurate with the lattice spacing.

This same mechanism is also responsible for the oscillatory interlayer exchange coupling in GMR structures [25, 26] and coupling of $4f$ electrons in rare earth elements. Furthermore the physics of spin glasses is discussed within the same context.

- **Superexchange**

In most of the magnetic insulators such as MnO, the magnetic atoms separated by diamagnetic atoms. Thus the magnetic ions are situated at distances too far for their $3d$ wave
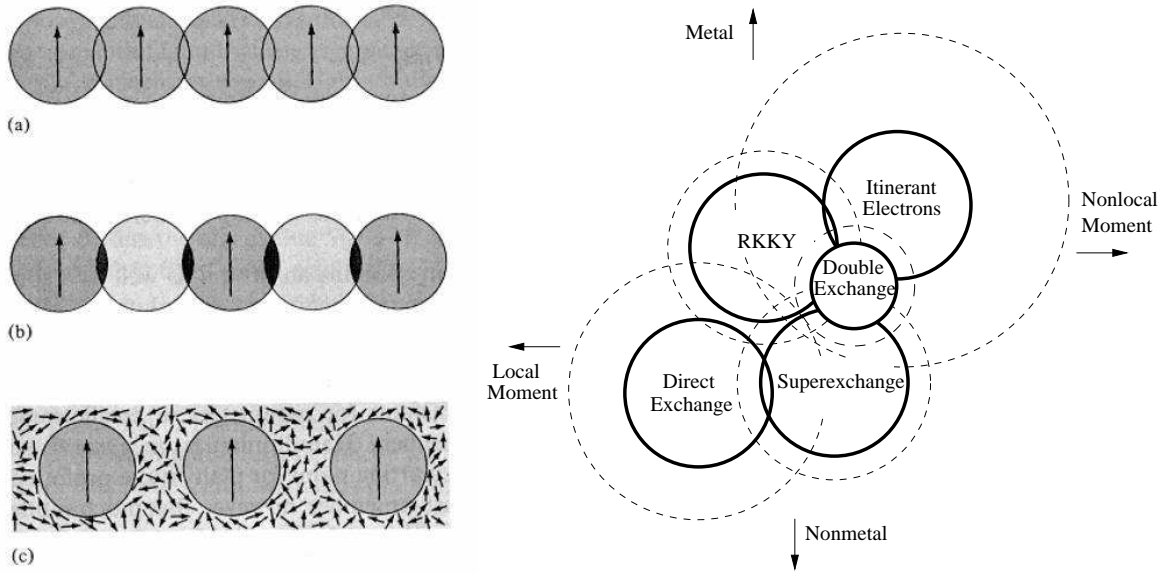
Figure 2.1: Left panel: Schematic illustrations of possible coupling mechanisms between localized magnetic moments: (a) direct exchange between neighboring atoms, (b) superexchange mediated by non-magnetic ions, and (c) indirect exchange mediated by the conduction electrons [27]. Right panel: The relationship among five exchange interactions [28].

functions to overlap and exchange interactions are mediated by the diamagnetic atoms, i.e, trough the overlap of $3d$ and $p$ wave functions. The value and sign of the this exchange (or so-called superexchange) interaction depend strongly on the types of $3d$ orbitals ($e_g$ or $t_{2g}$) involved, the number of electrons and also the angle Mn-O-Mn. This complex mechanism can initiate ferro- and antiferromagnetic coupling character. Finally, this interaction is effective only over short distances.

In left part of Fig. 2.1 we present the schematic representation of the these three main exchange mechanisms between localized moments. In addition to them there are also other mechanism which appear depending on whether the materials are insulators or metals and on which magnetic atoms (rare earths or transition metals) are involved such as double exchange and the exchange between the itinerant electrons. The most complicated situation is seen in $3d$ transition metals. In this systems $3d$ electrons are partly delocalized into the Fermi sea and partly localized around atomic sites. Furthermore, these two aspects can not be distinguished completely, and this is related to correlated features of the $3d$ electrons in these systems.

All these exchange interactions contribute to formation of diverse magnetically ordered structures through cooperative phenomena for macroscopic magnetism. Although these five kinds of exchange mechanisms were proposed for different cases and have been applied to various circumstances appropriately, there are no clear borderlines between them [28]. They are related to each other, and there are overlaps of their regions of applications. In right part of Fig. 2.1 we present the relationship between these five exchange interactions. The solid

circles represent the main region of application for each type of interaction, while the dashed circles indicates enlarged regions of applications. In fact in real systems it is possible that there are several exchange interactions which coexist and are mixed together.

Empirical values of the exchange interactions for various ferromagnetic metals have been calculated from specific heat measurements and from spin-wave spectra, whereas theoretical estimation of them have been one of the long standing and challenging problems in magnetism. Early attempts to calculate exchange integrals based on model Hamiltonian approaches resulted in unsatisfactory and even wrong results in some $3d$ systems [24]. For a quantitative study of magnetism and exchange interactions in solids the detailed consideration of electronic structure is necessary and should be introduced into the magnetic theory. This becomes possible with the recent developments of novel methods based on the results of numerical calculations of the electronic structure of solids [29]. Pioneering work in this field has been done mainly by two groups: the Russian group of Gubanov, Lichtenstein and others and Kübler and coworkers (Darmstadt) [8].

## 2.3   First-principles calculation of the exchange interactions

As mentioned in preceding section first-principles methods are the only way of obtaining exchange interactions in realistic systems. There are basically two different approaches, both rely on the adiabatic approximation in which the precession of the magnetization due to a spin-wave is neglected when calculating associated change of electronic energy. This approximation is valid under the conditions that the precession time of the magnetization should be large as compared to characteristic times of electronic motion, i.e., hopping time of an electron from a given site to a neighboring one and the precession time of the spin of an electron subject to the external field. Put differently, the spin-wave energies should be small as compared to the band with and exchange splitting. This is well justified for $3d$ systems (except Ni) and $4f$ rare earth elements. In principle, this approximation becomes exact in the limit of long wavelength magnons.

- **Real-space method**

Real-space approach was introduced by Liechtenstein *et al.,* in 1987 for the calculation of interatomic exchange interactions from first-principles [30]. It is based on multiple-scattering theory and employs the magnetic force theorem to calculate the energy change associated with a constrained rotation of the magnetic moments at sites $i$ and site $j$ (see Eq. (2.3)). The energy change can then be related to the exchange interactions as

$$J_{ij} = \frac{1}{4\pi} \int^{E_F} dE \, \text{Im} \, \text{Tr}_L (\Delta_i \hat{T}_\uparrow^{ij} \Delta_j \hat{T}_\downarrow^{ji}) \qquad (2.4)$$

This formula gives the expression for the pair exchange interaction parameter in the classical Heisenberg model (2.3). However, this approach has not been used in our calculations.

- **Frozen-magnon method**

In contrast to real space approach frozen-magnon approach is a reciprocal space method [31]. It is based on the total energy calculation for spiral magnetic configurations. With the help of the generalized Bloch theorem discussed in preceding chapter such calculations can be performed very efficiently without resorting to large super-cells. Additional help is provided by the force theorem that allows to use band energy of non-self-consistent frozen magnon states for the estimation of the total-energy differences. The following subsection is devoted to the discussion of frozen-magnon method for the case of multi-sublattice Heisenberg Hamiltonian.

The real-space and frozen-magnon methods are formally equivalent and complementary to each other. The quantities that are directly calculated are the $J_{ij}$ and $E(\mathbf{q})$ in the former case and in the latter case, respectively. They are also related to each other by a Fourier transformation. A detailed discussion on the comparison of both methods can be found in Ref.[32].

### 2.3.1 Frozen-magnon method for multi-sublattice systems

Let us consider the following classical multi-sublattice Heisenberg Hamiltonian

$$H_{eff} = -\sum_{\mu,\nu} \sum_{\substack{\mathbf{R},\mathbf{R}' \\ (\mu\mathbf{R}\neq\nu\mathbf{R}')}} J_{\mathbf{R}\mathbf{R}'}^{\mu\nu} \mathbf{s}_{\mathbf{R}}^{\mu} \mathbf{s}_{\mathbf{R}'}^{\nu} \tag{2.5}$$

In Eq.(2.5), the indices $\mu$ and $\nu$ number different sublattices and $\mathbf{R}$ and $\mathbf{R}'$ are the lattice vectors specifying the atoms within sublattices, $\mathbf{s}_{\mathbf{R}}^{\mu}$ is the unit vector pointing in the direction of the magnetic moment at site $(\mu, \mathbf{R})$.

Calculate interatomic Heisenberg exchange parameters involve few steps within frozen-magnon technique. In the first step, the exchange parameters between the atoms of a given sublattice $\mu$ are computed. The calculation is based on the evaluation of the energy of the frozen–magnon configurations defined by the following atomic polar and azimuthal angles

$$\theta_{\mathbf{R}}^{\mu} = \theta, \ \ \phi_{\mathbf{R}}^{\mu} = \mathbf{q} \cdot \mathbf{R} + \phi^{\mu}. \tag{2.6}$$

In the calculation discussed in this paper the constant phase $\phi^{\mu}$ is always chosen equal to zero. The magnetic moments of all other sublattices are kept parallel to the z axis. Within the Heisenberg model (**??**) the energy of such configuration takes the form

$$E^{\mu\mu}(\theta, \mathbf{q}) = E_0^{\mu\mu}(\theta) + \sin^2\theta J^{\mu\mu}(\mathbf{q}) \tag{2.7}$$

where $E_0^{\mu\mu}$ does not depend on $\mathbf{q}$ and the Fourier transform $J^{\mu\nu}(\mathbf{q})$ is defined by

$$J^{\mu\nu}(\mathbf{q}) = \sum_{\mathbf{R}} J_{0\mathbf{R}}^{\mu\nu} \exp(i\mathbf{q} \cdot \mathbf{R}). \tag{2.8}$$

$\phi_{\mathbf{R}}^{\mu} = \mathbf{q}.\mathbf{R} + \phi^{\mu}$ (a)

$\phi_{\mathbf{R}}^{\mu\nu} = \mathbf{q}.\mathbf{R} + \phi^{\mu\nu}$ (b)
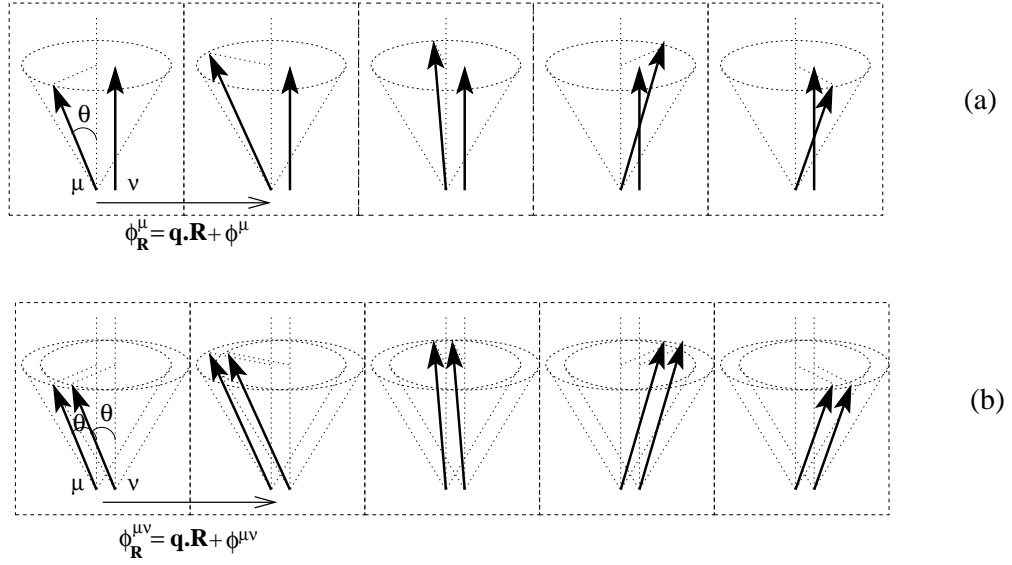
Figure 2.2: (a) Spin spiral to calculate intra-sublattice exchange interactions. (b) The same for inter-sublattice exchange interactions.

In the case of $\nu = \mu$ the sum in Eq. (2.8) does not include $\mathbf{R} = 0$. Calculating $E^{\mu\mu}(\theta, \mathbf{q})$ for a regular $\mathbf{q}$–mesh in the Brillouin zone of the crystal and performing back Fourier transformation one gets exchange parameters $J_{0\mathbf{R}}^{\mu\mu}$ for sublattice $\mu$.

To determine the exchange interactions between the atoms of two different sublattices $\mu$ and $\nu$ the frozen-magnon configurations (Eq. 2.6) are formed for both sublattices. The Heisenberg energy of such configurations takes the form

$$E^{\mu\nu}(\theta, \mathbf{q}) = E_0^{\mu\nu}(\theta) + \sin^2\theta \left[ J^{\mu\mu}(\mathbf{q}) + J^{\nu\nu}(\mathbf{q}) \right] + 2\sin^2\theta \, \mathrm{Re}J^{\mu\nu}(\mathbf{q}) \qquad (2.9)$$

where $E_0^{\mu\nu}(\theta)$ is a $\mathbf{q}$–independent part. Performing calculation of $[E^{\mu\nu}(\theta, \mathbf{q}) - E^{\mu\nu}(\theta, \mathbf{0})]$ and subtracting single-sublattice contributions known from the previous step one finds $[\mathrm{Re}J^{\mu\nu}(\mathbf{q}) - \mathrm{Re}J^{\mu\nu}(\mathbf{0})]$. The back Fourier transformation of this expression gives for $\mathbf{R} \neq 0$ the following combinations of the interatomic exchange parameters:

$$J_{\mathbf{R}}^{\mu\nu} \equiv \frac{1}{2}(J_{0\mathbf{R}}^{\mu\nu} + J_{0(-\mathbf{R})}^{\mu\nu}) \qquad (2.10)$$

$J_{\mathbf{R}}^{\mu\nu}$ does not contain information about the interaction of the atoms within the first unit cell corresponding to $\mathbf{R} = 0$. These exchange parameters can be found in a different way. For simplicity let assume that we have two magnetic atoms per unit cell. In this case we need at least two different magnetic configurations to calculate exchange interactions between these atoms. (see figure 2). The energies of such configurations is expressed as follows.

$$E^I(0, \mathbf{0}) = E_0 - 2J_0^{\mu\nu} \qquad (2.11)$$

$$E^{II}(\theta, \mathbf{0}) = E_0 - 2\cos\theta J_0^{\mu\nu} \qquad (2.12)$$
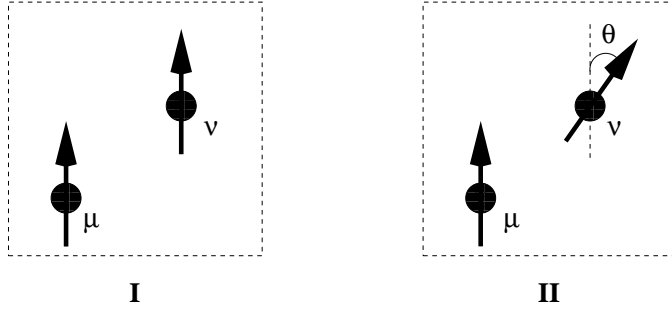
Figure 2.3: Magnetic moment configurations for the calculation of inter-sublattice exchange interactions.

where $J_0^{\mu\nu} = \sum_{\mathbf{R}} J_{0\mathbf{R}}^{\mu\nu}$. From Eqs. (2.11) and (2.12) one gets for $J_0^{\mu\nu}$

$$J_0^{\mu\nu} = \frac{E^I(0,\mathbf{0}) - E^{II}(\theta,\mathbf{0})}{2(1-\cos\theta)} \tag{2.13}$$

Combining Eq. (2.13 with the sum $\sum_{\mathbf{R}\neq 0} J_{0\mathbf{R}}^{\mu\nu}$ which is known from the preceding step one can access the parameters with $\mathbf{R} = 0$.

If one interested in estimation of the Curie temperature in mean field approximation the above procedure of obtaining inter-sublattice exchange interactions greatly simplifies the calculations. If there are $n$ magnetic atoms per unit cell then the number of different magnetic configurations required for estimation of intersublattice exchange parameters becomes

$$\frac{n(n-1)}{2} + 1 = \begin{cases} 2, & n = 2 \\ 4, & n = 3 \\ 7, & n = 4 \end{cases} \tag{2.14}$$

As it seen from the Eq. (2.14) the number of different configurations scale as $\sim \frac{n^2}{2}$ with number of magnetic atoms per unit cell. This requires few configurations for Heusler alloys with two or three magnetic atoms per unit cell studied in this thesis. However, the intra-sublattice exchange interactions should be obtained from the usual procedure.

# Chapter 3

# Magnetism at Finite Temperatures

## 3.1 Introduction

The study of the temperature dependence of the magnetic properties of itinerant ferromagnets is one of the fundamental problems of ongoing researches. Although density functional theory has been very successful in description of the ground-state properties of the magnetic systems, at finite temperatures it becomes rather difficult to calculate these properties from DFT, particularly the Curie and the Néel temperatures. These difficulties are mainly related to the Stoner picture of the magnetism in itinerant systems. Since the Stoner theory assumes that the magnetic moment gradually decreases with temperature, i.e., by means of spin-flip excitations across the Stoner gap $\Delta$ (see next section) and vanishes above $T_C$ (see Fig. 3.2). This process costs more energy than is actually needed to disorder magnetic moments and because of that the calculated values of $T_C$ for $3d$ transition metals (Fe, Co and Ni) are much higher than the experimental ones. There are also other weakness of the Stoner theory. For instance the behavior of magnetization at low temperatures and the Curie-Weiss behavior of the paramagnetic susceptibility cannot be described within the Stoner picture. Also the observed short range order above $T_C$ from neutron scattering experiments is not explainable within this picture.

On the other hand, the Heisenberg local moment model provides a better description of magnetism in itinerant systems at finite temperatures in spite of its failure at zero temperature in producing non-integer values of magnetic moments in $3d$ systems. In contrast to Stoner model, this model assumes that a magnetic moment on each atom that persists beyond $T_C$ and the magnetization vanishes by orienting the moments at random in the paramagnetic phase. The energy of these transverse fluctuations is smaller than the energy of the Stoner particle-hole transitions and they play a dominant role in the temperature behavior of an itinerant magnet. Within this model, not only the observed reduction of magnetization at low temperatures but also the Curie-Weiss behavior of the paramagnetic susceptibility of majority of ferromagnets are well described. In fact, Heisenberg model is well suited for systems with large exchange splitting like $3d$ transition metals and their alloys and rear
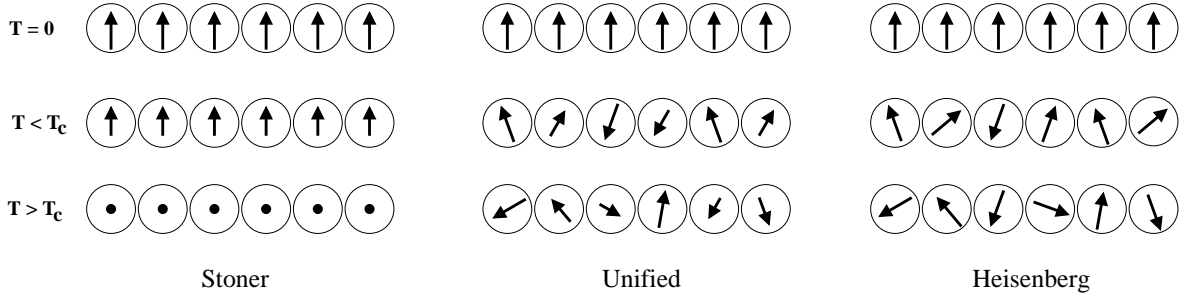
Figure 3.1: Comparison of the Stoner, Heisenberg and unified models.

earth elements where the spin-waves play a dominant role in a broad temperature interval in the thermodynamic properties.

In spite of the success of the Heisenberg model in description of finite temperature properties in broad classes of ferromagnets, there are some systems like weak ferromagnet $ZrZn_2$ which shows peculiar magnetic behavior at finite temperatures. This behavior can not be explained on the basis of either Stoner model or Heisenberg model and require the formulation of a more realistic model (unified theory), which combines the both models. A discussion and application of this approach is beyond the scope of this work.

In this thesis we will adopt the Heisenberg local moment picture in treatment of the finite temperature properties of the studied systems, i.e., Heusler alloys and subsequent interpretation of the obtained results. This means that Stoner excitations will be completely neglected. The use of Heisenberg model for these systems is well justified since they are considered to be the best local moment systems, where the electrons are itinerant, on the basis of experimental and theoretical information available.

## 3.2 Magnetic excitations

Temperature dependent properties of ferromagnets are governed by the magnetic excitations. At low temperatures spin-waves play an important role while with increasing temperature Stoner excitations become important.

- **Stoner excitations**

The fundamental single-particle excitations (or Stoner excitations) is a transition between bands of opposite spin. An electron is excited from an occupied state of the majority-spin band to an empty state of the minority-spin band and creates an electron-hole pair of triplet spin. It requires a minimum energy $\Delta$ in ferromagnets with a filled majority spin band, such as Co and Ni (strong ferromagnets). These excitations are associated with longitudinal fluctuations of the magnetization and play an important role in determination of high temperature properties of ferromagnets with small exchange splitting like Ni.
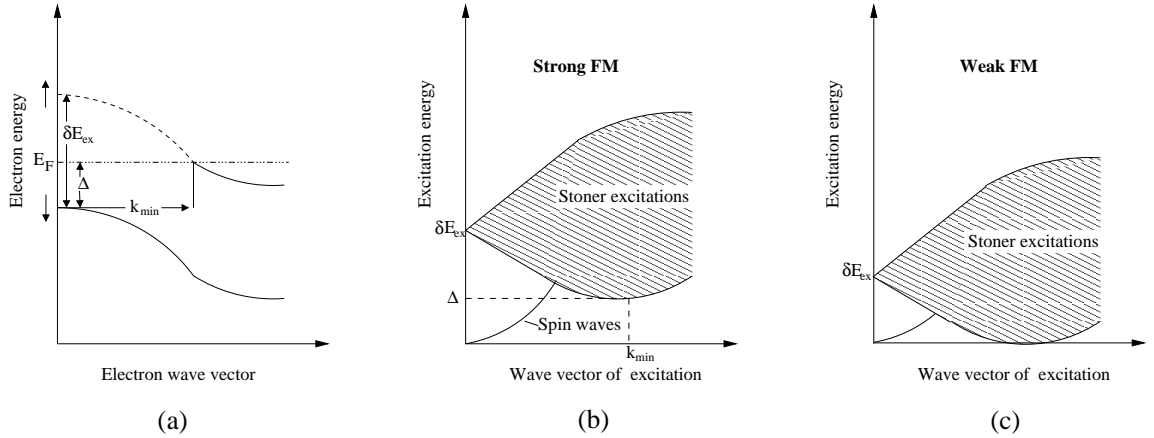
Figure 3.2: Magnetic excitations (a) Spin-split bands crossing the Fermi level in a strong ferromagnet. A spin flip can occur via a single electron excitation by lifting an electron from the majority band into the unoccupied part of the minority band (- - - ). Such excitations require a minimum energy transfer equal to the Stoner gap $\Delta$. (b) and (c) Schematic $E(\mathbf{q})$ diagram of magnetic excitations for strong and weak ferromagnets, respectively. One can distinguish between single-electron (Stoner) excitations and many-electron excitations (magnons) [33].

- **Spin waves or magnons**

The low temperature properties of ferromagnets are completely governed by the spin waves or magnons. These excitations correspond to collective transverse fluctuations of the direction of the magnetization. They start out with a parabolic $E(\mathbf{q})$ dispersion at $\mathbf{q} = 0$ and broaden out when they begin to overlap with single-particle excitations above the Stoner gap $\Delta$. At low temperatures they give rise to $T^{2/3}$ Bloch law for the reduction of the magnetization. For calculational purposes it is a good approximation to neglect the Stoner excitations up to the Curie temperature and to estimate the latter considering only spin-waves in ferromagnets with large exchange splitting. However, this is less justified for Ni that has a small exchange splitting.

## 3.3 Estimation of the Curie temperature

The discussion of the estimation of the Curie temperature will be based on two different statistical mechanics approaches to the Heisenberg Hamiltonian with exchange parameters calculated within a parameter-free DFT: mean-field (MF) and random phase approximation (RPA). RPA provides a quantitative description for the behavior of the magnetization in whole temperature interval while MFA captures qualitative features in this interval.

### 3.3.1   Mean field approximation

The finite temperature properties of magnetic systems and the phase transition temperature $T_C$ are first studied within mean-field theories. In 1907 Weiss proposed a phenomenological mechanism leading to the ferromagnetic ordering in $3d$ transition metals [18]. This approach is based on the assumption that each spin interacts with the same effective magnetic field created by all other spins. The interpretation of this phenomenological mechanism in terms of microscopic quantum models appears later with the work of Heisenberg. Due to its simplicity mean-field approximation is widely used. It usually yields qualitatively correct results, and provides insight into the nature of the magnetic phase transitions.

To illustrate the mean-field approximation let us consider following Heisenberg Hamiltonian with one magnetic atom per unit cell

$$H = -\frac{1}{S^2} \sum_{ij} J_{ij} \hat{\mathbf{S}}_i \hat{\mathbf{S}}_j - g\mu_B B \sum_i \hat{S}_i^z \tag{3.1}$$

where $\hat{\mathbf{S}}_i = (\hat{S}_i^x, \hat{S}_i^y, \hat{S}_i^z)$ and normalization factor $S^2$ is introduced to ensure that exchange parameters $J_{ij}$ are spin independent.

The partition function of the system in magnetic field $B$ is

$$Z = \text{Tr}[e^{-H/k_B T}] \tag{3.2}$$

where Tr stands for sum over all spin quantum numbers.

Without exchange couplings $J_{ij}$ one would have independent spins, each polarized by the magnetic field as

$$\frac{\langle \hat{S}_i^z \rangle}{S} = \frac{\text{Tr}[\hat{S}_i^z e^{-g\mu_B B \sum_i \hat{S}_i^z / k_B T}]}{S\,\text{Tr}[e^{-g\mu_B B \sum_i \hat{S}_i^z / k_B T}]} \tag{3.3}$$

But with the exchange couplings the problems becomes more complicated and can not be solved exactly. Instead we have to use approximations and the simplest approximation is the mean-field approximation. The central idea behind the mean-field approach is to approximate the interacting problem by a simpler interacting partition function. In this case each spin experiences an average field of many spins, and thus we can replace spin-spin interaction by an interaction of each spin with an average magnetization of spins around it.

With $\hat{\mathbf{S}}_i = (\hat{\mathbf{S}}_i - \langle \hat{\mathbf{S}}_i \rangle) + \langle \hat{\mathbf{S}}_i \rangle$ the product $\hat{\mathbf{S}}_i \hat{\mathbf{S}}_j$ in Hamiltonian becomes

$$\hat{\mathbf{S}}_i \hat{\mathbf{S}}_j = [(\hat{\mathbf{S}}_i - \langle \hat{\mathbf{S}}_i \rangle) + \langle \hat{\mathbf{S}}_i \rangle][(\hat{\mathbf{S}}_j - \langle \hat{\mathbf{S}}_j \rangle) + \langle \hat{\mathbf{S}}_j \rangle] \tag{3.4}$$

Expanding this to first order in the deviations $\delta \hat{\mathbf{S}}_i = \hat{\mathbf{S}}_i - \langle \hat{\mathbf{S}}_i \rangle$

$$\langle \hat{\mathbf{S}}_i \rangle \langle \hat{\mathbf{S}}_j \rangle + \langle \hat{\mathbf{S}}_j \rangle [\hat{\mathbf{S}}_i - \langle \hat{\mathbf{S}}_i \rangle] + \langle \hat{\mathbf{S}}_i \rangle [\hat{\mathbf{S}}_j - \langle \hat{\mathbf{S}}_j \rangle] + O(\delta \hat{\mathbf{S}}_i^2) \tag{3.5}$$

With this simplification our mean-field Hamiltonian becomes

$$\begin{aligned} H_{MF} &= -\frac{2}{S^2} \sum_{ij} J_{ij} \hat{\mathbf{S}}_i \langle \hat{\mathbf{S}}_j \rangle + \frac{1}{S^2} \sum_{ij} J_{ij} \langle \hat{\mathbf{S}}_i \rangle \langle \hat{\mathbf{S}}_j \rangle - g\mu_B B \sum_i \hat{S}_i^z \\ &= -\frac{2J_0 m + g\mu_B B S}{S} \sum_i \hat{S}_i^z + J_0 N m^2 \end{aligned} \tag{3.6}$$

where $J_0 = \sum_j J_{0j}$, $m = \langle \hat{S}_i^z \rangle / S$ and $N$ is the total number of sites. For the second part of Eq. (3.6) we assumed that $\langle \hat{\mathbf{S}}_i \rangle = \langle \hat{\mathbf{S}}_j \rangle$ in the lattice. The terms ignored in Eq. (3.6) correspond to correlation of the spins. This maybe questionable when interactions are nearest neighbor.In three dimensional systems for long range exchange interactions and for the lattices like fcc, due to a large number of interacting spins and the central limit theorem, the replacement of a sum of fluctuating spin variables by its average value is a reasonable approximation.

Using Eq. (3.3) one can calculate temperature dependence of the magnetization as

$$m(T) = \frac{\langle \hat{S}_i^z \rangle}{S} = \frac{\mathrm{Tr}[\hat{S}_i^z e^{-H_{MF}/k_B T}]}{S \mathrm{Tr}[e^{-H_{MF}/k_B T}]} = \frac{\mathrm{Tr}[\hat{S}_i^z e^{(-2J_0 m + g m_B BS)\hat{S}_i^z / Sk_B T}]}{S \mathrm{Tr}[e^{(-2J_0 m + g m_B BS)\hat{S}_i^z / Sk_B T}]} \tag{3.7}$$

In Eq. (3.7) the trace is a sum of all spin quantum numbers $\sum_{l=-S}^{S}$ so that

$$
\begin{aligned}
m(T) &= \frac{\sum_{l=-S}^{S} l e^{(-2J_0 m + g m_B BS)l/Sk_B T}}{S \sum_{l=-S}^{S} e^{(-2J_0 m + g m_B BS)l/Sk_B T}} \\
&= \frac{2S+1}{2S} \coth \frac{[(2S+1)(2J_0 m + g m_B BS)]}{2Sk_B T} - \frac{1}{2S} \coth \frac{(2J_0 m + g m_B BS)}{2Sk_B T} \\
&= B_S[(2J_0 m + g m_B BS)/k_B T]
\end{aligned} \tag{3.8}
$$

Here $B_S(x)$ is called Brillouin function. For $S = 1/2$ it is reduced to a simple form $B_{1/2}(x) = \tanh(x)$. Eq. (3.8) allows us to calculate temperature dependence of the magnetization. It is a self-consistent equation because the unknown variable $m(T)$ is on both sides of the equation.

Near $T_C$ where $m(T)$ is small the Brillouin function can be expanded,

$$B_S(x) = \frac{S(S+1)}{3S} x + O(x^3) \tag{3.9}$$

From Eq. (3.9) $T_C$ can be obtained as

$$T_C = \frac{2(S+1)J_0}{3S} \tag{3.10}$$

So far we have only considered quantum mechanical spins, the obtained formulas can easily be generalized to the classical limit. In this case $S \to \infty$ the Brillouin function reduces to Langevin function

$$L(x) = \coth(x) - \frac{1}{x} \tag{3.11}$$

and $T_c$ is given as follows

$$T_C = \frac{2J_0}{3} \tag{3.12}$$

As it is seen from Eqs. (3.10) and (3.12) $T_C$ in mean-field approximation is proportional to the on-site exchange parameter $J_0$ and does not depend on dimension of the system or crystal structure. These are the main disadvantages of the mean-field approach. However, in three dimensions MFA captures correctly all qualitative features of the magnetic phase transitions

and it gives numerically accurate results for the Curie temperature in systems with long range exchange interactions or large number of interacting neighbors like fcc lattice.

The above mean field formalism can easily be generalized to multi-sublattice systems. In this case one has to solve the system of coupled equations by the same way as one atom per unit cell. Here we only consider the calculation of Curie temperature in classical limit. The $T_C$ can be estimated by solving the system of coupled equations [34]

$$\langle S_\mu^z \rangle = \frac{2}{3k_B T} \sum_\nu J_0^{\mu\nu} \langle S_\nu^z \rangle \tag{3.13}$$

where $\langle S_\nu^z \rangle$ is the average $z$ component of $\mathbf{S}_\nu$. Eq.(3.13) can be represented in the form of eigenvalue matrix problem

$$(\Theta - T\mathbf{I})\mathbf{S} = 0 \tag{3.14}$$

where $\Theta_{\mu\nu} = \frac{2}{3k_B} J_0^{\mu\nu}$, $\mathbf{I}$ is a unit matrix and $\mathbf{S}$ is the vector of $\langle S_\nu^z \rangle$. The largest eigenvalue of matrix $\Theta$ gives the value of Curie temperature. [34]

### 3.3.2 Random phase approximation for multi-sublattice Heisenberg model

In this section we will go beyond the mean-field theory and calculate temperature dependence of the magnetization of a multi-sublattice Heisenberg model using Green function method within Tyablikov decoupling scheme. Tyablikov proposed a method of approximation for the Heisenberg model by suggesting a decoupling in the higher-order Green functions derived within the equation of motion method [35]. In contrast to the mean field approximation Tyablikov method takes properly into account the collective excitations (spin waves) and allows a reliable calculation of magnetization over the entire range of temperature of interest.

We start with the Heisenberg Hamiltonian for quantum spins neglecting the Zeeman energy

$$H = -\sum_{ij} \sum_{\mu\nu} J_{ij}^{\mu\nu} \mathbf{e}_{i,\mu} \mathbf{e}_{j,\nu} \tag{3.15}$$

where $\mathbf{e}_{i,\mu} = (\hat{s}_{i,\mu}^x, \hat{s}_{i,\mu}^y, \hat{s}_{i,\mu}^z)/(S_\mu)$ is the normalized spin operator corresponding to site $(i, \mu)$.

In terms of the creation and destruction operators $\hat{s}_{i,\mu}^{\mp} = \hat{s}_{i,\mu}^x \mp \hat{s}_{i,\mu}^y$ the Hamiltonian can be written in the form

$$H = -\sum_{ij} \sum_{\mu\nu} \tilde{J}_{ij}^{\mu\nu} [\hat{s}_{i,\mu}^+ \hat{s}_{j,\nu}^- + \hat{s}_{i,\mu}^z \hat{s}_{j,\nu}^z] \tag{3.16}$$

where $\tilde{J}_{ij}^{\mu\nu} = J_{ij}^{\mu\nu}/S_\mu S_\nu$.

Following Callen [36] let us introduce Green function

$$G_{ij}^{\mu\nu}(\tau) = -\frac{i}{\hbar}\theta(\tau)\langle [\hat{s}_{i,\mu}^+(\tau), \exp(\eta \hat{s}_{j,\nu}^z)\hat{s}_{j,\nu}^-]\rangle \tag{3.17}$$

where $\eta$ is a parameter, $\theta(\tau)$ is the step function ($\theta(\tau) = 1$ for $\tau \geq 0$), [...] denotes the commutator and $\langle \ldots \rangle$ is the thermal average over the canonical ensemble, ie., $\langle F \rangle = \text{Tr}[\exp(-\beta H)F]/\text{Tr}[\exp(-\beta H)]$ with $\beta = 1/k_B T$

In order to evaluate the problem we employ the equation of motion method. Writing the equation of motion for $G_{ij}^{\mu\nu}(\tau)$ we obtain

$$
\frac{\partial}{\partial\tau}G_{ij}^{\mu\nu}(\tau) = -\frac{i}{h}\delta(\tau)\langle[\hat{s}_{i,\mu}^{+}(\tau),\exp(\eta\hat{s}_{j,\nu}^{z})\hat{s}_{j,\nu}^{-}]\rangle - \frac{1}{\hbar^2}\theta(\tau)
$$
$$
\times\langle[[\hat{s}_{i,\mu}^{+}(\tau),\hat{H}],\exp(\eta\hat{s}_{j,\nu}^{z})\hat{s}_{j,\nu}^{-}]\rangle \tag{3.18}
$$

The last commutator term in Eq. (3.18) generates higher-order Green functions. These functions must be decoupled in order to make the problem numerically and analytically tractable. This is done using the Tyablikov decoupling (random phase approximation) scheme [35]. In the Tyablikov decoupling scheme $\hat{s}_{k,\mu}^{z}$ is separated from the spin-flip operators $\hat{s}_{i,\mu}^{\pm}$ in the high-order Green function via the substitution

$$
\langle[\hat{s}_{i,\mu}^{+}(\tau)\hat{s}_{k,\mu}^{z},\hat{s}_{j,\nu}^{-}]\rangle \approx \langle\hat{s}_{k,\mu}^{z}\rangle\langle[\hat{s}_{i,\mu}^{+}(\tau),\hat{s}_{j,\nu}^{-}]\rangle \tag{3.19}
$$

One then arrives at the equation

$$
\frac{\partial}{\partial\tau}G_{ij}^{\mu\nu}(\tau) = -\frac{i}{h}\delta(\tau)\langle[\hat{s}_{i,\mu}^{+}(\tau),\exp(\eta\hat{s}_{j,\nu}^{z})\hat{s}_{j,\nu}^{-}]\rangle + \frac{2i}{\hbar}\sum_{k,\xi}\tilde{J}_{i,k}^{\mu\xi}[\langle\hat{s}_{i,\mu}^{z}\rangle G_{kj}^{\xi\nu}(\tau)
$$
$$
-\langle\hat{s}_{k,\xi}^{z}\rangle G_{ij}^{\mu\nu}(\tau)] \tag{3.20}
$$

Eq. (3.20) can be solved for the Green function in momentum space with the standard Fourier transformation

$$
g_{\mu\nu}(\mathbf{q},\omega) = \frac{1}{2\pi}\sum_{i,j}\int d\omega\, e^{-i\mathbf{q}(\mathbf{R}_i-\mathbf{R}_j)}G_{ij}^{\mu\nu}(\tau) \tag{3.21}
$$

Thus we arrive at the expression

$$
\hbar\omega g_{\mu\nu}(\mathbf{q},\omega) = \frac{1}{2\pi}\langle[\hat{s}_{\mu}^{+},\exp(\eta\hat{s}_{\nu}^{z})\hat{s}_{\nu}^{-}]\rangle\delta_{\mu\nu} - 2\sum_{\xi}\{\tilde{J}_{\mu\xi}(\mathbf{q})\langle\hat{s}_{i,\mu}^{z}\rangle g_{\xi\nu}(\mathbf{q},\omega)
$$
$$
-\tilde{J}_{\mu\xi}(\mathbf{0})\langle\hat{s}_{k,\xi}^{z}\rangle g_{\mu\nu}(\mathbf{q},\omega)\} \tag{3.22}
$$

Eq. (3.22) can be written in a compact matrix form

$$
[\hbar\omega\mathbf{I} - \mathbf{M}(\mathbf{q})]\mathbf{g}(\mathbf{q},\omega) = \mathbf{u} \tag{3.23}
$$

where $\mathbf{g}(\mathbf{q},\omega)$ is a symmetric square matrix, $\mathbf{I}$ is a unit matrix and the inhomogeneity matrix $\mathbf{u}$ is expressed by

$$
u_{\mu\nu} = \frac{1}{2\pi}\langle[\hat{s}_{\mu}^{+},\exp(\eta\hat{s}_{\nu}^{z})\hat{s}_{\nu}^{-}]\rangle\delta_{\mu\nu}, \tag{3.24}
$$

matrix $\mathbf{M}(\mathbf{q})$ is defined by

$$
M_{\mu\nu}(\mathbf{q}) = \left\{\sum_{\xi}2\tilde{J}_{\mu\xi}(\mathbf{0})\langle\hat{s}_{\xi}^{z}\rangle\right\}\delta_{\mu\nu} - 2\tilde{J}_{\mu\nu}(\mathbf{q})\langle\hat{s}_{\mu}^{z}\rangle \tag{3.25}
$$

Next, we introduce the transformation which diagonalizes matrix $\mathbf{M(q)}$:

$$\mathbf{L(q)M(q)R(q)} = \Omega(\mathbf{q}) \tag{3.26}$$

where $\Omega(\mathbf{q})$ is the diagonal matrix whose elements give the spin wave energies $\omega_\mu(\mathbf{q})$. The number of branches in the spin wave spectrum is equal to the number of magnetic atoms in the unit cell. The transformation matrix $\mathbf{R(q)}$ and its inverse $\mathbf{R}^{-1}(\mathbf{q}) = \mathbf{L(q)}$ are obtained from the right eigenvectors of $\mathbf{M(q)}$ as columns and from the left eigenvectors as rows, respectively.

Using the spectral theorem and Callen's technique [36] one obtains the thermal averages of the sublattice magnetizations:

$$\langle \hat{s}_\mu^z \rangle = \frac{(S_\mu - \Phi_\mu)(1 + \Phi_\mu)^{2S_\mu + 1} + (S_\mu + 1 + \Phi_\mu)\Phi_\mu^{2S_\mu + 1}}{(1 + \Phi_\mu)^{2S_\mu + 1} - (\Phi_\mu)^{2S_\mu + 1}} \tag{3.27}$$

where $\Phi_\mu$ is an auxiliary function given by

$$\Phi_\mu = \frac{1}{N} \sum_q \sum_\nu L_{\mu\nu}(\mathbf{q}) \frac{1}{e^{\beta\omega_\nu(\mathbf{q})} - 1} R_{\mu\nu}(\mathbf{q}) \tag{3.28}$$

In Eq. (3.28), $N$ is the number of $\mathbf{q}$ points in the first BZ. Furthermore, Eq. (3.27) can be expressed in terms of Brillouin function using Callen-Shtrikman theorem as follows

$$\langle \hat{s}_\mu^z \rangle = S_\mu B_{S_\mu} \left[ S_\mu \ln \left( \frac{1 + \Phi_\mu}{\Phi_\mu} \right) \right] \tag{3.29}$$

where $B_{S_\mu}$ is the Brillouin function.

Eq. (3.27) is the central equation for the calculation of the sublattice magnetizations. It must be solved self-consistently. The Curie temperature $T_C$ is determined as the point where all sublattice magnetizations vanish.

Near $T_C$ ($\Phi_\mu \to \infty$ and $\langle \hat{s}_\mu^z \rangle \to 0$) Eq. (3.27) can be simplified. Expanding in $\Phi_\mu$ and using Eq. (3.28) one obtains

$$\langle \hat{s}_\mu^z \rangle = \frac{(S_\mu + 1)}{3S_\mu} \left\{ \frac{1}{S_\mu^2 N} \sum_{q,\nu} L_{\mu\nu}(\mathbf{q}) \frac{1}{e^{\beta\omega_\nu(\mathbf{q})} - 1} R_{\mu\nu}(\mathbf{q}) \right\}^{-1}. \tag{3.30}$$

From Eq. (3.30), it follows that for spin-independent Heisenberg exchange parameters [Eq. (3.15)] the dependence of the Curie temperature on the spin value is defined by the factor $(S_\mu + 1)/S_\mu$.

The classical limit can be obtained by letting $S_\mu \to \infty$ in Eqs. (3.27) and (3.30). Factor $(S_\mu + 1)/S_\mu$ in Eq. (3.30) becomes in this case unity. The temperature dependence of the magnetization can be calculated using the Eq. (3.29) which is reduced to Langevin function for $S_\mu = \infty$

$$\langle e_\mu^z \rangle = \mathcal{L}\left( \left\{ \frac{1}{N} \sum_{q,\nu} L_{\mu\nu}(\mathbf{q}) \frac{1}{e^{\beta\omega_\nu(\mathbf{q})} - 1} R_{\mu\nu}(\mathbf{q}) \right\}^{-1} \right) \tag{3.31}$$

where $\mathcal{L}(x) = \coth(x) - 1/x$ is the Langevin function and $\mathbf{e}_\mu$ is the angular momentum vector of size one.

# Chapter 4

# Heusler Alloys: Experimental and Theoretical Background

## 4.1   Introduction

The discovery of Heusler alloys dates back to 1903 when Heusler reported that the addition of *sp* elements (Al, In, Sn, Sb or Bi) turn Cu-Mn alloy into a ferromagnetic material even though the alloy contains none of the ferromagnetic elements [37]. The basic understanding of crystal structure and composition of these alloys remained unknown for a long time. In 1929 X-ray measurements of Potter [38] on Cu-Mn-Al alloy revealed that all constituents of this system was ordered on an fcc super lattice. Bradley and Rodgers [39] investigated Cu-Mn-Al system in detail using X-ray and anomalous scattering. The authors established a relationship between composition, chemical order and magnetic properties. After complete understanding of crystal structure numerous investigations were made. It is found that the Heusler structure is formed essentially from the ordered combination of two binary B2 compounds XY and XZ. Both compounds may have the CsCl type crystal structure, for instance CoMn and CoAl yield $Co_2MnAl$. Thus the ability of compounds to form B2 structure indicates the possibility of forming new Heusler compounds. It was also discovered that it is possible to leave one of the four sublattices unoccupied ($C1_b$ structure). The latter compounds are often called half- or semi-Heusler alloys, while the $L2_1$ compounds are referred to as full-Heusler alloys. Extensive experimental studies showed that the majority of Heusler compounds order ferromagnetically in stoichiometric composition. Crystal structure, composition and heat treatment were found to be important parameters for determining magnetic properties.

With the discovery of half-metallic ferromagnetism in NiMnSb and the observation of shape memory effect in $Ni_2MnGa$ compound, Heusler alloys received tremendous experimental and theoretical interest. In this chapter we will briefly present the previous experimental and theoretical studies on structural and magnetic properties of Heusler alloys. Also, an overview of the experimental and theoretical studies on exchange coupling will be given.
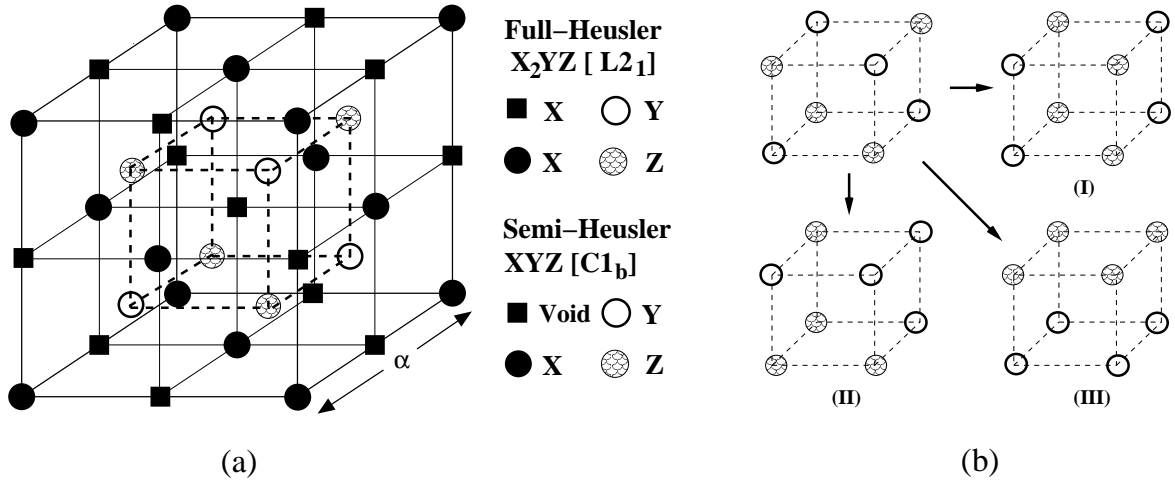
Figure 4.1: (a) $C1_b$ and $L2_1$ structures adapted by the half- and full-Heusler alloys. The lattice is consisted of 4 interpenetrating f.c.c. lattices. In the case of the half-Heusler alloys (XYZ) one of the four sublattices is vacant. Note also that if all atoms were identical, the lattice would be simply the bcc. (b) Three possible configuration of the occupation of Y and Z sublattices in B2-type disordered structure.

## 4.2 Structural properties

Heusler alloys are defined as the ternary intermetallic compounds. At the stoichiometric composition, full Heusler alloys ($X_2YZ$) and semi Heusler alloys (XYZ) crystallize in $L2_1$ and $C1_b$ structures (see figure4.1), respectively. The elements normally associated with the X, Y and Z are indicated in table1. The unit cell consists of four interpenetrating fcc sublattices with the positions (000) and $(\frac{1}{2}, \frac{1}{2}, \frac{1}{2})$ for X, $(\frac{1}{4}, \frac{1}{4}, \frac{1}{4})$ for Y and $(\frac{3}{4}, \frac{3}{4}, \frac{3}{4})$ for Z atom. The site $(\frac{1}{2}, \frac{1}{2}, \frac{1}{2})$ is vacant in semi Heusler compounds. The two structures are closely related with vacant cite. $C1_b$ structure can be obtained from $L2_1$ one by replacing the half of the X sites in an ordered manner. Consequently, the structure no longer centro-symmetric. In majority of the Heusler alloys Mn element enters as the Y element. The compounds where Mn assumes the X positions are very rare. Up to now, only two systems of this type were studied experimentally: $Mn_2VAl$ [40] and $Mn_2VGa$ [41].

At the stoichiometric composition, disorder can exist in the form of partial interchange of atoms in different sublattices. Johnston and Hall [42] proposed a single disordering parameter $\alpha$ to describe the effects of certain types of preferential disorder on the structure amplitudes of alloys of the type $X_2YZ$. For alloys ordered in $L2_1$ structure $\alpha$ is defined as the fraction of either Y or Z atoms being not on their correct sites. Partial occupation of Y and Z atoms on each others sublattices leads to $L2_1$-B2 type disorder. B2-type structure can be obtained by allowing half of the Y and Z atoms interchange their positions. The ratio of the $L2_1$/B2 depends on the heat treatments. Due to smaller interatomic distances in B2-type structure, an antiferromagnetic ordering becomes energetically favorable.

### 4.2.1 Martensitic phase transitions

At low temperatures several Heusler alloys, e.g. $Ni_2MnGa$, $Co_2NbSn$ etc., undergo a martensitic transition from a highly symmetric cubic austenitic to a low symmetry martensitic phase. Unlike atomic order-disorder transitions a martensitic transition is caused by non-diffusional cooperative movement of the atoms in the crystal [43]. It has been suggested that these transitions were driven by a band Jahn Teller mechanism [44] and there has not been any experimental evidence to confirm this conjecture for a long time. Recently the suggested model was confirmed by polarized neutron scattering experiments, where the transfer of magnetic moment from Mn to Ni was found in the martensitic phase of $Ni_2MnGa$ [45, 46].

In the case when the Heusler alloys are magnetic in the martensitic phase, they can exhibit the magnetic shape memory effect (MSM). This occurs especially when the Y constituent is Mn, but other transition elements are also possible. In these alloys, an external magnetic field can induce large strains when applied in the martensitic state. Extensive experimental and theoretical investigations of the martensitic phase transition in the ferromagnet $Ni_2MnGa$ have been made. This compound transforms martensitically at 202 K to a tetragonal structure below. There is a modulation of the (110) atomic planes with a periodicity of five atomic layers [50]. The transition is accompanied by a strong soft mode behavior in the transverse acoustic phonon branch with $\mathbf{q}$ along the [110] direction and polarization along [1-10] in the high-temperature phase. Below the transition the system becomes magnetically anisotropic. In the martensitic phase of $Ni_2MnGa$ an applied field of about 1 T can induce strains as large as 10% [47, 48]. The field induced strain is due to the reorientation of the tetragonal martensite variants by twin boundary motion [49].

## 4.3  Magnetic properties

Heusler alloys possess very interesting magnetic properties. One can study in the same family of alloys a series of interesting diverse magnetic phenomena like itinerant and localized magnetism, antiferromagnetism, helimagnetism, Pauli paramagnetism or heavy-fermionic behavior [50, 51, 52, 53].

### 4.3.1  Ferromagnets

The majority of the Heusler alloys order ferromagnetically and saturate in weak applied magnetic fields. If the magnetic moment is carried by Mn atoms, as it often is in the alloys $X_2MnZ$, a value close to $4\mu_B$ is usually observed. Although they are metals, these compounds have localized magnetic properties and are ideal model systems for studying the effects of both atomic disorder and changes in the electron concentration on magnetic properties.

In order to reveal the role of the $3d$ (X) and $sp$ (Z) atoms on magnetic properties of Heusler alloys extensive magnetic and other measurements have been performed on quaternary Heusler alloys [50]. It has been shown that $sp$ electron concentration is primarily

Table 4.1: Composition, magnetic order and crystal structure of Heusler alloys. The experimental information is taken from the reference [50].

| Y | X | Z | Magnetic order | Crystal structure |
|---|---|---|---|---|
| V | Mn | Al, Ga | FM* | L2$_1$ |
| | Fe | Al, Ga | FM | L2$_1$ |
| | Fe | Si | PM | L2$_1$ |
| | Co | Al, Ga, Sn | FM | L2$_1$ |
| Cr | Co | Al, Ga | FM | L2$_1$ |
| | Fe | Al, Ga | FM | L2$_1$ |
| Mn | Cu | Al, In, Sn | FM | L2$_1$ |
| | Cu | Sb | AFM | C1$_b$ |
| | Ni | Al | AFM | B2 |
| | Ni | Sb | FM | C1$_b$ |
| | Ni | Al, Ga, In, Sn, Sb | FM | L2$_1$ |
| | Co | Al, Si, Ga, Ge, Sn | FM | L2$_1$ |
| | Co | Sb | FM* | C1$_b$ |
| | Fe | Al, Si | FM | L2$_1$ |
| | Pd | Al | AFM | B2 |
| | Pd | In | AFM | L2$_1$-B2 |
| | Pd | Ge, Sn, Sb | FM | L2$_1$ |
| | Pd | Sb | FM | C1$_b$ |
| | Pd | Te | AFM | C1$_b$ |
| | Rh | Al, Ga, In | FM | B2 |
| | Rh | Ge, Sn, Pb | FM | L2$_1$ |
| | Rh | Sb | FM | C1$_b$ |
| | Ru | Ga | FM | C1$_b$ |
| | Au | Zn, Cu | AFM | B2 |
| | Au | Al, Ga, In | AFM | L2$_1$ |
| | Au | Sb | FM | C1$_b$ |
| | Pt | Al, Ga | AFM | L2$_1$ |
| | Pt | Ga | FM | C1$_b$ |
| | Ir | Al | AFM | L2$_1$ |
| | Ir | Ga | AFM | C1$_b$ |
| Fe | Fe | Al, Si | FM | D0$_3$ |
| | Co | Al, Si, Ga | FM | L2$_1$ |
| Co | Fe | Ga | FM | L2$_1$ |
| Ni | Fe | Al, Ga | PM | L2$_1$ |

FM*:Ferrimagnetic

important in establishing magnetic properties, influencing both the magnetic moment forma-
tion and the type of the magnetic order.

In table 4.1 we present magnetic Heusler alloys containing $3d$ transition metals (V, Cr,
Mn, Fe, Co, Ni) as the Y site and $3d$, $4d$ and $5d$ elements as the X site.

### 4.3.2 Antiferromagnets and ferrimagnets

Although the majority of Heusler alloys are ferromagnetic some of them order antiferro-
magnetically, in particular those compounds containing $3d$ element in which the magnetic
moment is only carried by Mn atoms at Y site. Experimentally antiferromagnetic order is
measured both in semi Heusler(in $C1_b$ structure) and in full Heusler alloys (in $L2_1$ and B2
structure). Antiferromagnetism is more favorable in full Heusler alloys which has B2-type
crystal structure due to smaller interatomic Mn-Mn distances. Indeed, antiferromagnetic be-
havior in several B2-type disordered $X_2MnZ$ (X=Ni, Pd; Z=Al, In) Heusler alloys has been
reported [50].

The situation is different in semi Heusler alloys. Due to large Mn-Mn distances in $C1_b$
structure the antiferromagnetic interaction between Mn atoms is assumed to be mediated
intermediate atoms (X or Z).

Ferrimagnetic ordering (antiferromagnetic coupling of X and Y atoms) is very rare in
Heusler alloys compared to ferromagnetic or antiferromagnetic one. Ferrimagnetism has been
detected [50] only in CoMnSb, Mn2VAl and $Mn_2VGa$ compounds. $Mn_2VAl$ received much
experimental attention. The neutron diffraction experiment gave the ferrimagnetic state of
compound with Mn magnetic moment of $1.5 \pm 0.3\mu_B$ and V moment $-0.9\mu_B$ [40].

### 4.3.3 Localized versus itinerant magnetism

Metals exhibiting local moment behavior are usually alloys and they are classified as dis-
ordered and ordered systems. Disordered alloys like Fe impurities in Cu or Ag have been
intensively studied during the last four decades and a variety of magnetic behavior has been
observed. Heusler alloys fall into the category of ordered systems. In these systems atoms car-
rying the magnetic moments are separated by other (usually non-magnetic) atoms and they
are believed to carry well-defined local moments. The manganese moment, which is usually
close to $4\mu_B$, remains fixed in amplitude when going from the ordered to the paramagnetic
state. The formation of local moments in Heusler alloys will be discussed below.

A qualitative evidence for the localized magnetic behavior can be obtained by comparing
ground state magnetic moment $p_0$ with that extracted from the slope of the Curie-Weiss
reciprocal susceptibility curve, i.e., $p_{eff} = \sqrt{p(p + 2\mu_B)}$. A ratio $p/p_0 \sim 1$ is expected for
localized systems whereas for itinerant magnetism a ratio greater than 1 is expected. This
allows one to analyze different mechanism for magnetic order. Indeed, a ratio close to one is
obtained in several Heusler alloys [50] which reveals the nature of magnetism in these systems
at least roughly.

The most direct quantitative evidence for localized magnetic behavior is provided by neutron scattering data. Measurements on $Pd_2MnSn$, $Ni_2MnSn$, $Cu_2MnAl$ and $Pd_2MnIn_{1-x}Sn_x$ Heusler compounds have been performed in order to study collective excitations [54, 55]. In all systems well defined spin waves were observed in the entire Brillouin zone below the Curie temperature $T_c$ and highest energy at the zone boundary was approximately 1-2$T_c$. Stoner excitations are well separated in energy from the collective excitations (spin waves) due to large exchange splitting $\triangle$ ($\triangle \sim 1 - 2\ eV$) and thus they can be neglected in consideration of thermodynamic properties. Also, measurements in the paramagnetic phase have established the absence of spatial magnetic correlations (spin waves), and have shown the value of atomic moment to be in agreement with that obtained from static susceptibility measurements.

However, the situation is different for those systems in which the moment is associated with the X atoms or both the X and Y atoms ($Co_2MnZ$ or $Mn_2VAl$). For such compounds the magnetic atoms are close enough for significant overlap of the $d$ wave function to occur and there is then a tendency towards itinerant behavior [50, 51]. Hence Stoner excitations may be important.

## 4.4  Band structure calculations

The band structure calculations of Heusler alloys has been initiated by Ishida *et al.,* in the early eighties. The authors used non-self-consistent spherical augmented plane wave method (SAPW) to study electronic structure of $Ni_2MnSn$, $Pd_2MnSn$ [56] and $Cu_2MnAl$ [57]. In 1983 Kübler *et. al.,* gave a detailed study on the formation and coupling of the magnetic moments in several Heusler alloys using self-consistent augmented spherical wave method (ASW). At the same year de Groot *et al.,* [59] discovered the half-metallic ferromagnetism in semi Heusler compounds NiMnSb and PtMnSb. Since then much effort has been devoted to the study of electronic and magnetic properties of these systems on the basis of band structure calculations.

### 4.4.1  Formation of local moments

The mechanisms of magnetic moment localization in transition metals and their alloys is one of the most interesting problems in modern magnetism. The origin of ferromagnetic behavior in Heusler alloys is rather complicated. The picture that emerged from the systematic calculations of Kübler *et. al.* for the microscopic mechanism responsible for the formation of magnetic moments in these systems is that the magnetization is very much confined to the Mn atoms [58]. The localized character of the magnetic moment results from the fact that the large exchange splitting of the Mn $d$ states implies that Mn atoms support $d$ states of only one spin direction. In the ferromagnetic state the spin-up $d$ electrons of the Mn atom hybridize with those of the X atoms in forming a common $d$ band, but spin-down $d$ electrons are almost completely excluded from the Mn sites. Thus we are left with the completely localized magnetic moments composed of completely itinerant electrons. In figure 4.2 we
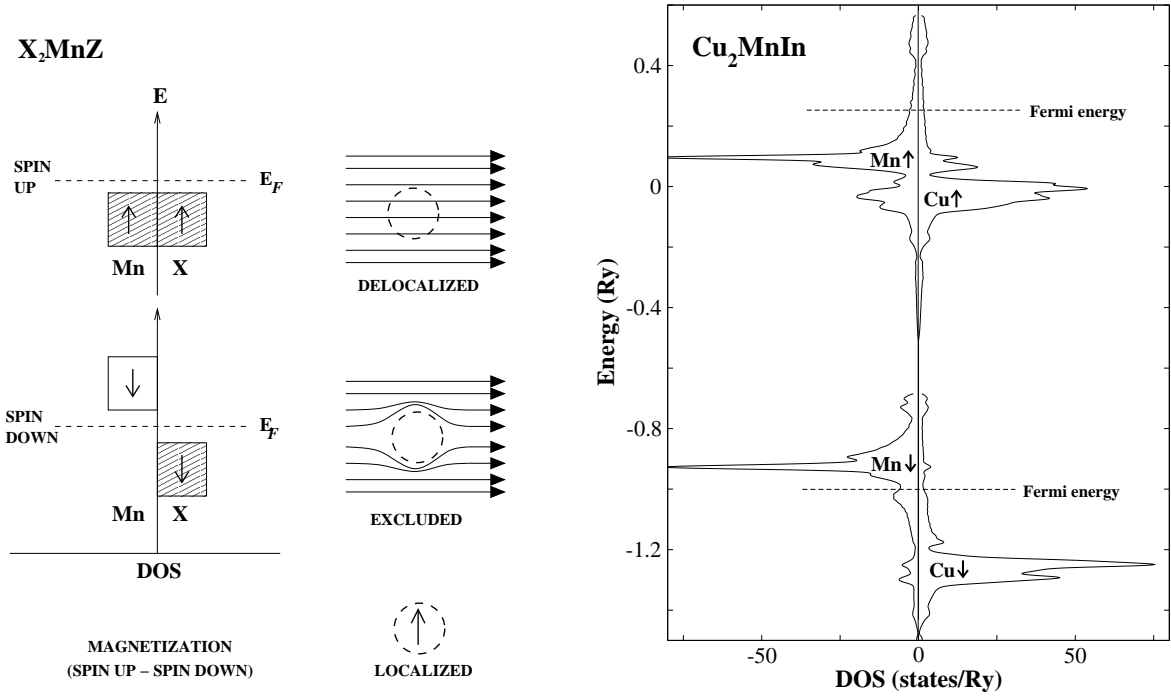
Figure 4.2: Left panel: Localized magnetic moments from delocalized electrons. Schematic diagram of up-spin and down-spin d electrons in Heusler alloys ($X_2MnZ$) [58]. Right panel: The corresponding non-schematic site and spin projected $d$ electron density of states for $Cu_2MnIn$.

present the physical picture that is just described. The same discussion is also valid for semi Heusler alloys (see next section).

Using the calculated total energies, it was possible to compare the relative stability of various magnetic phases (ferromagnetic one and two different antiferromagnetic ones) for a number of Heusler compounds [58]. Indeed, the magnetic moments of Mn atoms were found to be practically insensitive to the type of magnetic ordering. This behavior is obviously related to the localized nature of magnetism in these systems. Kübler *et al.,* also proposed that in full Heusler compounds, $X_2MnZ$, X atoms (e.g., Cu, Ni, Pd) serve primarily to determine the lattice constant, while Z atoms (Al, In, Sb) mediate the interaction between the Mn $d$ states. However, experiments, particularly on quaternary systems have demonstrated that both X and Z atoms play similar role in establishing the magnetic properties [60, 61]. Furthermore, the magnetic properties are primarily determined by the conduction electron concentration.

### 4.4.2   Half-metallic ferromagnetism

The concept of half-metallic ferromagnetism was introduced by de Groot et. al., on the basis of band structure calculations in NiMnSb and PtMnSb semi Heusler compounds [59]. In these materials one of the spin subbands (usually majority spin band) is metallic, whereas the Fermi level falls into a gap of the other subband (see Fig. 4.3). Ishida *et al.* have proposed that also the full-Heusler alloys of the type $Co_2MnZ$, (Z=Si,Ge), are half-metals [62]. Since
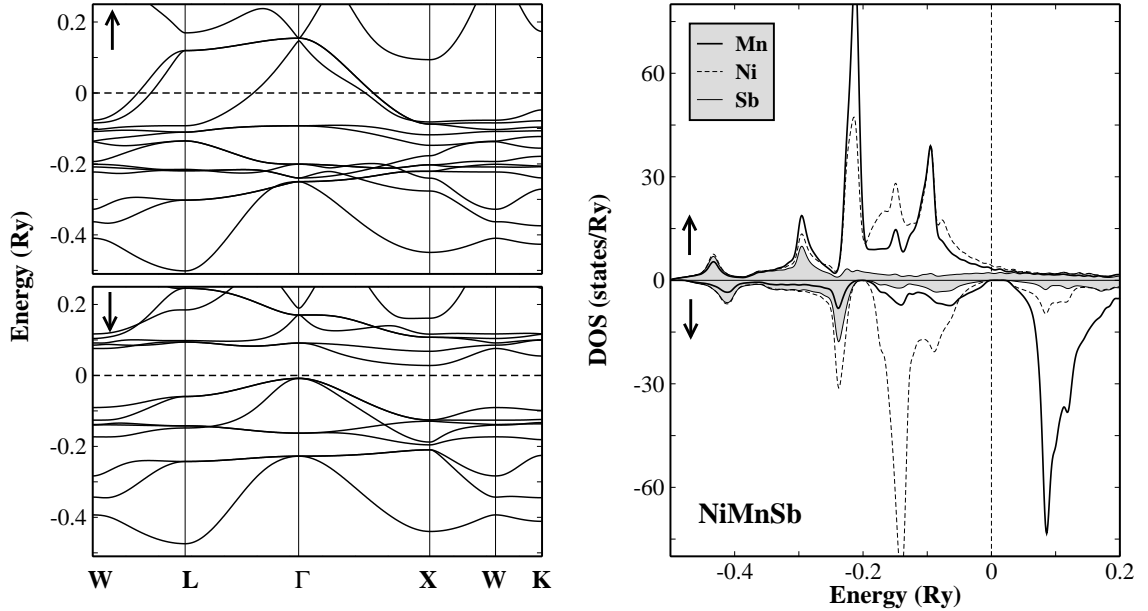
Figure 4.3: Left panel: Calculated band structure of half-metallic ferromagnet NiMnSb. The horizontal dashed line indicates the Fermi level. Right panel: Atom-resolved density of states (DOS) of NiMnSb. With shaded color we show the DOS of Sb.

then a number of further systems were predicted to be half-metallic. Among them are the binary magnetic oxides ($CrO_2$ and $Fe_3O_4$), colossal magnetoresistance materials ($Sr_2FeMoO_6$ and $La_{0.7}Sr_{0.3}MnO_3$) [63], diluted magnetic semiconductors ($Ga_{1-x}Mn_xAs$) and zinc-blende compounds MnAs and CrAs [64, 65, 66]. The origin of the appearance of half-metallic gap Heusler compounds will be discussed in detail in the following subsection.

- **Origin of the half-metallic gap**

The half-metallic ferromagnetism of semi Heusler alloys is intimately connected to their special so-called $C1_b$ crystal structure and consequently the symmetry of the system. Due to a vacant site at the position $(\frac{1}{2}\frac{1}{2}\frac{1}{2})$ in the $C1_b$ crystal structure the symmetry of the systems is reduced to tetrahedral from the cubic in the case of $L2_1$–type full Heusler alloys. Thus the gap originates from the strong hybridization between the $d$ states of the higher valent and the lower valent transition metal atoms [67]. This is shown schematically in figure 4.4. All Mn atoms are surrounded by six Z (Z is usually Sb) nearest neighbors (for the Mn atom at the (000) these neighbors are at $(\frac{1}{2}00)$, $(0\frac{1}{2}0)$, $(00\frac{1}{2})$, $(-\frac{1}{2}00)$, $(0-\frac{1}{2}0)$ and $(00\frac{1}{2})$). As a result the interaction of Mn with the Z-$p$ states splits the Mn-$3d$ states into a low-lying triplet of $t_{2g}$ states ($d_{xy}$, $d_{xz}$ and a higher lying doublet of $e_g$ states ($d_{x^2-y^2}$, $d_{3z^2-r^2}$). The splitting is partly due to the different electrostatic repulsion, which is strongest for the $e_g$ states which directly point at the Z atoms. In the majority band the Mn $3d$ states are shifted to lower energies and form a common $3d$ band with X (X=Ni, Co) $3d$ states, while in the
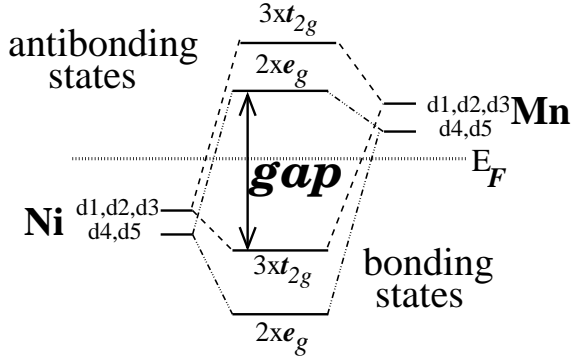
Figure 4.4: Schematic illustration of the origin of the gap in the minority band in semi-Heusler alloys [67].

minority band the Mn $3d$ states are shifted to higher energies and are unoccupied, so that a band gap at $E_F$ is formed, separating the occupied $d$ bonding states from the unoccupied $d$ antibonding states (see figure). Thus NiMnSb is a half-metal with a gap at $E_F$ in minority band and a metallic DOS at the fermi level in majority band.

The calculated total magnetic moment is 4 $\mu_B$ per unit cell and mostly located in Mn atom. NiMnSb has 22 valance electrons per unit cell, 10 from Ni, 7 from Mn and 5 from Sb. Because of the gap at $E_F$, in the minority band exactly 9 bands are fully occupied ( 1 Sb-like $s$ band, 3 Sb-like $p$ bands and 5 Ni-like $d$ bands) and remaining 13 electrons are accommodated in majority band resulting a magnetic moment of 13-9=4 $\mu_B$ per unit cell. Note that semi Heusler alloys like CoTiSb with 18 valence electrons shows semiconducting behavior.

It should be noted that the half-metallic character of semi Heusler compounds is highly sensitive to the crystal structure and symmetry e.g., the cubic point symmetry at Mn sites in ordinary $X_2$MnZ Heusler alloys gives rise to a symmetry of Mn-$3d$-$t_{2g}$ states that is different from the symmetry of the Sb-$p$ states. Hence, these states do not hybridize, so that no gap is opened in the minority spin band. The appearance of half-metallic ferromagnetism in full Heusler alloys is a subtle issue and explanation of it is very complicated. Recently Galanakis *et. al.* discussed this problem in detail [68].

- **Slater-Pauling behavior**

The total moment of the half-metallic semi- and full-Heusler alloys follows the simple rule: $M_t = Z_t - 18$ and $M_t = Z_t - 24$ where $Z_t$ is the total number of valence electrons [67, 68]. The total number of electrons $Z_t$ is given by the sum of the number of spin–up and spin–down electrons, while the total moment $M_t$ is given by the difference $Z_t = N_\uparrow + N_\downarrow$ , $M_t = N_\uparrow - N_\downarrow$. Since 9 (12) minority bands of semi (full) Heusler alloys are fully occupied, a simple rule of 18 (24) is obtained for half-metallicity in $C1_b$–type ($L2_1$) Heusler alloys.

This is analogues to the well-known Slater-Pauling behavior of the binary transition metal alloys [69]. The difference with respect to these alloys is, that in the half-Heusler alloys the minority population is fixed to 9 and 12, so that the screening is achieved by filling the majority band, while in the transition metal alloys the majority band is filled with 5 $d$-states or completely empty and charge neutrality is achieved by filling the minority or majority
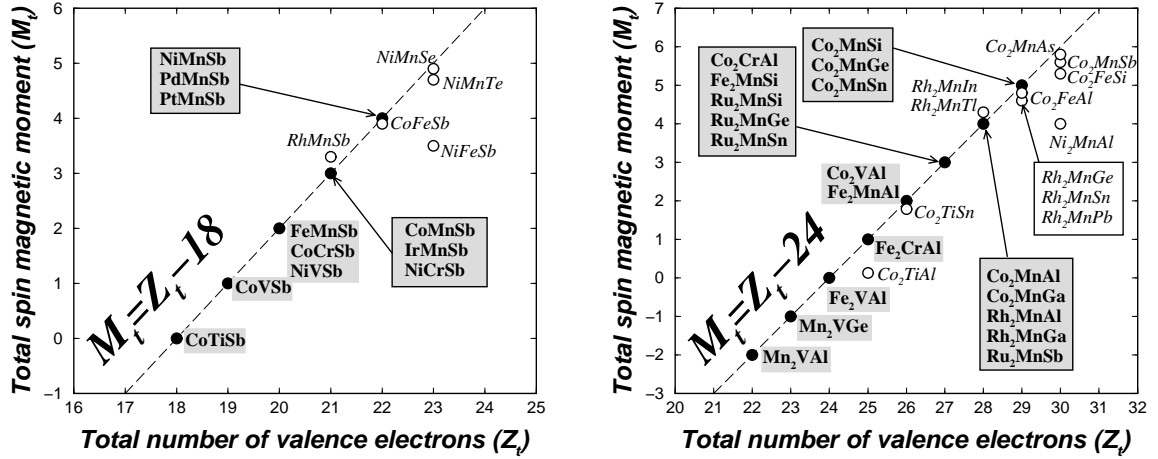
Figure 4.5: Left panel: Calculated total spin moments for semi Heusler alloys. The dashed line represents the Slater-Pauling behavior. Open circles indicates the compounds deviating from the SP curve [67]. Right panel: The same for the full Heusler alloys [68].

states. Therefore in the TM alloys the total moment is given by $M_t = 10 - Z_t$ for the systems on the left side and $M_t = Z_t$ for the systems on the right side of the Slater-Pauling curve.

For the half-metallic zinc-blende compounds like CrAs the rule is: $M_t = Z_t - 8$, since the minority As-like valence bands accommodate 4 electrons [70]. In all cases the moments are integer. In Fig. 4.5 we have gathered the calculated total spin magnetic moments for both Heusler alloys which we have plotted as a function of the total number of valence electrons. The dashed line represents the rule $M_t = Z_t - 18$ ($M_t = Z_t - 24$) obeyed by these compounds. The total moment $M_t$ is an integer quantity, assuming the values 0, 1, 2, 3, 4 and 5 if $Z_t = 18$. In the case of full Heusler alloys ($Z_t = 24$) $M_t$ can also take -2, -1 and 6. The value 0 corresponds to the semiconducting phase.

## 4.5 Exchange coupling: An overview

In view of the large separation of the Mn atoms ($> 4$ Å) and available inelastic neutron scattering experiments in Heusler alloys, the electrons of the unfilled Mn $3d$ shell can presumably be treated as very well localized, so that the $3d$ electrons belonging to different Mn atoms do not overlap considerably. The ferromagnetism in these systems is thought to arise from an indirect interaction, by way of conduction electrons, between the Mn moments. The first important information on the exchange coupling in these systems is provided by the inelastic neutron scattering experiments of Noda and Ishikawa in the late seventies [54]. The authors measured the spin wave spectra of $Ni_2MnSn$ and $Pd_2MnSn$ for various directions in the Brillouin zone and analyzed the results within the Heisenberg model. The obtained results for the exchange parameters were in good agreement with the assumption of indirect exchange coupling in Heusler alloys. Indeed, the pattern of exchange interactions was oscillatory and

long range reaching beyond the eight nearest neighborhood distance.

This behavior of exchange interactions has been taken as an evidence for Friedel oscillations and the results have been interpreted using either an RKKY model

$$J_R = -\frac{9\pi n^2 I^2}{8E_F} \frac{\cos(2k_F R)}{(k_F R)^3} \tag{4.1}$$

or Hartree-Fock treatment of double resonance model

$$J_R = -\frac{25}{4S} E_F \sin^2 \phi^- \frac{\cos(2k_F R - 2\phi^-)}{(k_F R)^3} \tag{4.2}$$

where $n$ is the number of conduction electrons, $I$ is the s-d exchange constant, $E_F$ and $k_F$ are Fermi energy and wave vector, respectively, and $\phi^-$ is the phase shift of the scattered wave function of the down spin electrons of the Mn atoms. $\phi^-$ is given by

$$\phi^- = \frac{\pi}{5}(5 - n_B) \tag{4.3}$$

where $n_B$ is the Mn magnetic moment divided by $m_B$.

Although both models gave good agreement with experiments for the exchange interactions at large distances, they were unable to account for either the sign and magnitude of the nearest and next nearest neighbor exchange parameters. The failure of these models for close distances was attributed to the involved asymptotic approximations. Price, however, showed that double resonance model unrestricted by any asymptotic approximation was able to capture qualitative features of the observed spin wave spectra in Pd$_2$MnSn [71]. Malmström and Geldart discussed the effect of the finite spin distribution on the RKKY interaction between the Mn moments [72]. The authors showed that, in spite of simplified treatment of electron band structure, finite spin distribution could bring the calculated values of the exchange interactions into agreement with that determined for the Ni$_2$MnSn and Pd$_2$MnSn compounds from the experimental studies. Reitz and Stearns, in addition to indirect s-d coupling, proposed two more coupling mechanisms to achieve agreement with experimental data: d-d exchange between itinerant and localized d electrons and super exchange via the Z atoms [73]. This model was capable of accounting for a wide range of properties in many different compounds because of the arbitrary adjustable parameters in latter mechanisms.

It is worth to note that all these model Hamiltonian approaches have certain advantageous and disadvantageous. The most prominent useful feature of them is that they provide a qualitative physical picture of magnetic interactions and reveal different intrinsic parameters for the mediation of exchange interactions between Mn atoms such as the number of conduction electrons, their polarization and finite spin distribution around Mn atoms. On the other hand, the main drawback of such approaches become obvious when one tries to predict the properties of new systems. This is mostly due to large number of arbitrary parameters and the use of simplified band structure model. Complete information on the magnetic interactions in solids can be, in principle, obtained from the solution of the Schrödinger equation as discussed in the preceding chapters.

The first quantitative study of the exchange interactions in Heusler alloys is given by Kübler *et al.,* within parameter free density functional theory [58]. The authors proposed a mechanism of super exchange type via the diamagnetic group III-V elements responsible for the Mn-Mn coupling. The calculation of the Mn-Mn exchange parameters is based on the comparison of the ferromagnetic and antiferromagnetic configurations of the Mn moments within the super cell relying on the Heisenberg model with localized moments. Although this approach works very well for systems with short range exchange interactions, i.e, interactions do not reach beyond the second nearest neighborhood (since in this case exchange parameters can be easily obtained from few magnetic configurations with the use of small super-cells), the situation is very different for systems with long range exchange coupling. In this case one needs large super cells and quite large number of magnetic configurations to extract all exchange parameters which obviously makes calculations very complicated and very expensive. This is also why Kübler *et al.,* reported only first two nearest neighbor exchange parameter in Heusler alloys, although they are known to be quite long range from experiments. It should be, however, noted that, in principle the obtained exchange parameters from simple calculations appear as the sum of all parameters if they are long range. Furthermore, within this method one can exactly get on-site exchange parameter $J_0 = \sum_{\mathbf{R}} J_{0\mathbf{R}}$, but this does not provide any information about the distribution of exchange parameters. Among the further findings of the Kübler *et al.,* is the absence of the considerable direct overlap of Mn $3d$ wave functions in Heusler alloys. The discussion is based on the comparison of the density of states for ferromagnetic and antiferromagnetic configurations.

Consequently, although the calculations of Kübler *et al.,* were an important step, however they were not able to explain the observed spin wave spectra of Heusler alloys. The most quantitative treatment of the exchange interactions in ferromagnets became possible after the implementation of the non-collinear magnetism in modern electronic structure codes. Developments in this field yields reliable and efficient calculation of exchange interactions up to the arbitrary distance from a magnetic atom in the crystal.

Coming back to the discussion of microscopic mechanisms for indirect exchange coupling in Heusler alloys we see on the the basis of model Hamiltonian approaches that two main points are central to understand them: conduction electrons and their spin polarization. Since the problem of interaction between local moments is rather closely connected with the problem of conduction electron polarization around a magnetic moment. To clarify this issue it is important to obtain information on the conduction electron spin polarization, and important information in this regard is provided by measurement and analysis of the hyperfine fields in non-magnetic sites (X,Z) in several Heusler alloys. The strength of the transferred hyperfine fields correlates with the amplitude of the $s$ conduction electron polarization. Indeed measurements by Campbell and Khoi *et al.,* shoved that maximum conduction electron polarization is found in the systems with high Curie temperatures such as $Cu_2MnAl$ and $Cu_2MnIn$ [74, 75].

However, hyperfine fields are only sensitive to the $s$ electron polarization and do not

say anything about the polarization of $p$ electrons which are dominated in Heusler alloys and expected to play the same role as $s$ electrons. To probe the whole conduction electron polarization we have to resort to another method. Compton scattering profiles are proved to be quite useful tool in this respect. Indeed, using this method, recent measurements of Zukowski *et al.*, on $Cu_2MnAl$ gave a large *sp* electron polarization which is antiferromagnetically coupled to Mn moment [76]. Also similar result is obtained for $Ni_2MnSn$ by Deb *et al.*, [77].

# Part II

# Results of Calculations

# Chapter 5

# Exchange Mechanisms in Heusler Alloys

## 5.1 Introduction

As we have seen in preceding chapter Heusler alloys exhibit very rich magnetic behavior. One can study in the same family of alloys a series of interesting diverse magnetic phenomena like itinerant and localized magnetism, antiferromagnetism, helimagnetism, or non-collinear magnetism. This diverse magnetic behavior reflects the complex nature of exchange interactions in these systems. Depending on the number of magnetic atoms within the unit cell there can be several exchange mechanisms which coexist and are mixed together. For instance in some Mn-based systems where the total magnetic moment is confined to Mn sublattice an indirect exchange mechanism seems most probable due to large distance between Mn magnetic moments. Indeed, for these systems early model Hamiltonian based studies assuming an indirect exchange coupling ($s$-$d$) between the Mn atoms via conduction electrons provided a qualitative information on the nature of magnetism. On the other hand, we know that in several full Heusler alloys ($X_2MnZ$; X = Fe, Co, Ni, Rh) X atoms also carry a substantial magnetic moment. In this case things get more complicated since there will be many exchange interactions between different magnetic atoms each of which will contribute to the formation of the magnetic state in a cooperative manner. For example, magnetic properties of quaternary Heusler alloys NiCoMnSb with three different magnetic atoms within the unit cell is governed by at least six different exchange interactions.

Our objective in this chapter as well as in the following chapters is a comprehensive study of exchange interactions and Curie temperature in both families of Heusler alloys. The calculational methods both for the exchange interactions and finite temperature properties are introduced in chapters 2 and 3, respectively. An overview of the previous experimental and theoretical studies on these materials is given in chapter 4. For a general discussion it is convenient to divide Heusler alloys into two groups. First group contains the systems with one magnetic atom per unit cell. Almost all semi Heusler alloys as well as some Mn-based

full Heusler alloys enter this group. Compounds with more than one magnetic atom per unit cell are included in the second group. The magnetism of the systems within the first group is relatively easy to understand but still very interesting since they present a diverse magnetic behavior as mentioned above. On the basis of available experimental information and early model Hamiltonian calculations an indirect exchange coupling mechanism is proposed for the first group of systems. This model is also supported by parameter-free first-principles calculations of Kübler *et al* [58]. However, the situation is not so easy for the compounds in the second group. Thus, the understanding of magnetism in these systems constitutes one of the aims of the present thesis.

Our extensive investigations on the second group of systems showed that the magnetism in these systems is rather complicated. First, due to Friedel oscillations there is always an indirect exchange interaction among the magnetic atoms, which strongly depends on conduction electron concentration. Second, because of the small distances between Mn and X atoms there is also a considerable overlap of $3d$ wave functions of these atoms (direct exchange). This interaction can be ferromagnetic or antiferromagnetic depending on the filling of the $3d$ orbitals of the atoms. Co$_2$MnZ and Mn$_2$VZ compounds which will be studied in the next chapter are the best examples for the former and latter case, respectively. Another distinct feature of this interaction is that it strongly depends on the value of the magnetic moment of the X atom. For small values of the X magnetic moment (0.1-0.3 $\mu_B$) this interaction plays a secondary role while it becomes extremely important with increasing X moment. The former case will be illustrated by the example of Ni$_2$MnZ compounds in the following section. Intermediate and large X moment limits will be considered in the next chapter.

In section 5.2 we discuss magnetism of the systems within the second group of alloys considering experimentally well known Ni$_2$MnZ compounds. Section 5.3 is devoted to a detailed study on the role of the conduction electrons in mediating exchange interactions between Mn atoms both in semi- and full-Heusler alloys from the first group. Many of the systems investigated in this thesis show half-metallic character. Due to the vital importance of these systems for spintronics applications the results for them are presented in a separate chapter (chapter 6).

## 5.2   Ni$_2$MnZ (Z = Ga, In, Sn, Sb) compounds

Recently these Ni-based Heusler alloys received tremendous experimental and theoretical interest because of the two unique properties that they exhibit: Shape memory effect and inverse magnetocaloric effect. In the preceding chapter we introduced shape memory effect. Shape memory alloys are promising materials for future applications. They can be used as sensors and actuators in different fields. The currently used materials (e.g. NiTi, CuAlNi alloys) use the temperature as a parameter to trigger the shape change. However, in ferromagnetic shape memory alloys magnetic field plays the same role as temperature. Thus,

Table 5.1: Experimental lattice parameters, magnetic moments (in $\mu_B$) and mean-field estimation of the Curie temperatures for Ni$_2$MnZ (Z = Ga, In, Sn, Sb). Lattice parameters and the experimental Curie temperature values are taken from Ref.[50]

| Compound | $a(\text{Å})$ | Mn | Ni | Z | Cell | MFA$_{[\text{Mn-Mn}]}$ | MFA$_{[\text{all}]}$ | Exp. |
|---|---|---|---|---|---|---|---|---|
| Ni$_2$MnGa | 5.825 | 3.570 | 0.294 | -0.068 | 4.090 | 302 | 389 | 380 |
| | | 3.43[a] | 0.36[a] | -0.04[a] | 4.11[a] | | | |
| | | | | | 4.17[b] | | | |
| Ni$_2$MnIn | 6.069 | 3.719 | 0.277 | -0.066 | 4.208 | 244 | 343 | 315 |
| Ni$_2$MnSn | 6.053 | 3.724 | 0.206 | -0.057 | 4.080 | 323 | 358 | 360 |
| | | 3.53[c] | 0.24[c] | -0.03[c] | 4.08[c] | | | |
| Ni$_2$MnSb | 6.004 | 3.696 | 0.143 | -0.033 | 3.950 | 343 | 352 | 365 |

[a]Ref.[85]
[b]Ref.[86] (Exp.)
[c]Ref.[87]

switching process can be made much faster and better controlled compared to conventional shape memory alloys. Among the ferromagnetic shape memory alloys Ni$_2$MnGa is the most studied one, it undergoes a magnetic phase transition at around 370 K and a martensitic phase transition at approximately 200 K. At the martensitic phase of Ni$_2$MnGa an applied field of about 1 T can induce strains as large as 10% [47, 48].

The inverse magnetocaloric effect (MCE) has its origin in a martensitic phase transformation that modifies the exchange interactions due to the change in the lattice parameters. For samples with compositions close to Ni$_2$MnZ (Z = Ga, Sn) stoichiometry an inverse MCE has been reported. This is an extrinsic effect arising from the coupling at the mesoscale between the martensitic and magnetic domains [78]. Applying a magnetic field adiabatically, rather than removing it as in ordinary MCE, causes the sample to cool. This is very important for room temperature refrigeration as an environment-friendly alternative to conventional vapor-cycle refrigeration. This has prompted intensive research in this field [79, 80, 81, 82].

In spite of substantial theoretical and experimental research aimed at understanding these two mechanisms, the study of exchange interactions in these systems received less attention. It is worth to note that the second effect (inverse MCE) is closely related to the distance dependence of the exchange interactions in these systems [82]. Recently Enkovaara *et al* studied the spin-spirals in Ni$_2$MnZ (Z = Al, Ga) and estimated Curie temperature from the calculated dispersions [83]. The authors showed that the Ni sublattice plays important role in the magnetic properties of the systems.

The main purpose of the present section is a detailed study of the exchange interactions in these systems. In particular we report a systematic study of the exchange interaction
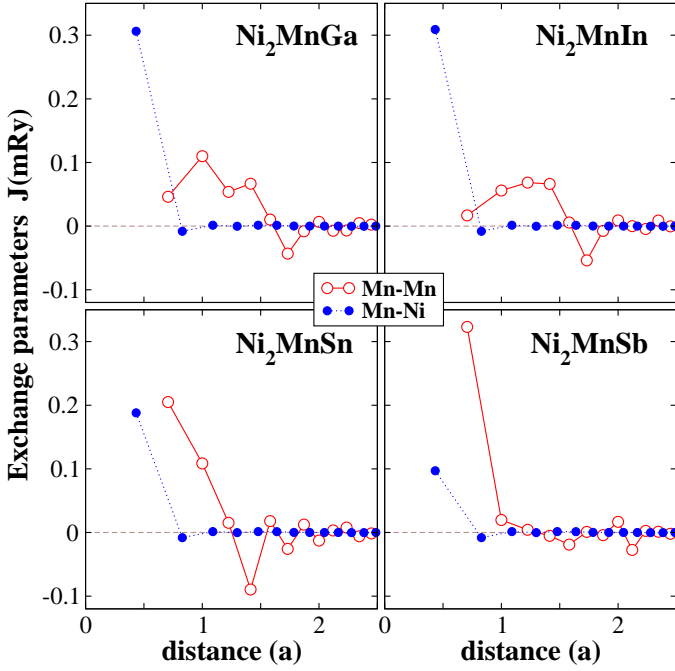
Figure 5.1: The parameters of the Mn-Mn (intra-sublattice) exchange interactions and Mn-Ni (inter-sublattice) exchange interactions in Ni$_2$MnZ (Z = Ga, In, Sn, Sb). The distances are given in the units of the lattice constant. The significance of the oscillations of the exchange parameters is verified by varying the **q** mesh in the frozen-magnon calculations.

between atoms of different sublattices and show that pattern of exchange interactions in these systems deviates strongly from the physical picture that can be expected on the basis of the experimental information available. Indeed common crystal structure, similar chemical composition and close experimental values of the Curie temperature make the assumption natural that the exchange interactions in these systems are similar. Our study shows, however, that this assumption is not correct [84]. The exchange interactions vary strongly depending on the Z constituent. In particular, the inter-sublattice interactions change strongly from system to system. We show that different exchange interactions lead, in agreement with experiment, to similar values of the Curie temperatures. We analyze the relation between the properties of the exchange interactions and the Curie temperatures.

- **Magnetic moments and exchange parameters**

In Table 5.1 we present calculated magnetic moments. For comparison, the available experimental values of the moments and the results of previous calculations are presented. Relative variation of the Mn moment is small. On the other hand, the moment of Ni and Z atoms show strong relative variation and are in Ni$_2$MnSb about two times smaller than in Ni$_2$MnGa or Ni$_2$MnIn. The values of the magnetic moments are in good agrement with the results of previous calculations.

The calculated Heisenberg exchange parameters are presented in Fig. 5.1. As mentioned in the introduction, the assumption that the closeness of the experimental Curie temperatures is the consequence of the similarity of the exchange interactions is not confirmed by the calculations. We obtain strong dependence of the exchange interactions on the type of the Z atom. For Z = Ga and Z = In that belong to the same column of the Mendellev's table (see
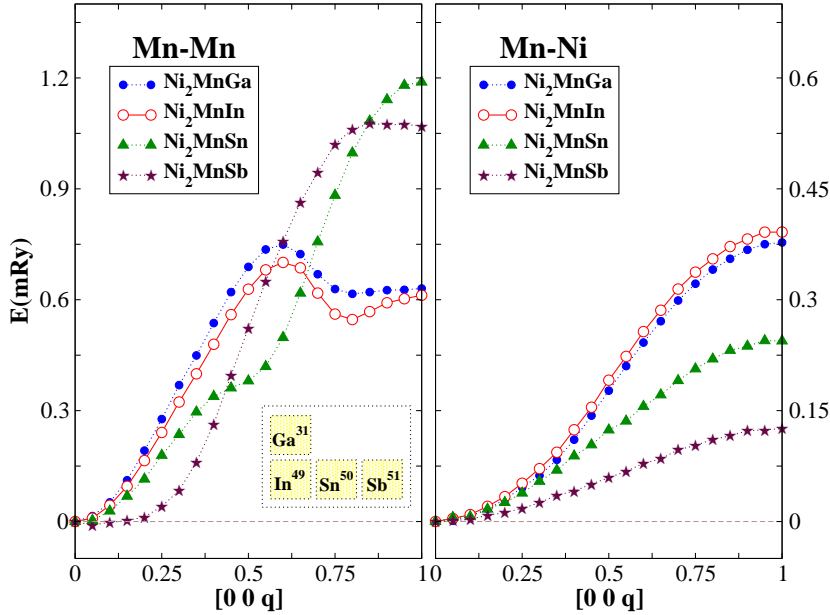
Figure 5.2: Frozen-magnon energies as a function of the wave vector **q** (in units of $2\pi/a$) in Ni$_2$MnZ for Mn-Mn (left) and Mn-Ni interactions (right).

inset in Fig. 5.2) we obtain similar pattern of Heisenberg exchange parameters. On the other hand, for Z atoms belonging to different columns the changes in the exchange interactions are very strong (Fig. 5.1). These changes concern both the Mn-Mn intra-sublattice interactions and the Ni-Mn inter-sublattice interaction.

Considering the Mn-Mn interactions we notice that in Ni$_2$MnGa and Ni$_2$MnIn the interaction with the coordination spheres from the first to the forth is positive. The interaction with the first coordination sphere is weaker than with the following ones. The interaction with the fifth sphere is very small. The interaction with the 6th sphere is negative. The interaction with further coordination spheres is very weak.

In Ni$_2$MnSn the interaction with the first sphere strongly increases compared with Ni$_2$MnGa and Ni$_2$MnIn. On the other hand, the interaction with the third sphere becomes small. The interaction with the forth sphere is strongly negative. The interaction with further neighbors are weak.

The trend observed in transition from Ni$_2$MnGa and Ni$_2$MnIn to Ni$_2$MnSn becomes even stronger in the case of Z = Sb. Here the interaction with the first neighbor increases further and is the only strong exchange interaction between the Mn atoms.

The inter-sublattice Mn-Ni interaction behaves very differently. A sizable direct interaction takes place only between nearest neighbors. This interaction is very strong in Ni$_2$MnGa and Ni$_2$MnIn and quickly decreases for Z = Sn and, especially, Z = Sb.

In spite of substantial experimental works on the structural and magnetic properties of Heusler alloys the information for the exchange interactions is very limited. Noda and Ishikawa [54] measured the spin wave spectra of Ni$_2$MnSn and Pd$_2$MnSn for various directions in the Brillouin zone and analyzed the results within the Heisenberg model. They found an long range and oscillatory character for the exchange interactions. Especially these oscillations were reaching beyond the the eight nearest neighbor distance in both compounds.
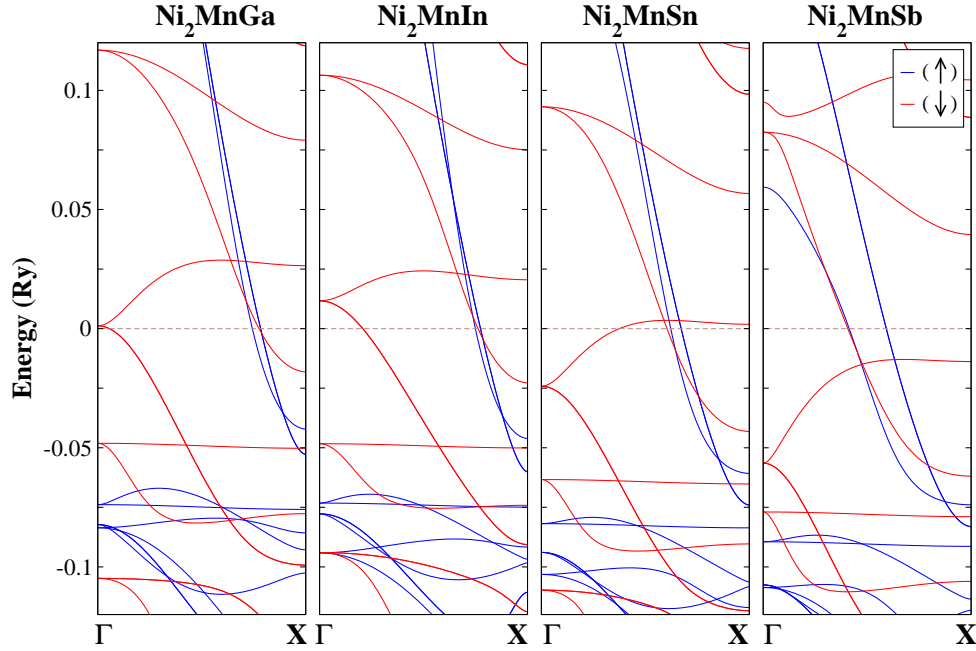
Figure 5.3: Band structure of Ni$_2$MnZ along the high symmetry line ($\Gamma$-X).

Interestingly, we obtained a very similar pattern of exchange parameters for Ni$_2$MnSn. Combining our theoretical findings with experimental results of Noda and Ishikawa we can draw a rough conclusion that exchange coupling in Mn-based Heusler alloys is indirect via the conduction electrons. A detailed analysis for the role of the conduction electrons in mediating exchange interactions will be given in the next section.

- **Frozen-magnon energies and band structure**

To reveal the physical origin of the strong difference in the exchange parameters of these systems we plot in Fig. 5.2 the frozen-magnon energies as a function of wave vector $\mathbf{q}$ for one direction in the Brillouin zone. The energy of the frozen magnon with a given $\mathbf{q}$ can be seen as a result of a complex interaction of the ferromagnetic states separated by vector $\mathbf{q}$ in the reciprocal space [6]. This interaction is stronger if the states have close energies and weaker for the states separated by a large energy interval. We remind the reader that the inter-atomic exchange parameters are Fourier transforms of the E($\mathbf{q}$) functions and therefore reflect their form. Indeed, E($\mathbf{q}$) curves for Ni$_2$MnGa and Ni$_2$MnIn are close to each other that leads to a similar set of interatomic exchange parameters (Fig. 5.1). These curves deviate strongly from a simple cosinusoid having a maximum at $\mathbf{q}$ about 0.6 and a rather weak variation at $\mathbf{q} > 0.6$. The complexity of E($\mathbf{q}$) means that several Fourier components are needed to describe the features of the function. This is reflected in the the Heisenberg's parameters of Ni$_2$MnGa and Ni$_2$MnIn.

On the other hand, the E($\mathbf{q}$) curve of Ni$_2$MnSb is well described by one cosinusoid (Fig. 5.2) that results in a single large Mn-Mn exchange parameter (Fig. 5.1). The E($\mathbf{q}$) of Ni$_2$MnSn
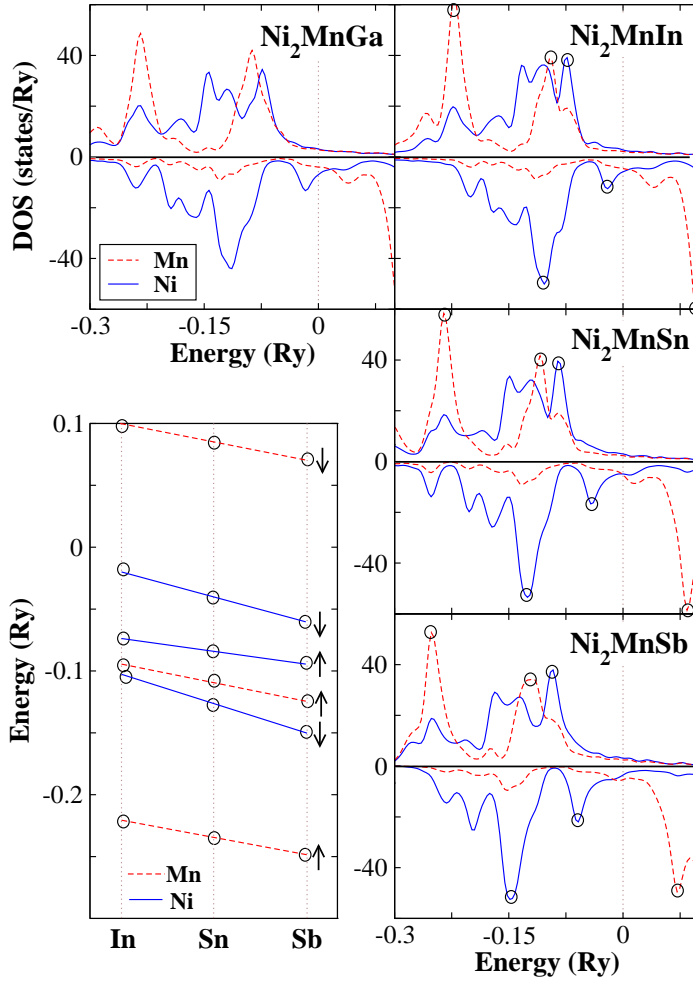
Figure 5.4: Spin-projected partial density of states of Ni$_2$MnZ. The separate graph in the left-hand bottom part of the figure shows the variation of the positions of a number of the DOS peaks for the In-Sn-Sb series of compounds. The lines in this graph are guides for the eye. The energies are measured with respect to the Fermi level of the corresponding system. The small open circles on the DOS curves mark the positions of the peaks. Arrows show spin projections. The analysis of the states at the Fermi level shows that the main contributions comes from the 3d states of Mn and Ni.

assumes an intermediate position from the viewpoint of the complexity of the function. This property is also reflected in the exchange parameters (Fig. 5.1).

- **Density of states and Curie temperature**

Note that the character of the **q**-dependence of the energy illustrated by Fig. 5.2 is a consequence of the properties of the electronic structure of the compounds. Indeed, in Fig. 5.3 we see that the electronic structures of Ni$_2$MnGa and Ni$_2$MnIn are similar. Transition along the row In-Sn-Sb leads to increasing difference in the electron spectrum. This increasing difference can be traced back to the change in the number of valence electrons: a Sb atoms has two more valence electrons than In and one more electron than Sn. As the result an important difference in the electron structure of the system is a relative shift of the Fermi level to a higher energy position in the sequence In-Sn-Sb. This shift is clearly seen in the DOS presented in Fig. 5.4. The positions of the same features of the DOS in different systems are well described by linear functions with negative angle coefficients. For the Mn peaks all three lines are almost parallel. This means that the change in the Mn DOS from system to system can be treated as a rigid shift with respect to the Fermi level. In the case of the Ni-

DOS the situation is more complicated since, besides the variation of the electron number, an additional influence on the peak positions is exerted by the variation of the Ni atomic moment (see Table 5.1).

The $E(\mathbf{q})$ curves determining the Mn-Ni interactions are presented in Fig. 5.2. The form of the curves is in all cases close to a cosinusoid. Therefore, only one exchange parameter has sizable value. The strength of the interaction is in correlation with the value of the magnetic moment of the Ni atoms.

The interatomic exchange parameters are used to evaluate the Curie temperature. If only the Mn-Mn interactions are taken into account we obtain values shown in Table 5.1. Despite very strong difference in the Mn-Mn exchange parameters in these systems the difference in the corresponding Curie temperatures is not very large. The explanation for this result is the property that in MFA to a one-sublattice ferromagnet the value of the Curie temperature is determined by the sum of the interatomic exchange interactions $J_0 = \sum_{\mathbf{R} \neq 0} J_{0\mathbf{R}}$. $J_0$ gives the average value of $E(\mathbf{q})$ and is less sensitive to the detailed form of the $E(\mathbf{q})$ function.

The comparison of the Curie temperatures calculated with the use of the Mn-Mn exchange parameters only with experimental Curie temperatures shows that the agreement with experiment is not in general good. In the case of $Ni_2MnGa$ the error is about 30%.

Account for inter-sublattice interactions improves the agreement with experimental $T_C$ values considerably (Table 5.1). This shows that the Ni moment provides a magnetic degree of freedom which plays important role in the thermodynamics of the system.

## 5.3 Role of the conduction electrons in mediating exchange interactions between Mn atoms

Our studies on experimentally well established Ni-based compounds in the preceding section revealed a complex character of the magnetism in these systems. In particular, long range and oscillatory behavior of the exchange interactions as well as their strong dependence on the Z constituent gave an evidence for the conduction electron mediated exchange interactions in Heusler alloys. Also, as we have seen in the preceding chapter an indirect exchange coupling model was used to interpret the observed spin wave spectra of several Heusler alloys. The first DFT calculations of the exchange interactions by Kübler *et al.* for a number of full Heusler alloys gave a strong support for the above indirect exchange coupling model.

To gain further insight into the role of the conduction electrons in exchange coupling we performed a systematic study on several Mn-based semi- and full Heusler alloys going beyond the stoichiometric compositions. In particular, we focus on the systems in which total magnetic moment is confined to Mn sublattice in order to avoid further complexities due to the additional exchange interactions between different magnetic atoms. These systems also provide a great simplification in calculations and subsequent interpretation of the results. Several Heusler compounds of XYZ and $X_2YZ$ type satisfy above condition if X element is chosen from the late transition metals (i.e., Cu, Pd, Ag, Pt, Au). Among them especially Pd-

Table 5.2: Experimental lattice parameters in $X_k MnZ$ ( X = Pd, Cu; k = 1, 2; Z = In, Sn, Sb, Te) for stoichiometric compositions. The last column gives the lattice constants used in calculations which are obtained by taking the average of lattice constants in sequence In-Sn-Sb-Te for experimentally existing compounds.

| Compound | $a_{[In]}(\text{Å})$ | $a_{[Sn]}(\text{Å})$ | $a_{[Sb]}(\text{Å})$ | $a_{[Te]}(\text{Å})$ | $a_{[Z]}(\text{Å})$ |
|----------|------|------|------|------|------|
| PdMnZ | - | - | 6.25 | 6.27 | 6.26 |
| CuMnZ | - | - | 6.09 | - | 6.09 |
| $Pd_2MnZ$ | 6.37 | 6.38 | 6.41 | - | 6.38 |
| $Cu_2MnZ$ | 6.20 | 6.17 | - | - | 6.18 |

and Cu-based stoichiometric full Heusler compounds $Pd_2MnZ$ (Z=In, Sn, Sb) and $Cu_2MnZ$ (Z=In, Sn) and non-stoichiometric ones $Pd_2MnZ_{1-x}Z'_x$ [(Z,Z')=(In, Sn), (Sn, Sb), (In, Sb)] and $Cu_2MnIn_{1-x}Sn_x$ received huge experimental interest. Early measurements by Webster *et al.* on quaternary full Heusler alloys $Pd_2MnIn_{1-x}Sn_x$ demonstrated the importance of the conduction electrons in establishing magnetic properties [50]. Recent experiments on quaternary semi Heusler compounds $Ni_{1-x}Cu_xMnSb$ and $AuMnSn_{1-x}Sb_x$ gave even more interesting results which reveal the decisive role of the conduction electron number in magnetic order and phase transition temperature $T_C$ [88, 89].

We consider Pd and Cu containing Mn-based semi and full Heusler alloys which is expressed in compact a form as $X_k MnZ_{1-m}Z'_m$ [X = Pd, Cu; k = 1, 2; (Z, Z')=(In, Sn), (Sn, Sb), (Sb, Te); $0 \leq m \leq 1$]. We use the virtual crystal approximation (VCA) to vary electron concentration. Half of the considered systems are not studied experimentally and thus their lattice constants are not known. As it is seen from Table 5.2 one or two compounds exist experimentally from semi-Heusler compounds and more in the case of full Heusler compounds. Therefore we use only an average lattice constant in the sequence In-Sn-Sn-Te. (see Table 5.2). This is a good approximation since, as we know from experiments, Heusler alloys containing different *sp*-atoms from the same row of Periodic Table have similar lattice parameters [50, 51]. Indeed, as it is seen in Table 5.2 the maximum variation of the lattice parameters from In to Te is less than 1%. An important increase is observed in transition from $3d$ to $4d$ systems due to large size of the $4d$ atoms.

Going beyond the stoichiometric compositions provided very important information on the nature of magnetism especially for semi Heusler alloys. For these systems we obtain a strong dependence of the exchange interactions on the number of the valence electrons. The systems with the same number of valence electrons, like PdMnSn and CuMnIn, have qualitatively similar patterns of exchange parameters and, as a result, similar Curie temperatures. We find a clear relationship between the strength of the exchange interactions and the conduction electron polarization. The larger the conduction electron polarization the stronger the exchange interactions. For zero polarization the calculated Curie temperature
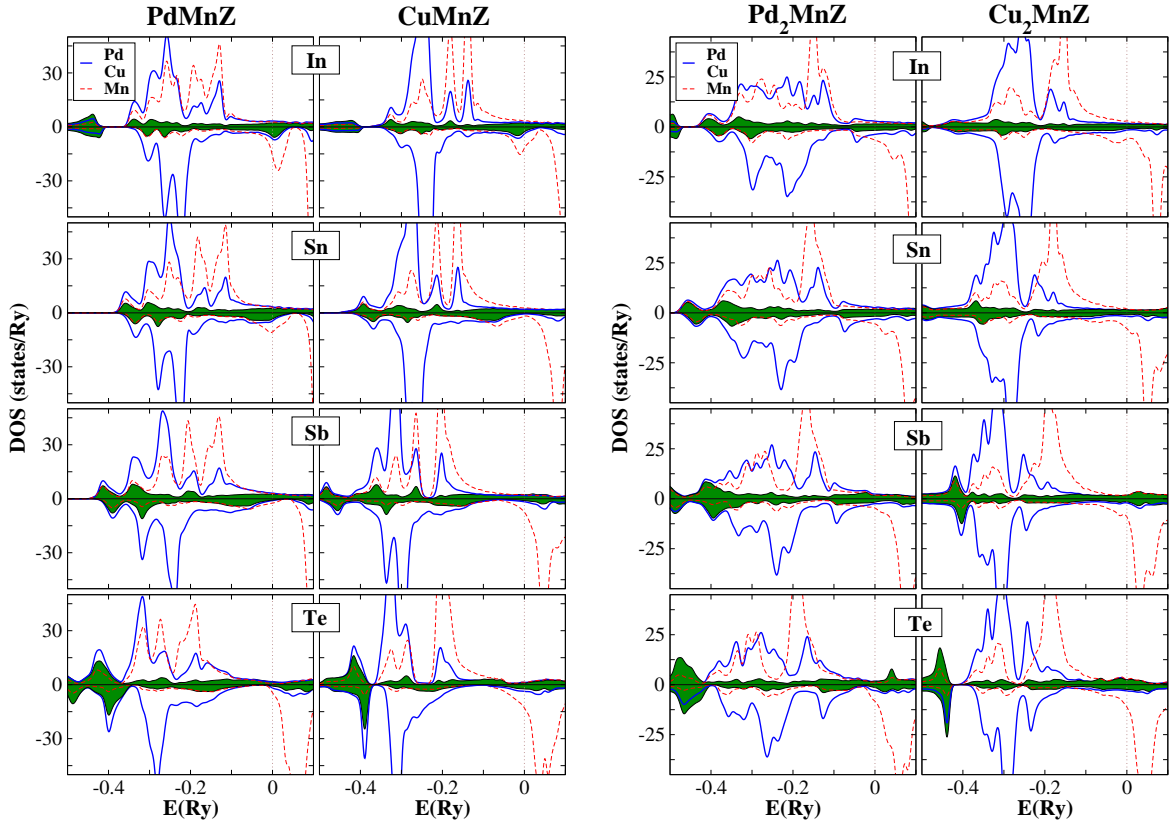
Figure 5.5: Left panel: Spin-projected atom-resolved density of states of PdMnZ and CuMnZ (Z=In, Sn, Sb, Te) for stoichiometric compositions. With shaded green color we show the DOS of Z constituent. The broken vertical lines denote the Fermi level. Left panel: The same for full Heusler compounds Pd$_2$MnZ and Cu$_2$MnZ.

also vanishes. However, the situation is not so evident for full Heusler alloys. We find a qualitative correlation between conduction electron polarization and Curie temperature but no relation between the exchange interactions for the systems with same number of valance electrons like Cu$_2$MnIn and Pd$_2$MnSb. In both families of systems the calculated exchange parameters are quite long range that indicates an indirect coupling between Mn atoms via the conduction electrons.

In last part of this section we investigate the role of $3d$ and $4d$ atoms in exchange coupling by comparing the results for Ni$_2$MnZ and Pd$_2$MnZ (Z=In, Sn, Sb, Te) for two different lattice parameters. Our calculations showed that $3d$ or $4d$-atoms have practically no effect on mediation of the exchange interactions. Magnetism of both systems appeared to be strongly depending on the Z constituent and conduction electron polarization. For the same Z constituent we obtain a similar pattern of exchange interactions in the case of almost equal conduction electron polarizations.

- **Density of states and magnetic moments**

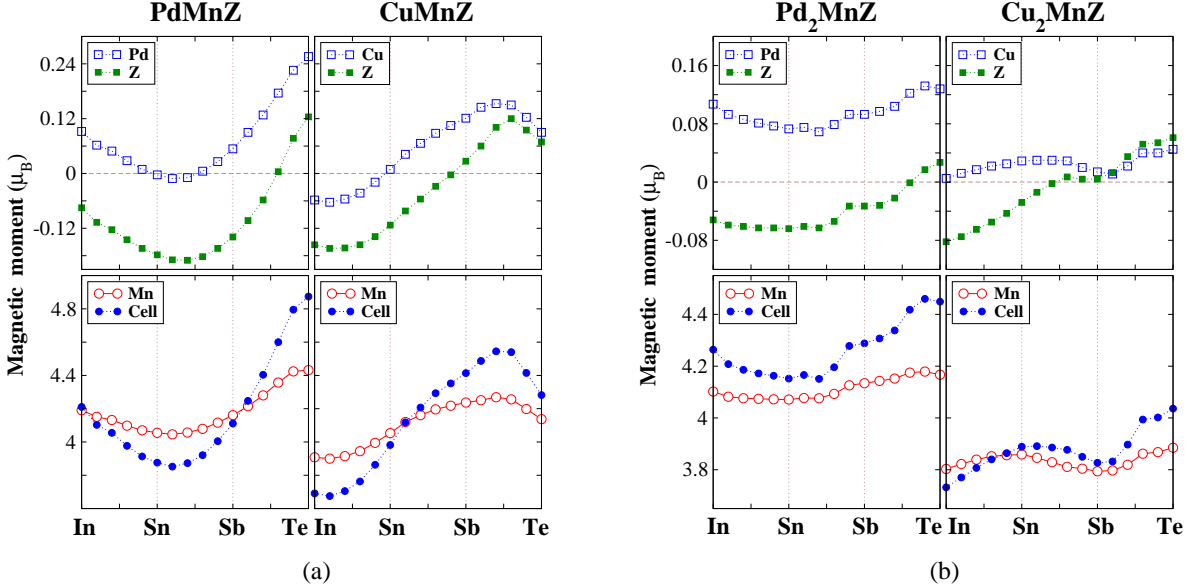In Fig. 5.5 we present the atom resolved density of states of X$_k$MnZ ( X = Pd, Cu; k = 1, 2;

Figure 5.6: (a) Calculated atom-resolved and total spin moments (in $\mu_B$) in PdMnZ and CuMnZ as a function of the *sp*-electron number of the Z constituent. (b) The same for full Heusler alloys Pd$_2$MnZ and Cu$_2$MnZ.

Z = In, Sn, Sb, Te) for stoichiometric compositions. In agreement with the commonly accepted picture of magnetism for Mn-based Heusler alloys we obtain a strong localization of magnetization on the Mn sublattice with a value of magnetic moment close to $4\mu_B$. The localized nature of magnetism will be further discussed in the next subsection. An important difference in the electron structure of these compounds is a relative shift of the Fermi level to a higher energy position in sequence In-Sn-Sb-Te due to change of the number of valance electrons within the same row of Periodic Table. This shift is clearly seen in the DOS presented in Fig. 5.5. Note that a Sb atom has two more valence electrons than In, one more electron than Sn and one less electron then Te. The DOS for semi-Heusler compounds show an interesting feature that different compositions give similar behavior if the total number of the *sp* electrons coming from different atoms is equal. This similarity is more pronounced near Fermi level. For example the peaks in Mn spin down states of PdMnSn and CuMnIn are very much similar to each other. This distinct feature of the DOS for semi-Heusler alloys is related to the symmetry properties of the wave functions in C1$_b$-type crystal structure [67, 68].

In Fig. 5.7 we present calculated atom resolved and total magnetic moments in both family of Heusler alloys PdMnZ, CuMnZ, Pd$_2$MnZ and Cu$_2$MnZ as a function of the *sp*-electron number of the Z constituent. As mentioned above, the magnetic moment is mostly confined to Mn sublattice. A small induced moment is found on Cu and Pd sublattices which is positive in a broad composition interval while this moment is negative for Z constituent. An interesting observation in Z dependent properties of the induced moments is that they almost follow the behavior of the Mn moment from In to Te. This correlation is more
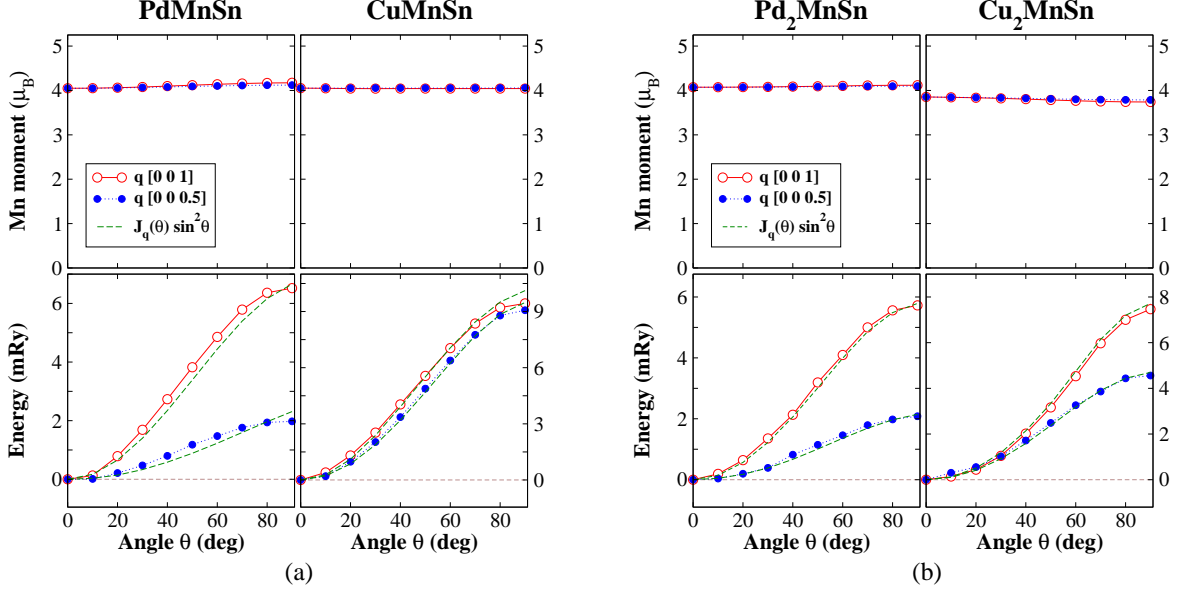
Figure 5.7: (a) Upper panel: Calculated Mn spin moment in PdMnSn and CuMnSn as a function of $\theta$ for spin spiral with $\mathbf{q} = (0\,0\,\frac{1}{2}), (0\,0\,1)$ in units of $\pi/a$. Lower panel: Corresponding total energies $\Delta E(\theta, \mathbf{q}) = E(\theta, \mathbf{q}) - E(0,0)$. For comparison results of force theorem (broken lines) is presented. $J_{\mathbf{q}}(\theta)$ stand for $J_{\mathbf{q}} \times M_{\theta}^2$, $M$ is the magnetic moment. (b) The same for $Pd_2MnSn$ and $Cu_2MnSn$ full Heusler compounds.

pronounced in semi-Heusler alloys (see Fig. 5.7). Furthermore, in semi Heusler compounds different compositions give similar values for magnetic moments with a small shift in the case of equal total number of valance electrons. This small shift stems from the different lattice constants. Additionally, the changes associated with total magnetic moment is very large in semi-Heusler compounds. In PdMnZ this is about 1 $\mu_B$, half of it comes from the change in Mn magnetic moment. On the other hand, the situation is different in full Heusler alloys, neither a correlation nor a substantial change in magnetic moments is obtained.

### 5.3.1 Local moment behavior

As we have seen in preceding chapter Mn-based Heusler compounds are considered to be ideal local moment systems on the basis of experimental information available. This feature was theoretically confirmed by early DFT calculations of Kübler *et al.* for a number of full Heusler compounds [58]. Considering PdMnSn, CuMnSn, $Pd_2MnSn$ and $Cu_2MnSn$ from semi and full Heusler compounds as a prototype we calculated magnetic moments an total energies as a function of $\theta$ for spin spiral with two different $\mathbf{q}$ values chosen in $z$ direction and compare the relative stability of the different magnetic configurations. Note that spin spiral technique allows one to treat all possible magnetic configurations between ferromagnetic and antiferromagnetic states. Here we restrict ourselves to the two $\mathbf{q}$ values: $\mathbf{q} = (0\,0\,\frac{1}{2})$ and $\mathbf{q} = (0\,0\,1)$. $\theta$ angle varied between 0 and 90. Note also that spin spiral having $\theta = 0$ with any value of $\mathbf{q}$ and $\theta = 90$ with $\mathbf{q} = (001)$ corresponds to ferromagnetic and antiferromagnetic
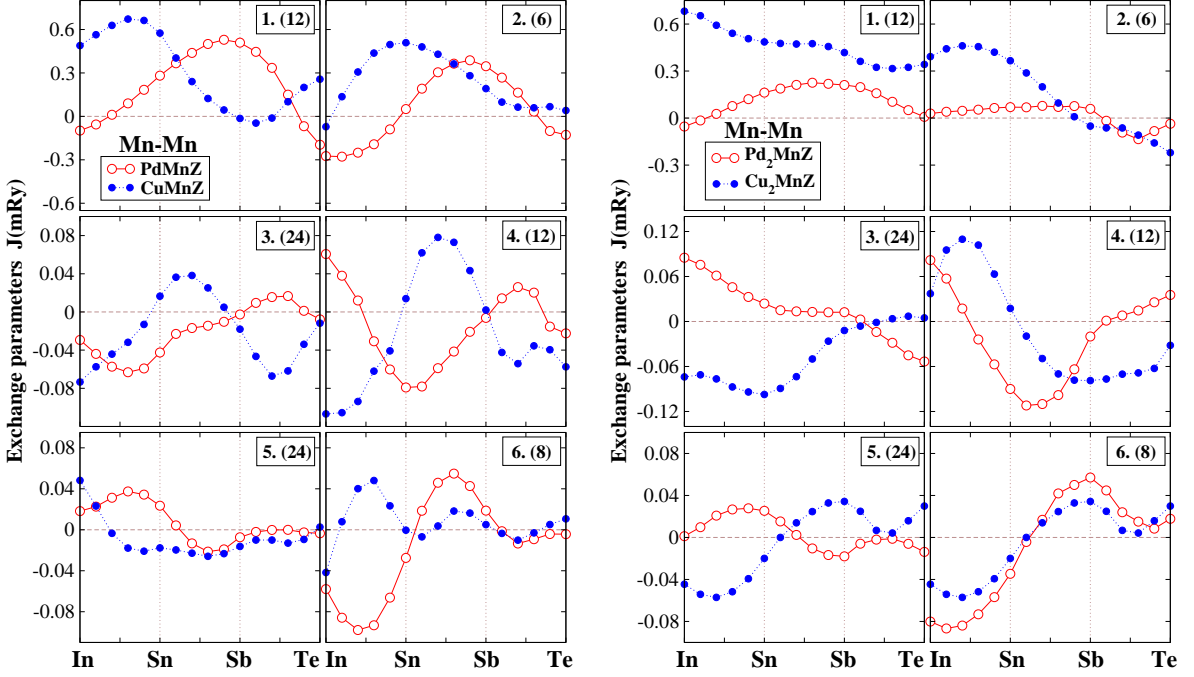
Figure 5.8: Left panel: First six nearest neighbor Mn-Mn exchange parameters in PdMnZ and CuMnZ as a function of the $sp$-electron number of the Z constituent. Also given are the number of atoms within corresponding coordination spheres. Right panel: The same for full Heusler alloys $Pd_2MnZ$ and $Cu_2MnZ$.

states, respectively.

The obtained results are presented in Fig. 5.7. For all considered systems the magnetic moment of the Mn atom is practically insensitive to the type of the magnetic ordering. The relative change of the Mn moment in transition from ferromagnetic to antiferromagnetic state is less than 3%. On the other hand, the calculated total energy increases with increasing $\theta$ angle and reaches the maximum value for $\theta = 90$ with $\mathbf{q} = (0\,0\,1)$ that corresponds to antiferromagnetic phase. This shows that ground state is ferromagnetic in all cases. The obtained stability of the magnetic moments reflects the localized nature of magnetism in both family of Heusler alloys as well as justifies the approach used in calculation of exchange parameters. Furthermore, the agreement between calculated values of $\Delta E(\theta, \mathbf{q})$ and $J_{\mathbf{q}}(\theta) \sin^2 \theta$ implies the possibility of using large angles ($30 < \theta < 90$) in calculation of exchange parameters in local moment systems which is not usually the case for $3d$ transition metals.

### 5.3.2 Indirect exchange coupling

In Fig. 5.8 we present calculated first six nearest neighbor Mn-Mn exchange parameters for both families of compounds as a function of $sp$-electron concentration together with number of atoms within corresponding coordination spheres. Behavior of the same quantities for larger distances ($\sim 10\,a$) is given in Fig. 5.9 for selected compounds PdMnIn, CuMnIn, $Pd_2MnIn$
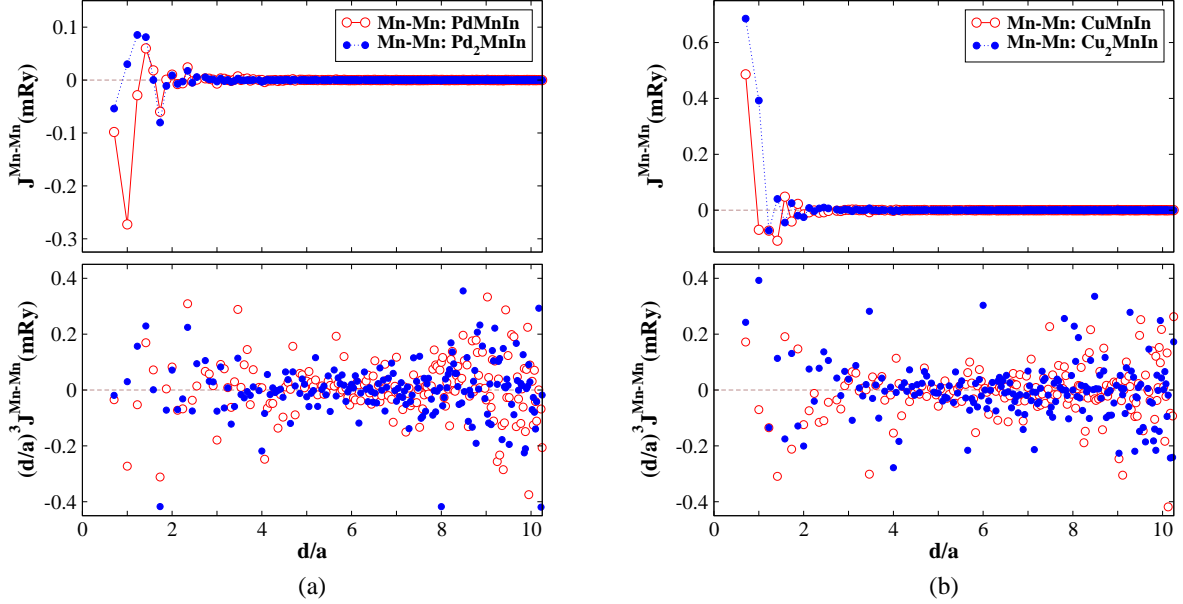
Figure 5.9: (a) Upper panel: Mn-Mn exchange interactions in $Pd_k MnIn$ (k = 1, 2) as a function of distance up to the $10a$. Lower panel: RKKY-type oscillations in exchange parameters for corresponding compounds. (b) The same for $Cu_k MnIn$ (k = 1, 2).

and $Cu_2 MnIn$. As it is seen from Figs. 5.8 and 5.9 the Mn-Mn interactions are long-ranged reaching beyond the 6th nearest neighborhood distance and have the RKKY-type oscillating character. The absolute value of the parameters decays quickly with increasing interatomic distance and the main contribution to $T_C$ comes from the interaction between atoms lying closer than $3a$. No sizable contribution is detected after $5a$. Nevertheless, even at very large distances RKKY-type oscillations becomes visible when exchange parameters are multiplied by $(d/a)^3$ (see Fig. 5.9) that reveal the indirect exchange coupling in these systems mediated by conduction electrons.

In agreement with the results of preceding section we obtain a strong dependence of the exchange parameters on the Z constituent for both families of Heusler compounds. As it is seen from Fig. 5.8 all exchange parameters oscillates between ferromagnetic and antiferromagnetic values with increasing $sp$-electron concentration. These oscillations are related to the detailed electron structure of the systems. Considering first two nearest neighbor exchange parameters we see that they have ferromagnetic character for a broad composition range and dominate over the rest of the parameters. The remaining ones are very weak and have similar energy dependencies. Note that it is these first two nearest neighbor exchange interactions which give rise to very high Curie temperatures in Cu-based full Heusler alloys as well as both classes of semi Heusler alloys. Furthermore, we obtain a strong correlation between strength of the exchange interactions and $sp$-electron (conduction electron) polarization (see Fig. 5.10). The larger the conduction electron polarization the stronger the obtained exchange parameters.

A distinct feature of the magnetism in semi-Heusler alloys is that the maximum of the
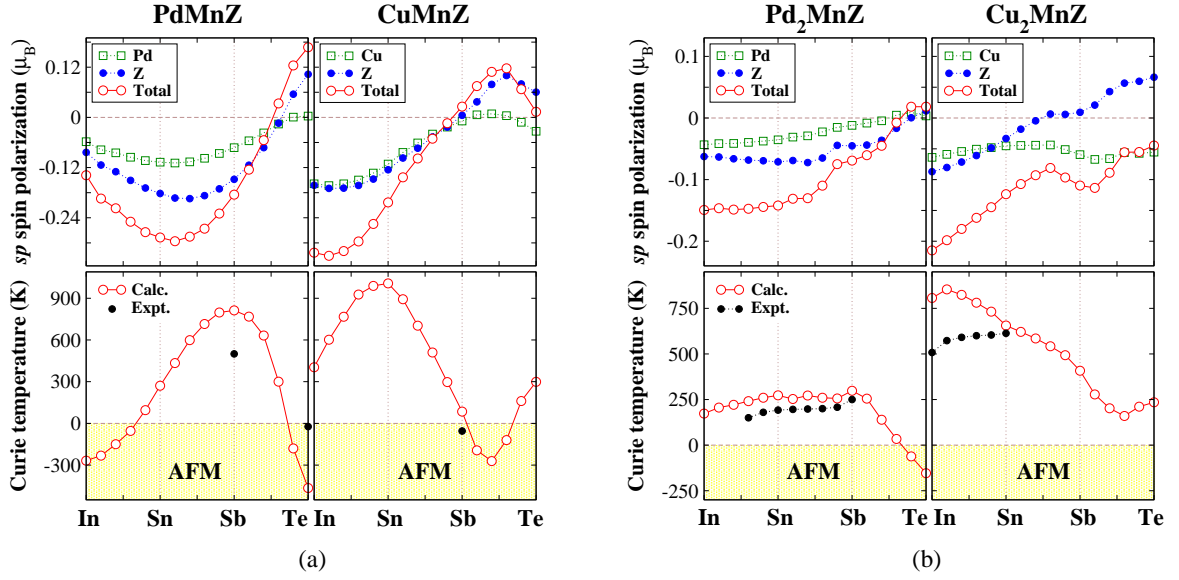
Figure 5.10: (a) Upper panel: The $sp$-electron spin polarization (in $\mu_B$) of the X=Pd,Cu and Z constituents. The total polarization is given as the sum of X and Z spin polarizations. Lover panel: Mean-field estimation of the Curie temperature in PdMnZ and CuMnZ. For comparison available experimental $T_C$ values taken from Ref.[50] are presented. (b) The same for the full-Heusler alloys Pd$_2$MnZ and Cu$_2$MnZ.

exchange interactions for both PdMnZ and CuMnZ corresponds to the similar number of the $sp$-electrons. The shift of the maxima for two systems is explained by the fact that Pd has one $sp$-electron less than Cu. The properties of the exchange interactions are reflected in the properties of the Curie temperature (see Fig. 5.10) where we also obtained a relative shift of the maxima of the two curves corresponding to one $sp$-electron. On the other hand, no such correlation is obtained for the full Heusler compounds.

### 5.3.3 Conduction electron polarization and Curie temperature

The problem of interaction between local moments and resulting Curie temperature is rather closely connected with the problem of conduction electron polarization around a magnetic moment. To clarify this issue it is important to obtain information on the conduction electron spin polarization. In Fig. 5.10 we present calculated $sp$-electron spin polarization and Curie temperatures for both families of Heusler alloys. For both classes of systems we obtain a qualitative correlation between the spin polarizations and Curie temperatures. In particular the systems with vanishing $sp$-electron spin polarization are characterized by the value of the Curie temperature that is very close to zero. Also, large spin polarization gives rise to high $T_C$ values in both families of alloys. Additionally, the sign of the spin polarization gives information on the nature of magnetic structure. For negative spin polarizations we obtain a ferromagnetic order in a large interval of compositions while positive polarization results in an antiferromagnetic order. A non-collinear magnetic structure is obtained for
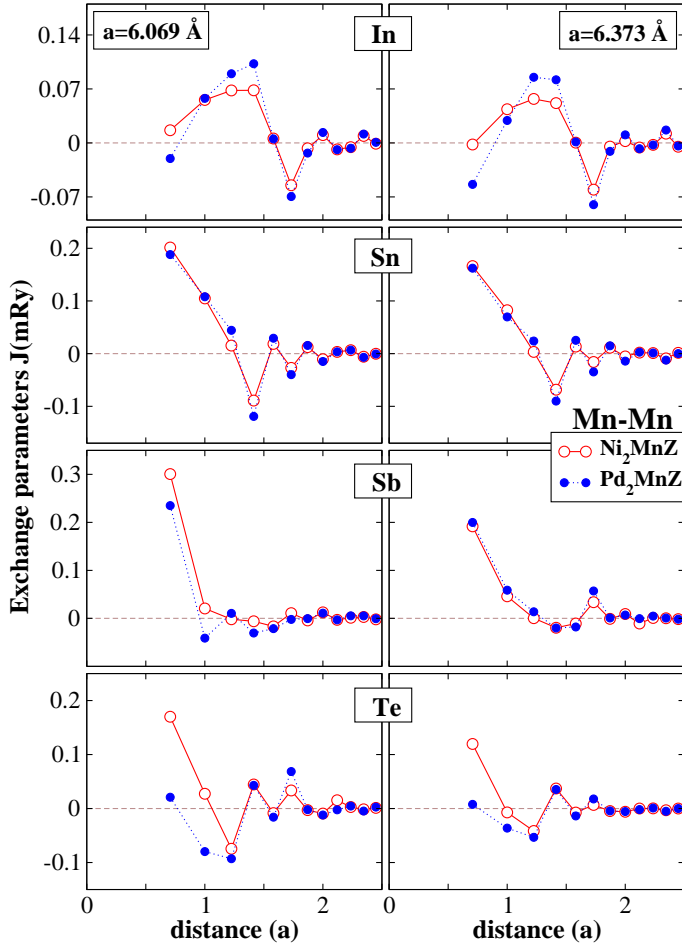
Figure 5.11: The parameters of the Mn-Mn exchange interactions in $Ni_2MnZ$ and $Ni_2MnZ$ (Z=In, Sn, Sb, Te) for two different lattice constants.

vanishing values of *sp*-electron spin polarization. These properties reveal the decisive role of the *sp*-electrons of the X and Z atoms in mediating the exchange interaction between the Mn spin moments as well as magnetic ordering. This makes spin-polarization of the *sp*-electrons important parameter for tuning the value of the Curie temperature in these systems. The obtained values of Curie temperatures are in good agreement with the available experimental data (see Fig. 5.10).

The first experimental information on the conduction electron polarization of Heusler alloys is provided by measurement and analysis of the hyperfine fields in non-magnetic sites (X,Z) in these systems. The strength of the transferred hyperfine fields correlates with the amplitude of the *s*-electron polarization. Indeed measurements by Campbell and Khoi *et al.*, shoved that maximum conduction electron polarization is found in systems with high Curie temperatures such as $Cu_2MnAl$ and $Cu_2MnIn$ [74, 75]. Recently, Zukowski *et al.*, using Compton scattering profiles, obtained a large conduction electron spin polarization in $Cu_2MnAl$ which is antiferromagnetically coupled to Mn moment [76]. Also, a similar result is obtained for $Ni_2MnSn$ by Deb *et al.*,[77]. Our calculations are in agreement with these recent experiments.

Table 5.3: Magnetic moments and $sp$-electron polarization (in $\mu_B$) in $Ni_2MnZ$ and $Pd_2MnZ$ (Z = In, Sn, Sb, Te) for two different lattice parameters.

| | $a = 6.07$ Å | | | | | $a = 6.37$ Å | | | | |
|---|---|---|---|---|---|---|---|---|---|---|
| Compound | X | Mn | Z | $sp$ | Cell | X | Mn | Z | $sp$ | Cell |
| $Ni_2MnIn$ | 0.27 | 3.72 | -0.07 | -0.16 | 4.19 | 0.27 | 3.99 | -0.07 | -0.17 | 4.45 |
| $Pd_2MnIn$ | 0.11 | 3.81 | -0.05 | -0.14 | 3.98 | 0.17 | 4.10 | -0.05 | -0.15 | 4.26 |
| $Ni_2MnSn$ | 0.21 | 3.74 | -0.06 | -0.13 | 4.10 | 0.21 | 4.00 | -0.06 | -0.14 | 4.35 |
| $Pd_2MnSn$ | 0.09 | 3.79 | -0.06 | -0.13 | 3.91 | 0.07 | 4.07 | -0.06 | -0.14 | 4.15 |
| $Ni_2MnSb$ | 0.15 | 3.76 | -0.03 | -0.09 | 4.04 | 0.22 | 4.04 | -0.02 | -0.06 | 4.46 |
| $Pd_2MnSb$ | 0.08 | 3.82 | -0.03 | -0.08 | 3.95 | 0.09 | 4.13 | -0.03 | -0.07 | 4.29 |
| $Ni_2MnTe$ | 0.22 | 3.83 | 0.03 | 0.01 | 4.31 | 0.21 | 4.04 | 0.02 | -0.03 | 4.48 |
| $Pd_2MnTe$ | 0.14 | 3.89 | 0.04 | 0.04 | 4.21 | 0.13 | 4.17 | 0.03 | 0.02 | 4.45 |

### 5.3.4  $3d$ versus $4d$ electrons

The role of the $sp$-electrons in mediating exchange interactions is further emphasized by a correlation between exchange parameters of different systems with a similar polarization. Fig. 5.11 present the exchange parameters of $Ni_2MnZ$ and $Ni_2MnZ$ (Z=In, Sn, Sb, Te) for two different lattice spacings. For each lattice parameter we obtain a similar pattern of exchange parameters for X=Ni and Pd also in the case of similar $sp$-electron spin polarizations (see Table 5.3). As it is seen from Table 5.3 and Fig. 5.11 this similarity is more pronounced for $Ni_2MnSn$ and $Pd_2MnSn$ compounds that they have equal $sp$-electron spin polarizations. For both lattice parameters the strong deviations in exchange parameters occur in the case of Z=Te where also the conduction electron spin polarizations assume quite different values.

In conclusion, we have shown that the magnetism of the Heusler alloys is characterized by the complex pattern of the exchange interactions that cannot be predicted without direct calculation. On the other hand our calculations show that the magnetic properties of the broad classes of the Heusler alloys can be tuned by the variation of the number and spin-polarization of the $sp$-electrons. This finding suggests a practical tool for the design of the materials with given properties.

# Chapter 6

# Magnetism of Half-Metallic Heusler Compounds

## 6.1  Introduction

This chapter is devoted to the study of half-metallic Heusler compounds because of their potential applications in the field of spintronics. The concept of half-metallicity and its origin is introduced in chapter 4. In these systems at the Fermi energy $E_F$ one spin direction is metallic and the other has an energy gap, resulting in 100 % spin polarization while normal transition metal ferromagnets (Fe, Co, and Ni) possess the spin polarization of $40\% - 50\%$. Consequently, half-metallic ferromagnets are expected to provide the huge tunnel magnetoresistance (TMR) and giant magnetoresistance (GMR) in magnetoelectronics devices. They can also be used as perfect spin filters and spin-injection devices as an alternative to ferromagnetic $3d$ metals. Since $3d$ systems cause serious problems due to large difference between the resistances of metal and semiconductor substrate.

Among the half-metallic ferromagnets the Heusler compounds are much more suitable for device applications due to their very high Curie temperatures, low coercivities and crystal structure compatibility with the zincblende semiconductors used industrially. Recently, several groups achieved very large TMR values using half-metallic Heusler alloys.

Our extensive investigations on ferromagnetic Heusler alloys (non-half metallic) presented in the preceding chapter provided a clear physical picture for the exchange coupling mechanism, in particular the role of conduction electrons in mediating interactions between Mn atoms is revealed. In principle, the same discussion also holds for the half-metallic Heusler compounds considered in this chapter. The only difference is that in these systems the calculated pattern of exchange interactions are rather short range. This behavior originates from the absence of Fermi surface for one spin direction in half-metallic ferromagnets which introduce an additional damping factor in RKKY model.

However, in this chapter we will discuss rather specific problems related to the nature of magnetism in half-metallic Heusler compounds aiming to provide a guideline for the further

experimental studies. For experimentally well established systems like NiMnSb and Co$_2$MnSi (section 6.2) we consider effect of the half-metallic gap on the stability of exchange interactions and resulting Curie temperature by contracting the lattice spacing which moves the position of Fermi level within the gap. Role of the inter-sublattice exchange interactions is revealed for the formation of very high Curie temperatures in some full Heusler compounds such as Co$_2$MnSi. We also study spin wave spectra and temperature dependence of the magnetization employing multi-sublattice Green function technique within Tyablikov decoupling scheme. In section 6.3 we demonstrate the role of the strong antiferromagnetic intersublattice exchange interactions in establishing ferrimagnetic order. Last section of this chapter is reserved for the discussion of predicted new semi Heusler compounds with very high $T_C$. Last part of this section dwells on an important problem which is the relation between half metallicity and Curie temperature by the example of these new systems.

## 6.2    NiMnSb, CoMnSb, Co$_2$CrAl and Co$_2$MnSi compounds

Recently, these compounds received considerable theoretical and experimental interest as promising device candidates due to their high Curie temperatures, large minority-spin band gaps and the possibility to grow on common semiconductors.

Experimental investigations were in the direction of the utilization of these materials in fundamental spintronics devices. Kämmerer *et al.* integrated Co$_2$MnSi, as a representative of the full-Heusler compound family, as one magnetic electrode in magnetic tunnel junctions and found a tunnelling magnetoresistance effect much larger than in the case that the Ni$_{0.8}$Fe$_{0.2}$ or Co$_{0.3}$Fe$_{0.7}$ are used as magnetic electrodes [90]. Similar experiments have been undertaken by Okamura and collaborators using Co2Cr$_{1-x}$Fe$_x$Al as the magnetic electrode [91]. Girgis *et al.* have fabricated current-in-plane giant magnetoresistive (GMR) devices based on multilayers of epitaxial NiMnSb and sputtered Cu and CoFe. They measured magnetoresistance of up to 3.5% at room temperature [92].

On the theoretical side, the studies are mainly focused on the stability of the half-metallic gap under different circumstances. For NiMnSb and Co$_2$MnSi compounds it was shown that half-metallicity is preserved under tetragonalization of the crystal lattice [93]. For a number of Heusler alloys Mavropoulos *et al.* studied the influence of the spin-orbit coupling on the spin-polarization at the Fermi level and found the effect to be very small [94] that is in agreement with a small orbital moment calculated by Galanakis. [95] Larson *et al.*[96] have shown that the structure of Heusler alloys is stable with respect to the interchange of atoms and Orgassa and collaborators and Picozzi and collaborators have demonstrated that a small degree of disorder does not destroy the half-metallic gap.[97, 98] Dowben and Skomski have shown that at non-zero temperatures the spin-wave excitations lead to the presence at the Fermi level of the electron states with opposite spin projections leading to decreasing spin-polarization of the charge carriers [99].

Despite very strong interest to the half-metallic ferromagnetism in Heusler alloys the
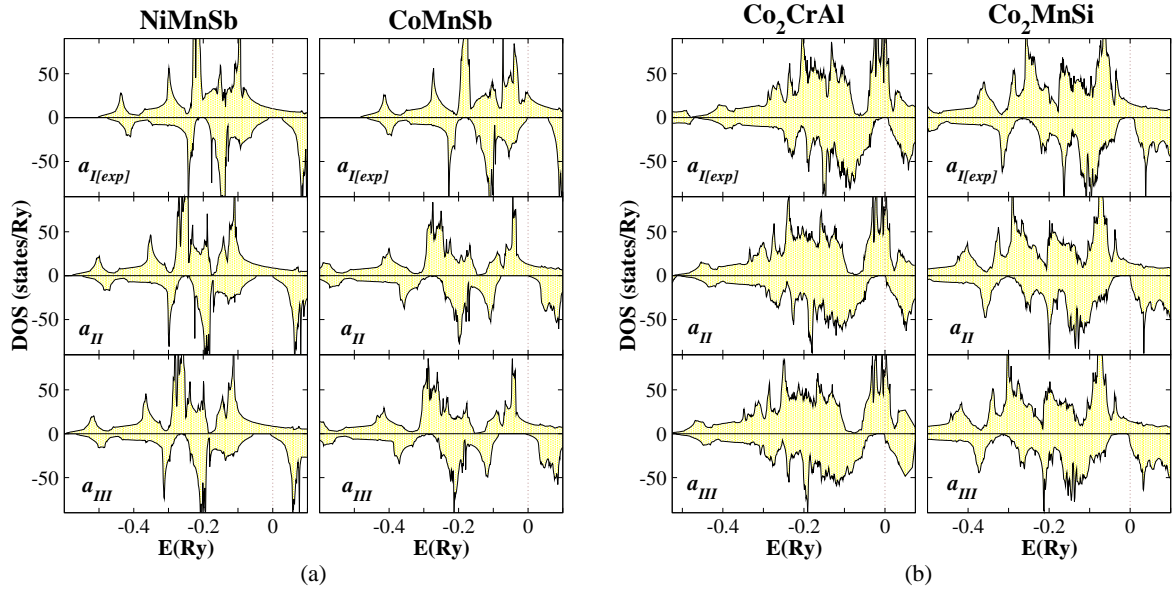
Figure 6.1: (a) Calculated spin-resolved density of states of NiMnSb and CoMnSb for three values of the lattice parameter. (b) The same for Co₂CrAl and Co₂MnSi. The upper panels present the results for the experimental lattice constant [50]. The middle panels show the results for the lattice parameter $a_{II}$ that is determined by the coincidence of the Fermi level with the upper edge of the half-metallic gap. The bottom panels present the results for lattice parameter $a_{III}$ that is obtained by a 1% contraction of $a_{II}$.

study of the exchange interactions and finite temperature magnetic properties received less attention. The latter constitutes the main purpose of the present section. Here we study the exchange interactions and Curie temperatures in both half- and full-Heusler alloys for three different lattice spacings. The investigation of the influence of the value of the lattice parameter on the properties of the Heusler alloys is important since the samples grown on different substrates can have different lattice spacings. The last part of this section is devoted to the consideration of the temperature dependence of magnetization at the experimental lattice parameters.

## 6.2.1 Effect of lattice parameter on magnetic properties

In this subsection we report the calculation of density of states, magnetic moments, interatomic exchange interactions and Curie temperatures at different lattice parameters for all four compounds.

- **NiMnSb and CoMnSb**

The electronic structure of both compounds has been extensively studied earlier and the reader is referred to the review [100] and references therein for detailed discussion. Here we present a brief description of the calculational results aiming to provide the basis for further considerations and to allow the comparison with previous work.

In Table 6.1 we collect the atomic and total spin moments for three different lattice parameters. The first calculation is performed for the experimental bulk lattice constant [50]. The calculated densities of states (DOS) for this case are presented in the upper panel of Fig. 6.1. For both NiMnSb and CoMnSb the Fermi level lies in the low-energy part of the half-metallic gap. The compression of the lattice pushes the majority $p$ states to higher energies that results in increased energy position of the Fermi level with respect to the half-metallic gap. At the lattice parameter $a_{II}$ the Fermi level coincides with the upper edge of the gap (Fig. 6.1). In the next step we further contracted the lattice constant by 1% (lattice parameter $a_{III}$, bottom panel in Fig. 6.1). In this case the Fermi level is slightly above the gap and the total spin moment is slightly smaller than the integer values of 3 and 4 $\mu_{\rm B}$ for CoMnSb and NiMnSb respectively.

The contraction of the lattice leads to an increase of the hybridization between the $d$ orbitals of different transition-metal atoms. This results in a decrease of the spin moment of Mn. In the case of NiMnSb this change is small: the reduction of the Mn spin moment under lattice contraction from the experimental lattice parameter to $a_{II}$ is $\sim$0.2 $\mu_B$. The Ni spin moment increases by about the same value to preserve the integer value of the total spin moment of 4 $\mu_{\rm B}$.

In CoMnSb, the half-metallic gap is larger than in NiMnSb. As a result, the transition of the Fermi level to the upper gap-edge requires a large lattice contraction of 11% (Table 6.1). This leads to a strong decrease of the Mn moment by $0.84\mu_{\rm B}$. To compensate this decrease the Co moment changes its sign transforming the magnetic structure from ferrimagnetic to ferromagnetic.

In Fig. 6.2 we present the exchange constants calculated for various lattice spacings. The Co-Co, Ni-Ni exchange interactions as well as the exchange interactions between the moments of the $3d$ atoms and the induced moments of Sb atoms are very weak and are not shown. The weakness of the effective Co-Co and Ni-Ni exchange interactions can be explained by a relatively large distance between atoms and relatively small atomic moments.

On the other hand, each Ni(Co) atom is surrounded by four Mn atoms as nearest neighbors that results in strong Mn-Ni(Co) exchange interaction (Fig. 6.2). Also the exchange interaction between large Mn moments is strong.

The ferromagnetic Mn-Mn interactions are mainly responsible for the stable ferromagnetism of these materials. For both systems and for all lattice spacings studied the leading Mn-Mn exchange interaction is strongly positive. In NiMnSb, the Mn-Ni interaction of the nearest neighbors is positive for all three lattice parameters leading to the parallel orientation of the spins of the Mn and Ni atoms. In CoMnSb the situation is different. At the experimental lattice parameter the leading Mn-Co interaction is negative resulting in the ferrimagnetism of the system. For the contracted lattices the interaction changes sign resulting in the ferromagnetic ground state of the alloy.

The analysis of the strength of the exchange interaction as a function of the lattice parameter shows that in CoMnSb the contraction leads to a strong increase of both leading

Table 6.1: Calculated atom-resolved and total spin moments in $\mu_B$ for NiMnSb, CoMnSb, Co$_2$CrAl and Co$_2$MnSi. All compounds are half-metallic at the experimental lattice constants taken from Ref. [50]. a$_{II}$ means the use of the lattice constant that places the Fermi level at the upper edge of the half-metallic gap and a$_{III}$ corresponds to 1% contraction of the lattice constant with respect to a$_{II}$.

| Compound | a(Å) | X | Y | Z | Void | Total |
|---|---|---|---|---|---|---|
| NiMnSb - a$_{I[exp]}$ | 5.93 | 0.20 | 3.85 | -0.09 | 0.04 | 4.00 |
| NiMnSb - a$_{II}$ | 5.68 | 0.32 | 3.68 | -0.05 | 0.05 | 4.00 |
| NiMnSb - a$_{III}$ | 5.62 | 0.33 | 3.64 | -0.04 | 0.05 | 3.97 |
| CoMnSb - a$_{I[exp]}$ | 5.87 | -0.32 | 3.41 | -0.11 | 0.02 | 3.00 |
| CoMnSb - a$_{II}$ | 5.22 | 0.45 | 2.57 | -0.06 | 0.04 | 3.00 |
| CoMnSb - a$_{III}$ | 5.17 | 0.48 | 2.52 | -0.05 | 0.04 | 2.99 |
| Co$_2$CrAl - a$_{I[exp]}$ | 5.74 | 0.62 | 1.83 | -0.08 | | 3.00 |
| Co$_2$CrAl - a$_{II}$ | 5.55 | 0.69 | 1.68 | -0.06 | | 3.00 |
| Co$_2$CrAl - a$_{III}$ | 5.49 | 0.69 | 1.66 | -0.05 | | 2.99 |
| Co$_2$MnSi - a$_{I[exp]}$ | 5.65 | 0.93 | 3.21 | -0.06 | | 5.00 |
| Co$_2$MnSi - a$_{II}$ | 5.49 | 0.97 | 3.10 | -0.04 | | 5.00 |
| Co$_2$MnSi - a$_{III}$ | 5.43 | 0.97 | 3.01 | -0.04 | | 4.97 |

Mn-Co and Mn-Mn interactions. On the other hand, in NiMnSb the increase of the Mn-Ni interaction is accompanied by a decrease of the leading Mn-Mn interaction. Simultaneously, the interaction between the second-nearest Mn atoms increases with contraction in the case of NiMnSb staying almost unchanged in CoMnSb. This complexity of the behavior reflects the complexity of the electronic structure of the systems.

The interatomic exchange parameters are used to evaluate the Curie temperature within two different approaches: MFA and RPA. In Table 6.2 we present the values of the Curie temperature obtained, first, by taking into account the Mn-Mn interactions only and, second, with account for both Mn-Mn and Mn-Ni(Co) interactions. The contribution of the inter-sublattice interactions to the Curie temperature appears to be less than 5 % for both compounds and the Curie temperature is mainly determined by the intra-sublattice Mn-Mn interaction.

The MFA and RPA estimations of the Curie temperature differ rather strongly (Table 6.2). The relative difference of two estimations is about 20%. The reason behind this difference will be discussed below. For the systems considered here the RPA estimations of the Curie temperatures are in good agreement with the experiment, somewhat overestimating the experimental values.

Recently Kübler [101] reported estimations of the Curie temperature of NiMnSb. His approach is based on the evaluation of the non-uniform magnetic susceptibility on the basis of the Landau-type expansion for the free energy. Within some approximations the parameters
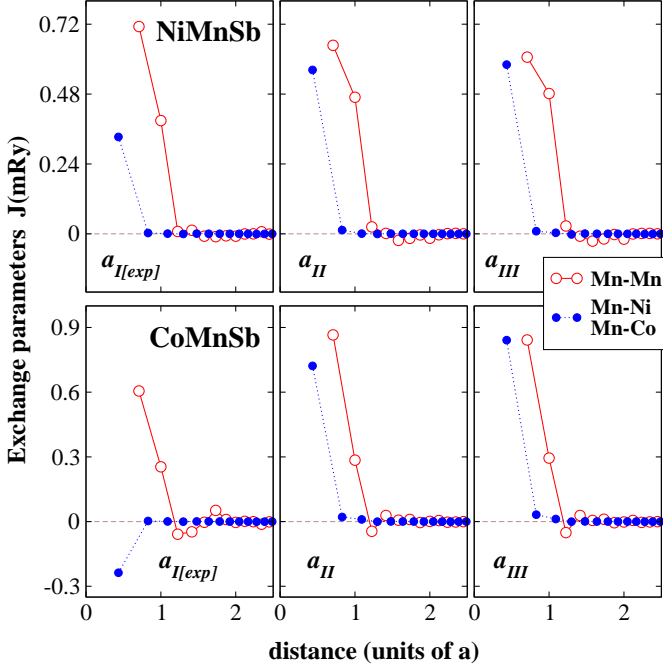
Figure 6.2: The variation of the interatomic exchange parameters for NiMnSb (upper panel) and CoMnSb (bottom panel) as a function of the interatomic distance. The left panel corresponds to the experimental lattice constant, the middle and right panels correspond respectively to $a_{II}$ and $a_{III}$ parameters.

used in the study of the thermodynamical properties can be expressed in terms of the quantities evaluated within the first-principles DFT calculations. The estimated values of the Curie temperature are 601 K for a static approach and 701 K if the frequency dependence of the susceptibility is taken into account. These estimations are somewhat lower than the value of 880 K given by the RPA approach (Table 6.2). A detailed comparative analysis of the two calculational schemes is needed to get an insight in the physical origin of this difference.

The contraction of the lattice in the case of the NiMnSb compound leads to an increase of the Mn-Ni interactions (Fig. 6.2). This results in increased difference between the Curie temperatures calculated with the Mn-Mn interactions only and with both Mn-Mn and Ni-Mn interactions taken into account (Table 6.2). For CoMnSb, the leading exchange interactions of both Mn-Mn and Mn-Co types increase in the value under transition from the experimental lattice constant to $a_{II}$ (Fig. 6.2). As a result, the Curie temperature increases with contraction by about 50%.

- **Co$_2$CrAl and Co$_2$MnSi**

The second group of materials studied in the paper is formed by the full-Heusler compounds Co$_2$MnSi and Co$_2$CrAl. The electronic structure of these systems has been studied earlier [68]. Compared to half-Heusler systems, the presence of two Co atoms per formula unit results in an increased coordination number of Co atoms surrounding Mn atoms (eight instead of four in CoMnSb). This leads to an increased hybridization between the $3d$ orbitals of the Mn and Co atoms. The spin moment of Co in Co$_2$MnSi is about 1 $\mu_B$ that is considerably larger than the Co moment in CoMnSb. In Co$_2$CrAl the Co moment is about 1/3rd smaller than in Co$_2$MnSi that reflects a smaller value of the Cr moment compared to the Mn moment (Table 6.1).

Table 6.2: Calculated Curie temperatures. The second and third columns contain the $T_C^{MFA(RPA)}$ obtained with the account for Mn-Mn (Cr-Cr) interactions only. In the next two columns all interactions are taken into account. The last column presents the experimental values of the Curie temperature from Ref. [50].

| Compound | MFA$_{[Y-Y]}$ | RPA$_{[Y-Y]}$ | MFA$_{[all]}$ | RPA$_{[all]}$ | Exp. |
|---|---|---|---|---|---|
| NiMnSb - a$_{I[exp]}$ | 1096 | 880 | 1112 | 900 | 730 |
| NiMnSb - a$_{II}$ | 1060 | 853 | 1107 | 908 | - |
| NiMnSb - a$_{III}$ | 1008 | 802 | 1063 | 869 | - |
| CoMnSb - a$_{I[exp]}$ | 785 | 619 | 815 | 671 | 490 |
| CoMnSb - a$_{II}$ | 1185 | 940 | 1276 | 1052 | - |
| CoMnSb - a$_{III}$ | 1140 | 893 | 1252 | 1032 | - |
| Co$_2$CrAl - a$_{I[exp]}$ | 148 | 141 | 280 | 270 | 334 |
| Co$_2$CrAl - a$_{II}$ | 168 | 159 | 384 | 365 | - |
| Co$_2$CrAl - a$_{III}$ | 164 | 154 | 400 | 379 | - |
| Co$_2$MnSi - a$_{I[exp]}$ | 232 | 196 | 857 | 740 | 985 |
| Co$_2$MnSi - a$_{II}$ | 142 | 118 | 934 | 804 | - |
| Co$_2$MnSi - a$_{III}$ | 110 | 75 | 957 | 817 | - |

As in the case of the half-Heusler compounds discussed above, the variation of the lattice parameter leads to the change in the position of the Fermi level. At the experimental lattice parameter the Fermi level of Co$_2$CrAl lies in the lower part of the half-metallic gap while for Co$_2$MnSi it is close to the middle of the gap (Fig. 6.1b). The contraction of the lattice needed to place the Fermi level at the upper edge of the gap is smaller than for CoMnSb. As a result, the change in the magnetic moments is also relatively weak (Table 6.1).

The presence of an extra Co atom in the full-Heusler alloys makes the interactions more complex than in the case of the half-Heusler alloys. In CoMnSb the important interactions arise between nearest Mn atoms (Mn-Mn interactions) and between nearest Mn and Co atoms (Mn-Co interaction). In the case of Co$_2$MnSi (Fig. 6.3) the interactions between Co atoms at the same sublattice (Co-Co) and between Co atoms at different sublattices (Co$^1$-Co$^2$) must be taken into account. The cobalt atoms at different sublattices have the same local environment rotated by $90^o$ about the [001] axis. The leading interaction responsible for the stability of the ferromagnetism is the Mn-Co interaction between Mn atoms and eight nearest Co atoms (Fig. 6.3). This interaction changes weakly with the contraction of the lattice. Our exchange parameters agree well with the parameters of Kurtulus *et al.* (Fig. 6.3) who also found the Co-Mn exchange interaction to be leading [124].

The interaction between nearest Co atoms at different sublattices (filled green spheres in Fig. 6.3) favors the ferromagnetism also and is stronger than the ferromagnetic interaction between the nearest Mn atoms (empty spheres). Although the spin moment of Mn atoms
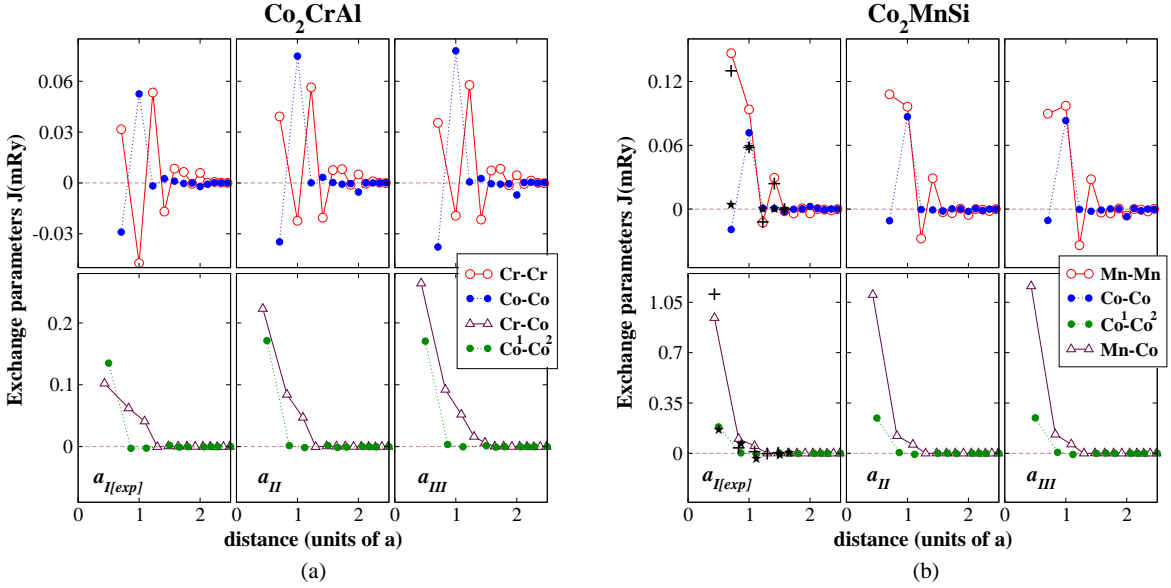
Figure 6.3: (a) The exchange constants for Co₂CrAl as a function of the interatomic distance. (b) The same for Co₂MnSi. The left panels correspond to the experimental lattice constant, the middle and right panels to $a_{II}$ and $a_{III}$ parameters respectively. The superscripts 1 and 2 denote Co atoms belonging to different sublattices. For comparison, the exchange parameters of Co₂MnSi obtained in Ref. [124] at the experimental lattice parameter ($a_{I[exp]}$) are shown. The following symbols are used in the presentation: + for the Mn-Mn and Mn-Co interactions and ⋆ for the Co-Co and Co¹-Co² interactions.

is larger than the moment of Co atoms (Table 6.1) the opposite relation between exchange parameters can be the consequence of the smaller distance between the Co atoms: $a/2$ between the Co atoms and $\sqrt{2}a/2$ between the Mn atoms. An interesting feature of the intra-sublattice Mn-Mn and Co-Co interactions is different signs of the exchange parameters for different distances between atoms. This leads to a RKKY-like oscillations of the parameters (Fig. 6.3).

In Co₂CrAl the leading Cr-Co interactions (empty triangles) are much smaller than corresponding Mn-Co interactions in Co₂MnSi. On the other hand, the leading inter-sublattice ferromagnetic Co-Co interactions are comparable in both systems. The compression of the lattice leads to an increase of the magnitude of the inter-sublattice Co-Cr and Co¹-Co² coupling. The intra-sublattice Cr-Cr and Co-Co interactions oscillate with varying inter-atomic distances.

The difference in the properties of the exchange parameters of the half- and full-Heusler alloys is reflected in the calculated Curie temperatures (Table 6.2). In contrast to CoMnSb where the Mn-Mn exchange interactions are dominant, in Co₂MnSi they play a secondary role. The $T_C^{MFA(RPA)}$ calculated taking into account these interactions only is much smaller than the Curie temperature calculated with all inter-atomic exchange interactions taken into account (Table 6.2). The same conclusion is valid for Co₂CrAl where the Cr-Cr interactions give about half of the Curie temperature obtained with all interactions included into
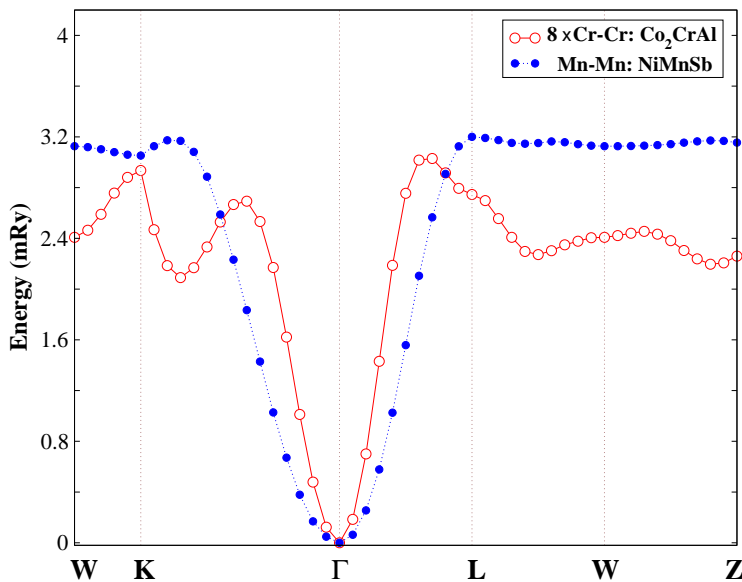
Figure 6.4: The frozen-magnon dispersions for NiMnSb and Co$_2$CrAl along the symmetry lines in the Brillouin zone. The magnons correspond to the Mn sublattice in the case of NiMnSb and to the Cr sublattice in the case of Co$_2$CrAl. For Co$_2$CrAl, the frozen-magnon energies are multiplied by a factor of 8.

consideration.

A striking feature of the full Heusler compound Co$_2$CrAl that differs it strongly from the half-Heusler systems considered in the previous Section is a very small difference between the $T_C$ values calculated within the MFA and RPA approaches. A similar behavior was obtained for the Curie temperatures of the zincblende MnSi and MnC [102]. In Co$_2$MnSi, the relative difference of the MFA and RPA estimations assumes an intermediate position between the half-Heusler systems and Co$_2$CrAl.

To understand the origin of the strong variation of the relative difference of the MFA and RPA estimations of the Curie temperature we compare in Fig. 6.4 the frozen magnon dispersions for two compounds. The magnons correspond to the Mn sublattice in the case of NiMnSb and to the Cr sublattice in the case of Co$_2$CrAl. As seen from Table 6.2 the MFA and RPA estimations obtained with the use of these dispersions differ by 20% for NiMnSb and by 5% for Co$_2$CrAl.

The Curie temperature is given by the average value of the magnon energies. In MFA this is the arithmetic average while in RPA this is harmonic average. Therefore we need to understand why for Co$_2$CrAl these two averages are much closer than for NiMnSb. The following properties of the averages are important for us. The arithmetic average takes all the magnon values with equal weight whereas in the harmonic average the weight decreases with increasing energy of the magnon. It is an arithmetic property that the MFA estimation is larger than the RPA one or equal to it if all numbers to be averaged are equal to each other. In terms of magnon energies, $T_C^{MFA}$ is equal to $T_C^{RPA}$ in the case that the magnon spectrum is dispersion-less.

Considering the frozen-magnon dispersions from the viewpoint of these properties we indeed can expect that the arithmetic and harmonic averages will be closer for Co$_2$CrAl. In Fig. 6.4 both curves are scaled to have almost the same maximal value. It is seen that

the Co$_2$CrAl dispersion has smaller relative contribution of the low-energy magnons because of the steeper increase of the curve at small wave vectors. It has also smaller contribution of the magnons with the largest energies because the maxima have the form of well-defined peaks opposite to NiMnSb where we get a plateau. Thus the main contribution in the case of Co$_2$CrAl comes from intermediate energies that makes the MFA and RPA estimations closer.

Coming back to the considerations of the Curie temperatures, we conclude that, in general, the Curie temperatures of Co$_2$MnSi and Co$_2$CrAl calculated within both MFA and RPA are in good agreement with experiment while the MFA values in the case of NiMnSb and CoMnSb overestimate the Curie temperature strongly.

The lattice contraction leads in both compounds to an enhancement of the Mn-Co(Cr-Co) exchange constants that results in an increase of the Curie temperature.

Kurtulus and collaborators have calculated the Curie temperature for Co$_2$MnSi within MFA and found the value of 1251 K that is considerably larger than our MFA estimate of 857 K. This difference is unexpected since the values of the exchange parameters obtained by Kurtulus *et al.* agree well with our parameters (Fig.6.3). To reveal the origin of the discrepancy we performed the MFA calculation of the Curie temperature with the exchange parameters of Kurtulus *et al.* and obtained the $T_C$ value of 942 K which is in reasonable agreement with our estimate. Apparently the reason for the inconsistency is in the procedure of the solving of the multiple-sublattice MFA problem used by Kurtulus *et al.* that should deviate from the standard one [34].

### 6.2.2   Spin-wave spectra

In Fig. 6.5 we present the calculated spin-wave spectra for NiMnSb and Co$_2$CrAl. The spin-wave energies are obtained by the diagonalization of the matrix of exchange parameters that contains all important intra- and inter-sublattice interactions. The number of branches in the spectrum is equal to the number of magnetic atoms in the unit cell: two in NiMnSb and three in Co$_2$CrAl. One of the branches is acoustic and has zero energy for zero wave vector. Also in the spin-wave spectra, we see strong difference between two systems. In NiMnSb, the acoustic branch is predominantly of the Ni type stemming from the weak interaction between Mn and Ni magnetic moments (see Fig. 6.2). On the other hand, the optical branch is of predominantly the Mn type. The strong hybridization between two sublattices is obtained only about $\mathbf{q} = 0$. In Co$_2$CrAl, the energy scale of the branches differs much smaller and the hybridization between sublattices is stronger than for NiMnSb.

### 6.2.3   Temperature dependence of the magnetization

In this section we will present the results of the calculation of the temperature dependence of magnetization that is based on the consideration of the Heisenberg hamiltonian with exchange parameters calculated within a parameter-free DFT approach. To calculate the temperature dependence of the magnetization we use the RPA method as described in chapter 3. We
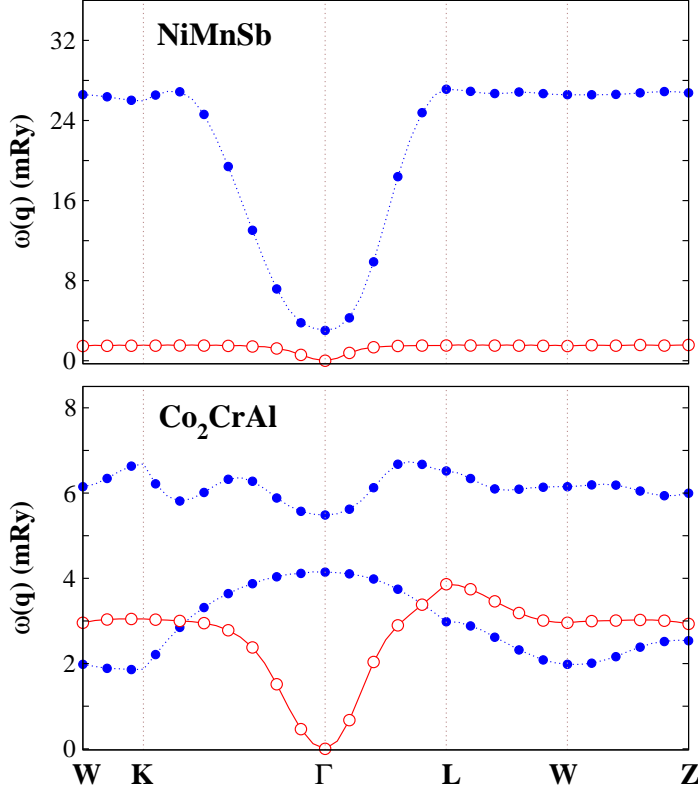
Figure 6.5: The spin wave dispersions for NiMnSb and Co$_2$CrAl along the symmetry lines in the Brillouin zone. Filled and empty spheres denote the acoustic and optical branches, respectively.

consider both classical-spin and quantum-spin cases.

In the classical-spin calculations the calculated values of the magnetic moments (Table 6.1) are used. To perform quantum-mechanical RPA calculation we assign integer values to the atomic moments. In the semi Heusler compounds we ignore the induced moments on Ni and Co atoms and assign the whole moment per formula unit to the Mn atom: $4\mu_B$ ($S = 2$) in NiMnSb and $3\mu_B$ ($S = 3/2$) in CoMnSb. In Co$_2$MnSi we take the values of $3\mu_B$ ($S = 3/2$) and $1\mu_B$ ($S = 1/2$) for Mn and Co atoms respectively. This assignment preserves the value of the total spin moment per chemical unit. In Co$_2$CrAl we use in the quantum-RPA calculations the atomic moment of $2\mu_B$ ($S = 1$) for Cr and $1\mu_B$ ($S = 1/2$) for Co.

In Fig. 6.6(a), we present in the normalized form the calculated temperature dependence of the magnetization for both families of Heusler compounds. The calculations are performed for the experimental lattice parameter. For comparison, the experimental curves are presented. The nature of the spin (quantum or classical) influences the form of the curves considerably. The classical curve lies lower than the quantum one. This results from a faster drop of the magnetization in the low-temperature region in the case of classical spins. In general, the quantum consideration gives better agreement of the form of the temperature dependence of the magnetization with experiment.

In Fig. 6.6(b) we present the temperature dependence of the magnetization of individual sublattices. As expected from the previous discussions in half-Heusler systems the main contribution to the magnetization comes from the Mn sublattice while for the full-Heusler
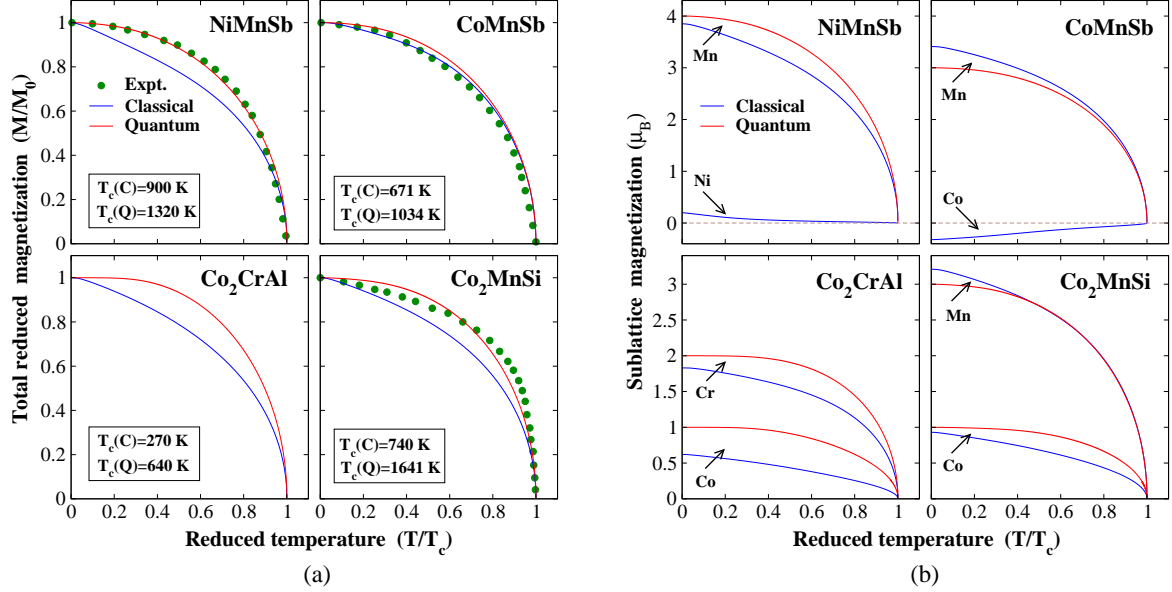
Figure 6.6: (a) The calculated temperature dependence of the total magnetization for both families of Heusler alloys. For comparison the experimental temperature dependencies [50, 51] are presented. The calculations are performed for both classical and quantum Hamiltonians. Both the magnetization and the temperature are given in reduced form. (b) Calculated sublattice magnetizations as a function of temperature. The temperature is given in reduced form.

systems both $3d$ atoms contribute substantially.

Considering the calculated Curie temperatures we notice that the value of $T_C$ calculated within the quantum-mechanical RPA is substantially larger than the corresponding classical estimation (see Fig. 6.6). This property is well-known and has its mathematical origin in the factor $(S+1)/S$ entering the RPA expression for the Curie temperature. In Fig. 6.7 we show the dependence of the Curie temperature calculated within the quantum mechanical RPA approach on the value of $S$. The exchange parameters are kept unchanged in these calculations. We see that the dependence has a monotonous character tending to a classical limit for large $S$.

Presently we do not have an explanation why quantum-mechanical calculations give better form of the temperature dependence while the classical calculation provides better value of the Curie temperature. We can suggest the following arguments. The quantum treatment is more appropriate than the classical one in the low-temperature region. At high temperatures characterized by strong deviation of the atomic spins from the magnetization axis the quantum treatment gives too slow decrease of the magnetization. It is worth noting that the consequent theory should take into account not only the orientational disorder of the atomic moments but also the single-particle (Stoner-type) excitations leading to the decrease of atomic moments. Another important aspect is related to the fact that the exchange parameters used in the calculations are estimated within the picture of classical atomic moments described above. It is possible that the values of the exchange parameters must be modified
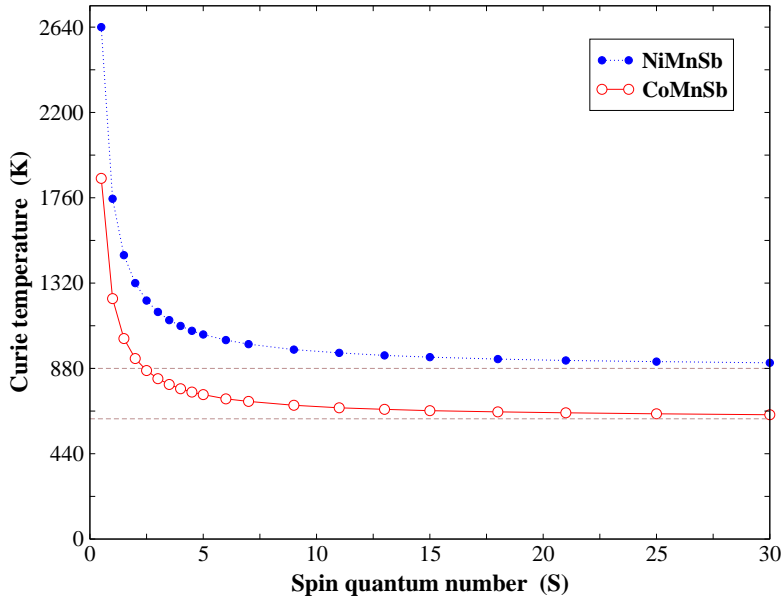
Figure 6.7: Curie temperature of NiMnSb and CoMnSb as a function of spin quantum number $S$. The horizontal broken lines correspond to the classical limit ($S = \infty$).

for the use in the quantum-mechanical case. These questions belong to fundamental problems of the quantum-mechanical description of the magnetic systems with itinerant electrons.

## 6.3 Competing Mn-Mn exchange interactions in ferrimagnetic Mn$_2$VZ (Z = Al, Ge) compounds

Half-metallic ferrimagnetic materials, like FeMnSb or the Mn$_2$VAl compounds, are much more desirable than their ferromagnetic counterparts in magnetoelectronics applications. This is mostly due to the fact that the small value of the total magnetic moment in these systems provides additional advantageous. For example they do not give rise to strong stray fields in devices or are less affected by the external magnetic fields.

The ideal case for applications would be a half-metallic antiferromagnet like CrMnSb. It is a special antiferromagnet in the sense that the majority spin and minority spin densities of states are not identical, as for common antiferromagnets and the material is better described as a fully compensated ferrimagnet, having a magnetic moment that is, due to the half-metallic character, precisely equal to zero. Such a half-metallic antiferromagnet would be a very interesting magnetoelectronics material since it would be a perfectly stable spin-polarized electrode in a junction device. And moreover if used as a tip in a spin-polarized STM, it would not give rise to stray flux, and hence would not distort the domain structure of the soft-magnetic systems to be studied. Unfortunately, CrMnSb does not crystallize in the ordered C1$_b$ crystal structure adopted by the semi-Heusler alloys. However, these results show that such an important magnetoelectronics material could exist. Van Leuken and de Groot have recently suggested a possible route towards a half-metallic antiferromagnet starting from the semiconducting C1$_b$-type compound FeVSb [103]. It is isoelectronic with the non-existing half-metallic antiferromagnet CrMnSb. A 12.5% substitution of Mn for V,

Table 6.3: Lattice parameters, magnetic moments (in $\mu_B$) and mean-field estimation of the Curie temperatures for Mn$_2$VZ (Z= Al, Ge). The second (third) column gives the Curie temperature calculated with account for Mn-Mn (Mn-V) interactions only. In the fourth column both types of interactions are taken into account. The experimental value of Curie temperature for Mn$_2$VAl is taken from Ref.[50].

| | $a$(Å) | Mn | V | Z | Cell | MF$_{[Mn\text{-}Mn]}$ | MF$_{[Mn\text{-}V]}$ | MF$_{[all]}$ | Exp |
|---|---|---|---|---|---|---|---|---|---|
| Mn$_2$VAl | 5.93 | 1.53 | -1.02 | -0.03 | 2.00 | 30 | 623 | 638 | 760 |
| | 5.87[a] | 1.50[a] | -0.90[a] | -0.10[a] | 2.00[a] | | | | |
| | 5.93[b] | 1.41[b] | -0.79[b] | -0.02[b] | 2.02[b] | | | | |
| | 5.92[c] | | | | 1.94[c] | | | | |
| Mn$_2$VGe | 6.09 | 1.00 | -0.97 | -0.04 | 1.00 | -170 | 488 | 413 | - |
| | 5.93[b] | 0.75[b] | -0.48[b] | -0.02[b] | 1.00[b] | | | | |

[a]Ref.[106]
[a]Ref.[68]
[c]Ref.[104]

and (in order to keep the system isoelectronic, In for Sb) was predicted to already yield half-metallic ferrimagnetism, with local Mn moments of about 2.3 $\mu_B$ and a band gap of about 0.35 eV.

Here we consider experimentally well established Mn$_2$VAl compound and theoretically predicted Mn$_2$VGe compound. The latter one close to ideal case. Both systems have half-metallic ferrimagnetic ground state. Mn$_2$VGe is not yet synthesized. On the other hand, Mn$_2$VAl received much experimental and theoretical attention. The neutron diffraction experiment by Itoh *et al.* [40] gave the ferrimagnetic state of compound with Mn magnetic moment of $1.5\pm0.3\mu_B$ and V moment $-0.9\mu_B$. Jiang *et al.* examined the magnetic structure of Mn$_2$VAl by X-ray diffraction and magnetization measurements [104]. They found that Mn$_2$VAl was nearly half-metallic with the total magnetic moment of $1.94\mu_B$ at 5 K. The Curie temperature of the sample was found to be about 760 K and the loss of half-metallic character was attributed to the small amount of disorder. The electron structure calculation by Ishida *et al.* performed within the local-density approximation (LDA) to the density functional theory resulted in a ground state of Mn$_2$VAl close to half-metallicity [105]. Recently a detailed theoretical study of the magnetism of Mn$_2$VAl was reported by Weht and Pickett [106] who used the generalized gradient approximation (GGA) for the exchange correlation potential and have shown that Mn$_2$VAl is a half-metallic ferrimagnet with the atomic moments of $1.5\mu_B$ and $-0.9\mu_B$ on Mn and V in very good agreement with experiment. The Fermi level was found to lie in the minority spin band.

Our main purpose here is a detailed study of the exchange interactions in two half-metallic Mn$_2$VZ compounds: Mn$_2$VAl and Mn$_2$VGe. It is shown that the pattern of exchange interactions in these systems deviates from the physical picture that can be expected on the basis

of the experimental information available [107]. Indeed, the Mn-Mn distance of 2.96Å(3.04Å)
in Mn$_2$VAl (Mn$_2$VGe) is substantially smaller than the Mn-Mn distance of about 4.2Å in the
X$_2$MnZ-type Heusler alloys [50]. (For Mn$_2$VGe we use the interatomic distance of Mn$_2$VGa
[108]). On the other hand, it is comparable with the Mn-Mn distance in the antiferromag-
netic fcc Mn (2.73Å) [109]. According to the Bethe-Slater curve [110] there are physical
reasons to expect that smaller distances between the 3$d$ atoms stimulate the formation of
the antiferromagnetic structure whereas larger distances make the ferromagnetic structure
energetically preferable. Among the Heusler alloys, a smaller distance between pairs of the
Mn atoms is obtained in the case of random occupation by Mn and Z atoms of the Y and Z
sublattices (see, e.g., the system with the B2-type crystal structure in Ref. [50]). Indeed, the
experiment gives for such systems the antiferromagnetic ordering [50]. Therefore in the case
of Mn$_2$VAl an antiferromagnetism of the two Mn sublattices can be expected. Our study
shows, however, that the situation is more complex. Although a large magnetic moment
is carried by Mn atoms, competing ferromagnetic (inter sublattice) and antiferromagnetic
(intra sublattice) Mn-Mn interactions in Mn$_2$VAl almost cancel each other in the mean-field
experienced by the Mn atoms. In Mn$_2$VGe the leading Mn-Mn exchange interaction is an-
tiferromagnetic. In both compounds the ferromagnetism of the Mn subsystem is favored by
strong antiferromagnetic Mn-V interactions.

The crystal structure is presented in chapter 4. The two Mn sublattices are equivalent.
The nearest Mn atoms belong to two different sublattices. In Table 6.3 we present calculated
magnetic moments. For comparison, the available experimental values of the moments and
the results of previous calculations are given. The net magnetic moment per unit cell is 2$\mu_B$
for Mn$_2$VAl and 1$\mu_B$ for Mn$_2$VGe. The magnetic alignment is ferrimagnetic in both systems.
The Mn moments are parallel and assume the values close to 1.5 $\mu_B$ in Mn$_2$VAl and to 1 $\mu_B$
in Mn$_2$VGe. The moment of V is close to $-1\mu_B$ in both systems. The values of the moments
are in agreement with the results of previous calculations.

- **Exchange parameters and Curie temperature**

The calculated Heisenberg exchange parameters are presented in figure 6.8. We obtained a
strong dependence of the pattern of the Mn-Mn and V-V exchange interactions on the type
of the Z atom. Actually, this is an expected result on the basis of our theoretical findings for
the exchange mechanism in Heusler alloys presented in previous chapter. The nearest Mn-
Mn distance is half of the lattice constant $a$. The exchange interaction between the nearest
Mn atoms is ferromagnetic (Fig. 6.8) for both compounds while second nearest neighbor
interaction is antiferromagnetic. In both systems substantial Mn-Mn interactions reach only
fourth nearest neighbor and show RKKY-type oscillations.

If only Mn-Mn exchange interactions are considered, in Mn$_2$VAl prevail ferromagnetic
interactions while in Mn$_2$VGe the Mn-Mn dominate antiferromagnetic interactions. The
corresponding Curie and Néel temperature are given in table 6.3.

The interactions between V atoms are very small and can be neglected. The formation of
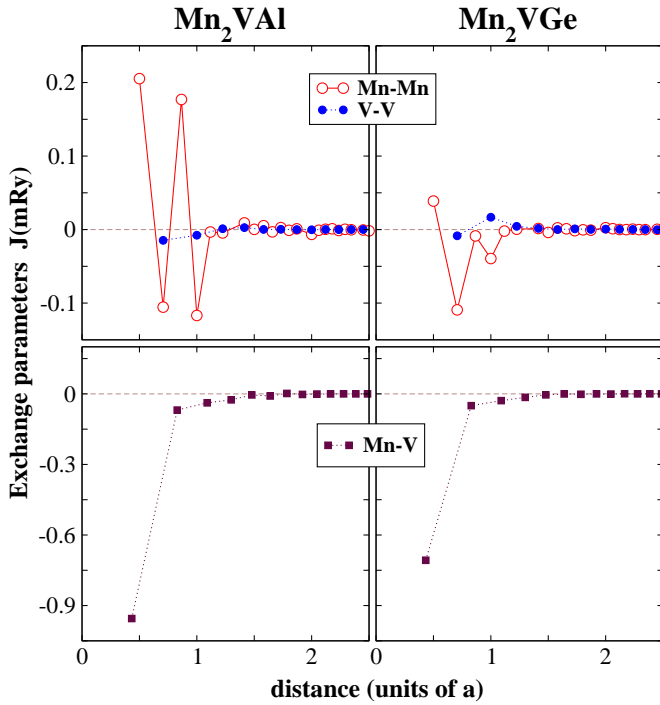
Figure 6.8: Upper panel: Mn-Mn and V-V exchange interactions in $Mn_2VZ$ (Z=Al and Ge) as a function of the distance given in units of the lattice constant. Lower panel: The same for Mn-V intersublattice exchange interactions.

the ferrimagnetic structure with all Mn moments being parallel to each other and the V moments directed oppositely is determined by the strong antiferromagnetic exchange interactions between the nearest Mn and V moments. In $Mn_2VAl$ this interaction is 5 times larger than the nearest neighbor Mn-Mn interaction. In $Mn_2VGe$ this factor increases to 10. The strong Mn-V antiferromagnetic coupling makes a parallel direction of the Mn moments surrounding a V atom energetically preferable leading to the ferromagnetism of the Mn sublattices. In $Mn_2VGe$ this trend overcomes the direct antiferromagnetic Mn-Mn interaction.

In the 8th column of Table 6.3 we present the Curie temperature calculated with the Mn-Mn exchange interaction being neglected. The Curie temperature given in the last column takes into account both Mn-V and Mn-Mn interactions. It is clearly seen that the main contribution for both systems comes from the Mn-V interaction. In $Mn_2VAl$, the correction of $T_C$ due to the Mn-Mn exchange interaction is positive and very small. In $Mn_2VGe$, it is negative and amounts to 15%.

In $Mn_2VAl$, where the experimental estimation of the Curie temperature is available, both the theoretical and experimental values are in good agreement. The theoretical Curie temperature of $Mn_2VGe$ should be considered as prediction.

## 6.4  Prediction of high $T_c$ in NiVAs and NiCrZ (Z = P, Se, Te) compounds

In recent years, the first-principles calculations have become established as a complementary tool to experiments in the design of new materials. In this section we illustrate this in the

Table 6.4: Lattice parameters, magnetic moments (in $\mu_B$) and MFA and RPA estimations of the Curie temperatures for NiVAs, NiCrZ (Z=P, Se, Te) and NiMnSb. The last column represents the relative difference of the MFA and RPA estimations.

|  | $a(\text{Å})$ | Ni | V,Cr,Mn | Void | Z | Cell | MFA | RPA | $[\frac{MFA-RPA}{RPA}]$ |
|---|---|---|---|---|---|---|---|---|---|
| NiVAs | 5.85 | -0.02 | 2.05 | 0.06 | -0.09 | 2.0 | 723 | 603 | % 20 |
|  | $5.87^{(a)}$ | -0.03 | 2.06 | 0.06 | -0.09 | 2.0 | 715 | 595 | % 20 |
| NiCrP | 5.59 | -0.01 | 3.08 | 0.07 | -0.15 | 3.0 | 1030 | 848 | % 21 |
|  | $5.65^{(b)}$ | -0.06 | 3.16 | 0.06 | -0.16 | 3.0 | 938 | 770 | % 22 |
| NiMnSb | 5.93 | 0.19 | 3.86 | 0.04 | -0.10 | 4.0 | 1096 | 880 | % 24 |
| NiCrSe | 5.64 | 0.24 | 3.64 | 0.12 | -0.01 | 4.0 | 537 | 508 | % 6 |
|  | $5.65^{(b)}$ | 0.23 | 3.65 | 0.12 | -0.01 | 4.0 | 543 | 515 | % 5 |
| NiCrTe | 5.84 | 0.24 | 3.68 | 0.11 | -0.03 | 4.0 | 868 | 805 | % 8 |
|  | $5.87^{(a)}$ | 0.23 | 3.70 | 0.11 | -0.03 | 4.0 | 874 | 812 | % 8 |

[a] Lattice constant of InP

[b] Lattice constant of GaAs

case of Ni-based half-metallic semi-Heusler compounds NiCrZ (Z = P, Se, Te) and NiVAs by calculating the magnetic phase transition temperatures. Our aim is to provide a guideline for experimental work, stimulating the fabrication of these new materials.

These systems were recently predicted to be half-metals [111, 112]. For each compound we performed calculations for two values of the lattice parameter (Table 6.4): the theoretical equilibrium parameter [111, 112] and the lattice parameter of a binary semiconductor that can be considered as a possible substrate for growing the corresponding Heusler alloy: GaAs for NiCrP and NiCrSe and InP for NiVAs and NiCrTe.

The two lattice parameters used in the calculations resulted for all systems in very similar physical properties (see, e.g., Table 6.4). Therefore the most of the results will be presented for one lattice constant. All the discussion in this section is valid for both lattice spacings.

- **DOS and magnetic moments**

In Fig. 6.9, we present the calculated electron densities of states (DOS) of the ferromagnetic phases of the four Heusler compounds. All systems are found to be half-metallic with the Fermi level lying in the semiconducting gap of the minority-spin channel. Our DOS are in good agreement with the DOS obtained in Refs.[111, 112].

In Table 6.4, the calculated magnetic moments are collected. Since the systems are half-metallic, the magnetic moments per formula unit are integer: $2\mu_B$ for NiVAs, $3\mu_B$ for NiCrP and $4\mu_B$ for NiCrSe and NiCrTe. The major part of the magnetic moment comes from the second formula atom (V,Cr). Small induced magnetic moments are found on Ni and *sp* atoms.
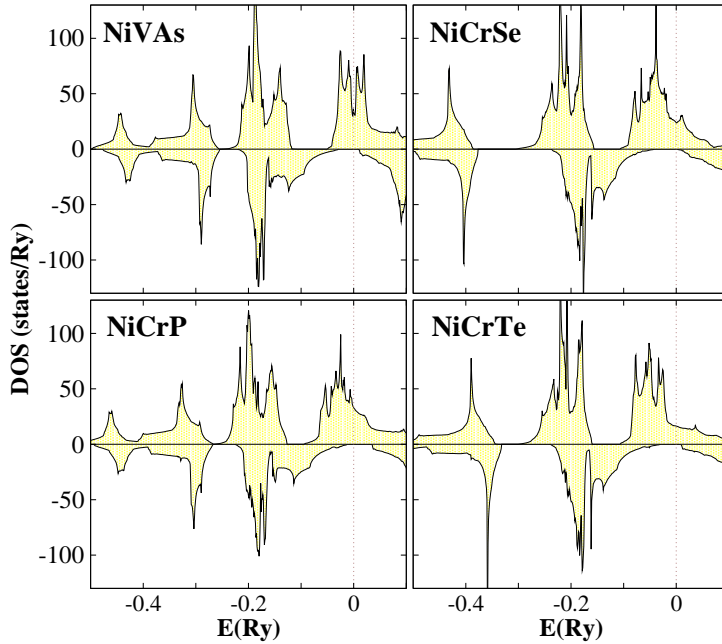
Figure 6.9: Spin-projected density of states of NiVAs and NiCrZ (Z=P, Se, Te).

### 6.4.1 Frozen-magnon dispersions and exchange parameters

Figure 6.10(a) presents the frozen-magnon dispersion for NiCrZ (Z=P, Se, Te) and NiVAs. To compare we show the results for NiMnSb as well. The five systems can be subdivided into two groups. One group contains NiVAs, NiCrP and NiMnSb. Here the frozen-magnon dispersions are monotonous and resemble, visually, a simple cosinusoid. The second group contains NiCrSe and NiCrTe and is characterized by non-monotonous dispersions with a maximum close to the center of the q-interval (Fig. 6.10a). Note, that the $sp$ elements (the third chemical-formula constituents) within each of the group belong to the same column of the Mendeleev's table whereas for different groups these columns are different. The importance of the valency of the $sp$ element for magnetic properties of Heusler alloys has been already observed in our earlier studies (see previous chapter).

The calculated exchange parameters are given in Fig. 6.10(b). Since the inter-atomic exchange parameters are the Fourier transforms of the frozen-magnon dispersions they reflect the properties of the dispersions: The exchange parameters belonging to the same group show similar qualitative behavior. On the other hand, there is strong difference between the systems belonging to different groups (Fig. 6.10(b)). In the first group (Fig. 6.10(b), left panel), the strongest exchange interaction takes place between nearest magnetic $3d$ atoms. This strongest interaction determines the cosinusoidal form of the corresponding magnon dispersion. The sizable interaction between the second-nearest magnetic $3d$ atoms describes the deviation of the dispersion from a simple cosinusoid.

In the second group of compounds (Fig. 6.10(b), right panel), the strongest interaction is between the second-nearest magnetic atoms. Because of the decreased period of the Fourier component corresponding to the second exchange parameter the dispersions are nonmonotonous and have the maximum not at the boundary of the Brillouin zone but inside
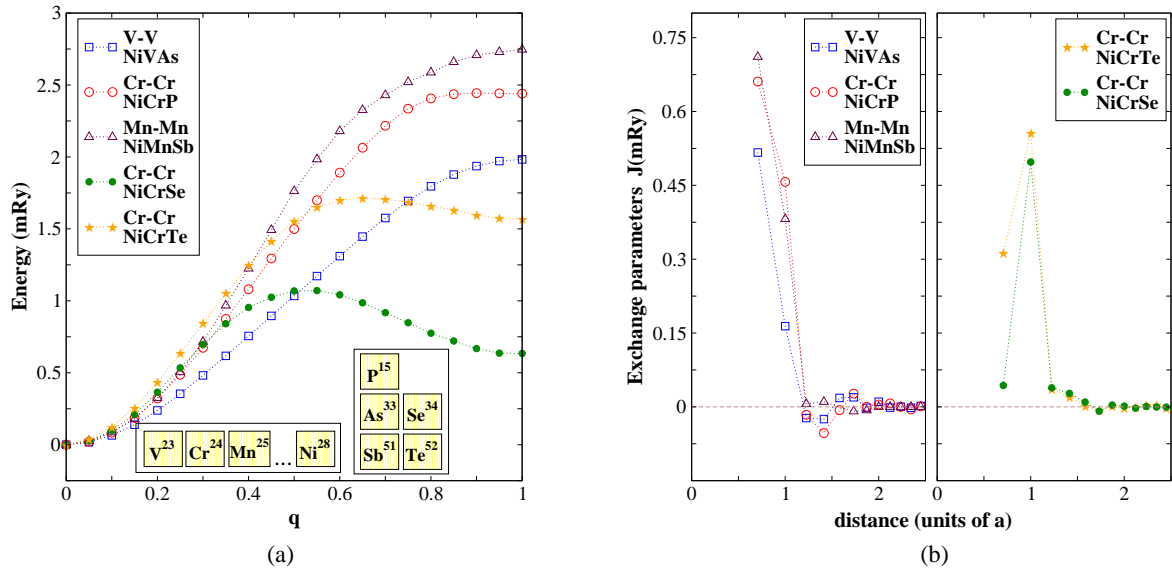
Figure 6.10: (a) Frozen-magnon dispersions for NiVAs, NiMnSb and NiCrZ (Z=P, Se, Te). The spectrum is shown for [0 0 q] direction in the reciprocal space. The wave vector is given in the units of $2\pi/a$. In the calculations only the V-V, Cr-Cr and Mn-Mn interactions were taken into account. (b) Interatomic exchange interactions. The calculational data for NiVAs and NiCrZ are presented for the theoretical equilibrium lattice constant.

of it.

A remarkable feature of the exchange interactions is their short range character: the leading contribution into the Curie temperature of all systems is provided by the interactions within the first two coordination spheres. The interactions with further coordination spheres are very weak and can be neglected in the calculation of the Curie temperature. The interactions between Ni atoms and the interactions of Ni with V and Cr are very weak and are not presented.

- **Curie temperature**

The calculated exchange parameters are used to evaluate the Curie temperature (Table 6.4). It is important to note that the similarity of the form of the magnon dispersions within one group of compounds is not accompanied by a quantitative closeness of the curves (Fig. 6.10a). Therefore the Curie temperatures can differ strongly for compounds belonging to the same group.

The Curie temperatures are estimated within two different schemes: MFA and RPA. For all systems and for both theoretical schemes the calculated Curie temperatures are substantially higher than room temperature. The MFA always gives the value of $T_c$ that is larger than the corresponding RPA value and usually overestimates the experimental Curie temperature.

The analysis of the calculational data allows to make a number of important conclusions. First, there is a strong influence of the $sp$ atom on the value of $T_c$. Indeed, the comparison of NiCrSe and NiCrTe that differ by the $sp$ atom shows that the Curie temperature changes

from about 500 K in NiCrSe to about 800 K in NiCrTe. This strong dependence reveals the sensitivity of the exchange interactions and the Curie temperature to the details of the electron structure.

An interesting feature of the calculated Curie temperatures (Table 6.4) is a large difference between the MFA and RPA estimations for the first group of compounds in contrast to a small difference for the second group. Characterizing the relative difference of the MFA and RPA values of the Curie temperature by the relation $[T_c^{MFA} - T_c^{RPA}]/T_c^{RPA}$ we get for the first group of compounds a large value of 20-24% compared to a small value of 5-8% for the second group. This feature reflects the properties of the corresponding frozen-magnon spectra.

From Fig. 6.10(a) we see that the frozen-magnon curves of the second group of compounds are flat in the second half of the $\mathbf{q}$ interval demonstrating here very weak dispersion. On the other hand, the first group of compounds have considerable dispersion in this part of the $\mathbf{q}$ interval. In addition, the low-$\mathbf{q}$ part of the curves for the second group of compounds lie higher than the corresponding part of the curves for the first group. Therefore, the relative contribution of the low-energy magnons to the RPA value of the Curie temperature is smaller in the second group of compounds. This combination of features of the wave-vector dependencies of the frozen-magnon energies is responsible for a larger difference between the RPA and MFA estimations of the Curie temperature of the first group of compounds.

### 6.4.2 Curie temperature and half-metallicity

An important question concerning the magnetism of the half-metallic systems is the relation between half-metallicity and Curie temperature. Indeed, a number of studies has shown that the half-metallicity can stimulate an increase of the Curie temperature [101, 113, 114]. The analysis of Fig. 6.11 allows us to establish a correlation between the value of the Curie temperature and the energy distance $\delta$ between the Fermi level and the upper edge of the semiconducting gap. This quantity determines the spacing between the highest occupied spin-up state and the lowest empty spin-down state. For very small $\delta$ of 0.03 eV in NiCrSe we obtained the lowest Curie temperature of 508 K. On the other hand, for large $\delta$ in NiCrP and NiMnSb we obtained the Curie temperature substantially above 800 K.

Since the value of the Curie temperature is determined by the magnetic excitations to interpret the $\delta - T_C$ correlation we need to understand the origin of the influence of the $\delta$ value on the spin-wave energies.

The magnon energies reflect the energy prize for the deviations of the atomic moments from parallel directions [6]. In the ground-state ferromagnetic configuration the spin-projection is a good quantum number and the electron states with opposite spin projections do not interact. The deviation of the atomic moments from parallel directions leads to the mixing of the majority-spin and minority-spin states. The hybridization of a pair of the states leads to their repulsion. As a result, the energy of the lower state decreases (bonding state) and the energy of the upper state increases (antibonding state). If the lower state is occupied and the
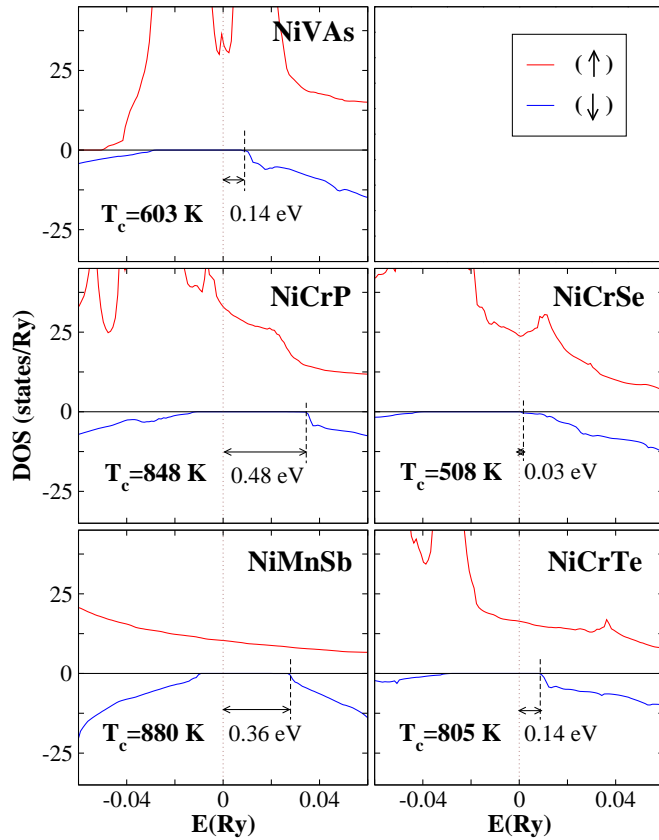
Figure 6.11: Spin-projected density of states of NiVAs, NiCrP, NiMnSb, NiCrSe and NiCrTe near Fermi level. Also shown are the RPA estimations of the Curie temperature and the energy distances between the Fermi level and the bottom of the spin-down conduction band.

upper state is empty this process leads to the decrease of the energy of the magnon making ferromagnetic state energetically less favorable. The smaller is the energy distance between interacting states the stronger is the effect.

Coming back to the half-metallic compounds considered in the paper we note that the hybridizational interaction of this type takes place between the occupied majority-spin states below the Fermi level and the empty spin-down states at the bottom of the conduction band. The distance between these states is given by parameter $\delta$. Therefore this process provides a mechanism for the correlation between $\delta$ and Curie temperature.

Since the strength of the hybridizational repulsion increases with decreasing energy distance between interacting states the negative contribution to the spin-wave energies is larger in the case of smaller $\delta$. However, the correlation between parameter $\delta$ and $T_C$ or, more general, between the half-metallicity and $T_C$ should not be considered as a universal rule. The hybridizational repulsion considered above is only one of numerous processes arising in a complex multi-band system with the deviation of the atomic moments from the parallel directions. The combined result of these processes cannot be predicted without the direct calculation of the excitation energies. Such a calculation must take into account the complexity of the electron structure of a real system. Indeed, the comparison of NiVAs and NiCrTe shows that both systems have the same $\delta$ of 0.14eV. However, their Curie temperatures differ strongly.

# Chapter 7

# Effect of Pressure on Magnetic Properties of Heusler Alloys

The understanding of the magnetic properties of transition metals and their alloys is one of the chief aims of the theory of itinerant magnetism. The pressure dependence of the Curie temperature in ferromagnetic systems provides an important information in this respect and is an object of intensive studies both experimental and theoretical. The key question here is the character of the variation of various magnetic properties with decreasing distances between magnetic atoms. Considering $Ni_2MnSn$ Heusler compound as an example we study pressure dependence of electronic structure, exchange interactions and Curie temperature focusing on the low pressure region where the experimental information is available. We relate the theoretical dependence of $T_C$ on the lattice constant (and pressure for large $a$) to the corresponding dependence predicted by the empirical interaction curve. The Mn-Ni atomic interchange observed experimentally is simulated to study its influence on the Curie temperature.

## 7.1 Empirical interaction curve

In an early work, Castellitz [115] proposed an empirical rule (interaction curve) that describes the dependence of the Curie temperature of the Mn-containing ferromagnetic alloys with 4-5 valence electrons per molecule on the ratio $R/d$ where $R$ is the nearest-neighbor Mn-Mn distance and $d$ is the radius of the atomic Mn 3d shell. The curve is supposed to represent the Curie temperatures of various systems at ambient pressure as well as the pressure dependence of $T_c$ of a given system. The function is not monotonous and has a maximum at the $R/d$ value of about 3.6 (see Fig. 7.6). According to the interaction curve, one can expect $dT_c/dP > 0$ for alloys with $R/d > 3.6$ (e.g., $Ni_2MnSn$ and $Cu_2MnIn$). On the other hand, the systems with $R/d < 3.6$ (e.g., NiAs-type MnAs, MnSb and MnBi) are expected to have negative pressure dependence of the Curie temperature. These predictions are in agreement with experiment [116, 117, 118].

Recently Kanomata *et al.* suggested a generalization of the interaction curve to the case
of 6-7 valence electrons per chemical formula [119]. These systems form a new branch of
the dependence of the Curie temperature on the Mn-Mn distance (Fig. 7.6). The available
experimental values of the pressure derivative of the Curie temperature, $dTc/dP$ , for Heusler
alloys are consistent with those expected from the interaction curve [120, 121, 122].

## 7.2   Pressure dependence of the exchange interaction and Curie temperature in Ni$_2$MnSn

The Heusler compound Ni$_2$MnSn received much interest from the experimental point of view.
Early experiments on the pressure dependence of the Curie temperature of this system have
been performed in a low pressure region (less than 0.5 GPa) [120]. Recently Gavriliuk *et al.*
[123] have studied structural and magnetic properties of Ni$_2$MnSn in the pressure interval
up to 10.8 GPa. The authors have found an increasing linear dependence of the Curie
temperature on applied pressure. The Mössbaurer spectroscopy revealed partial interchange
of the Mn and Ni atoms.

Motivated by this recent experiment and empirical interaction curve we studied the elec-
tronic structure, exchange interactions and Curie temperature in Ni$_2$MnSn as a function of
pressure. The main attention is devoted to the interval of the interatomic Mn-Mn distances
from $4.26 \mathring{A}$ to $4.06 \mathring{A}$ that corresponds to the available experimental variation of this param-
eter. These values of the Mn-Mn distance are far above the value of $3.6 \mathring{A}$ that, according
to interaction curve, separates the regions of positive and negative pressure gradients of the
Curie temperature for this group of systems. To verify the appearance of the non-monotonous
behavior we extended the calculation to smaller values of the lattice constant correspond-
ing to larger applied pressures. We compare empirical and calculated dependencies. The
influence of the Mn-Ni atomic interchange on the magnetism of the system is also studied.

We will subdivide the discussion of the influence of the pressure on the electronic properties
of Ni$_2$MnSn in two parts. First, we present a detailed study of the low-pressure region
where an experimental information is available (We extend this interval up to $\sim$20 GPa).
In particular we verify the monotonous increase of the Curie temperature with increasing
pressure in this region. Then we consider a much larger interval of the variation of the lattice
parameter to study the occurrence of the non-monotonous behavior of the Curie temperature.

### 7.2.1   Low pressure region

To establish the relation between the lattice parameters and applied pressure we use the
following expression obtained experimentally in Ref.[123]

$$\frac{(V - V_0)}{V_0} = -aP + bP^2$$

Table 7.1: Lattice parameters, magnetic moments and Curie temperatures in Ni$_2$MnSn at ambient pressure and applied pressure of 16 GPa with and without Mn-Ni swap.

| | Ni$_2$MnSn | | Ni$_2$MnSn (Mn-Ni swap) | |
| --- | --- | --- | --- | --- |
| | $a = 6.02$ Å$_{[0\ \text{GPa}]}$ | $a = 5.82$ Å$_{[16\ \text{GPa}]}$ | $a = 6.02$ Å$_{[0\ \text{GPa}]}$ | $a = 5.82$ Å$_{[16\ \text{GPa}]}$ |
| Ni$^1$ | 0.21 | 0.19 | 0.21 | 0.26 |
| Ni$^2$ | 0.21 | 0.19 | 0.08 | 0.05 |
| Mn | 3.73 | 3.47 | 3.24 | 2.80 |
| Sn | -0.05 | -0.05 | -0.04 | -0.03 |
| Total | 4.09 | 3.81 | 3.50 | 3.09 |
| $T_c$[Calc] | 362 | 400 | 340 | 562 |
| $T_c$[Expt] | (338-360)[a] | - | - | - |

[a]Ref.[50, 123, 125]

where $a = 8.64 \cdot 10^{-3} GPa^{-1}$, $b = 1.13 \cdot 10^{-4} GPa^{-2}$ and $V_0$ is the volume of the unit cell at the ambient pressure.

We begin with the discussion of the effect of pressure on the electronic structure. In Fig. 7.1(a), we compare the density of states calculated for the ambient pressure and the applied pressure of 16 GPa. As expected, the pressure leads to the broadening of the bands that stems from the decreasing inter-atomic distances and, therefore, increasing overlap of the atomic states. One of the consequences of the band broadening is the trend to the decrease of the magnetic moments. This trend is demonstrated in table 7.1 and Fig. 7.1(b). In Fig. 7.1(b) we present a detailed information on the atomic and total magnetic moments for the range of pressures up to 20.6 GPa. The dependence of the Mn magnetic moment on pressure can be well represented by a linear function with a negative slope. The behavior of the induced moment of Ni is more peculiar. The dependence deviates strongly from the straight line and shows weak oscillations in the high-pressure part of the curve. This behavior reflects the details of the pressure dependence of the band structure, in particular, the form of the DOS in the energy region close to the Fermi level and the character of the Mn-Ni hybridization. Since these weak oscillations do not play noticeable role in the issues we focus on in this paper we do not further investigate their origin. The induced moment on Sn has the direction opposite to the direction of the Mn moment. Its value decreases slowly with increasing pressure. The spin polarization at the Fermi level shows very weak pressure dependence.

Thus the decreasing lattice constant produces a clear trend to a monotonous decrease of the atomic magnetic moments. For our purpose of the investigation of the pressure dependence of the Curie temperature it is important to relate the increasing band width and decreasing magnetic moments to the properties of the inter-atomic exchange interactions.

In the spirit of the Heisenberg model of localized moments one expects that decreasing atomic moments produce the trend to the decrease of the inter-atomic exchange interactions
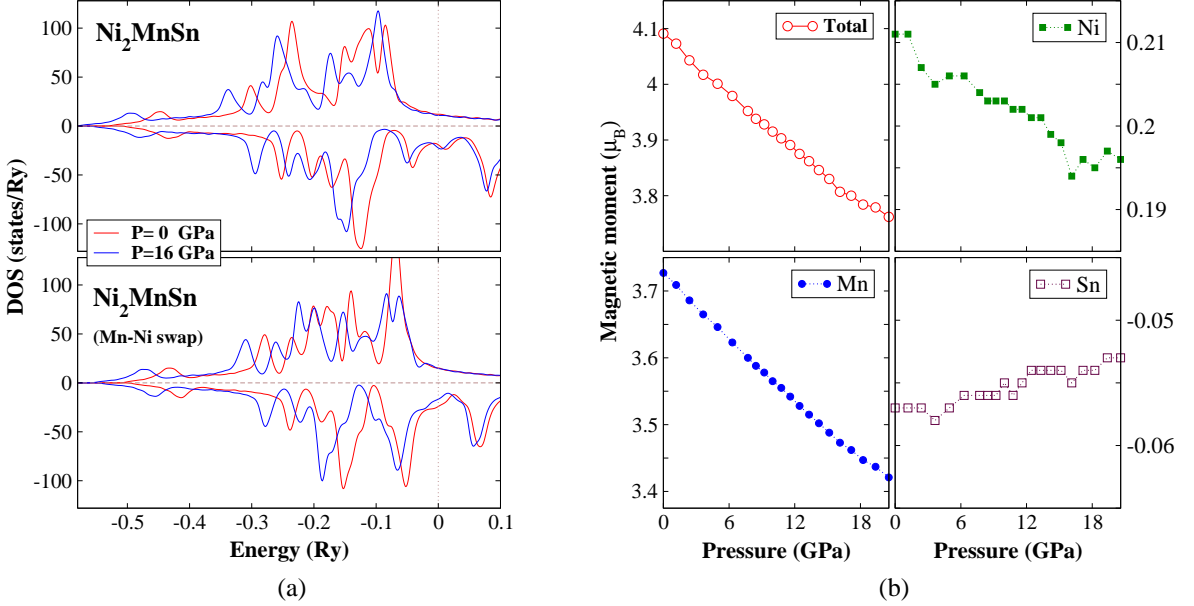
Figure 7.1: (a) Upper panel: Spin projected density of states of Ni$_2$MnSn for ambient pressure and applied pressure of 16 GPa. Lower panel: The same for the case of Mn-Ni atomic interchange. (b) Pressure dependence of magnetic moments in Ni$_2$MnSn.

by the factor of $M_p^2/M_0^2$ where $M_p$ is the atomic moment at pressure $P$ and $M_0$ is the moment at the ambient pressure. Correspondingly, one expects the trend to decreasing Curie temperature resulting from decreasing atomic moments.

An opposite monotonous trend to increasing interatomic exchange interactions is produced by increasing electron hopping and, as a result, more efficient mediation of the exchange interactions between magnetic atoms. The competition of two opposite trends opens possibility for both increase and decrease of the Curie temperature with applied pressure as well as for a nonmonotonous pressure dependence in a larger pressure interval.

In Fig. 7.2(a), we present the calculated inter-atomic exchange parameters of Ni$_2$MnSn for pressures of 0 and 16 GPa. For comparison, a zero-pressure result of previous calculation is also presented. At both pressures the patterns of inter-atomic exchange interactions are very similar. This similarity involves both Mn-Mn and Mn-Ni exchange interactions. The Mn-Mn interactions are long-ranged reaching beyond the 8th nearest neighborhood distance and have the RKKY-type oscillating character. The inter-sublattice Mn-Ni interaction behaves very differently. A sizable interaction takes place only between nearest neighbors. Note that Fig.7.2(a) does not present all calculated exchange parameters: the exchange parameters have been evaluated up to the inter-atomic distances of $8.7a$ that corresponds to about 70 coordination spheres. The absolute value of the parameters decays quickly with increasing interatomic distance. In Fig. 7.2(b), we demonstrate the convergence of the calculated Curie temperature with respect to increasing number of the atomic coordination spheres. The main contribution to $T_C$ comes from the interaction between atoms lying closer than $3a$. After $5a$ no sizable contribution is detected.
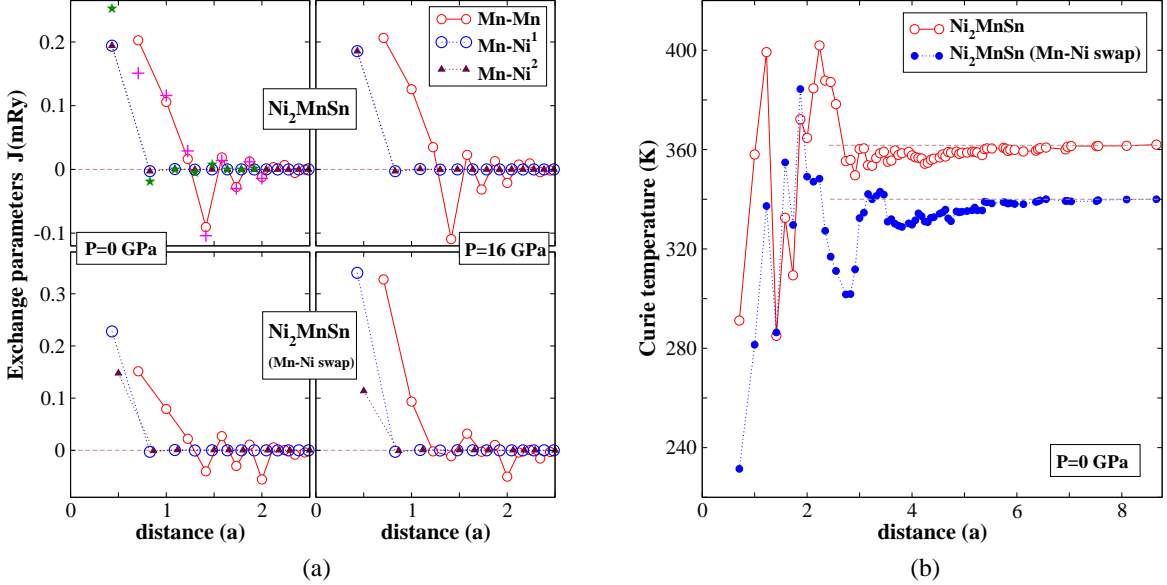
Figure 7.2: (a) Upper panel: Interatomic exchange parameters of Ni$_2$MnSn for ambient pressure and applied pressure of 16 GPa. Lower panel: The same for the case of Mn-Ni atomic interchange. Zero pressure comparison of both Mn-Mn (+) and Mn–Ni ($\star$) exchange parameters with Ref.[124] is also shown. (b) Pressure variation of the Curie temperature with increasing number of coordination spheres with and without Mn-Ni atomic interchange.

In Fig.7.2(a), we compare our exchange parameters for Ni$_2$MnSn at zero pressure with the exchange parameters calculated recently by Kurtulus *et al.* [124] Kurtulus *et al.* used TB-LMTO-ASA method and local spin-density approximation (LSDA). The inter-atomic exchange parameters were evaluated using the real-space approach by Liechtenstein *et al.* [30] This approach and the frozen-magnon technique employed in the present paper are equivalent to each other. In the real-space method by Liechtenstein *et al.* the inter-atomic exchange parameters are calculated directly whereas in the frozen-magnon approach they are obtained by the Fourier transformation of the magnon dispersion.

In Table 7.1 we present the MFA estimation of the Curie temperature. It is in good agreement with available experimental values overestimating them somewhat. An overestimation of the Curie temperature is a usual feature of the MFA as discussed in previous chapter.

The pressure dependence of the interatomic exchange parameters is presented in Fig. 7.3. The corresponding Curie temperature is shown in inset in Fig 7.6. The analysis shows that the leading contribution into Curie temperature is given by the Mn-Mn exchange interactions within the first three coordinations spheres. The numbers of the atoms in these spheres are 12, 6 and 24, respectively for the first, second and third spheres. The exchange parameters corresponding to the second and third coordination spheres increase monotonously with increasing pressure determining the increase of the Curie temperature (Fig 7.6). Thus, the increase of the experimental Curie temperature with pressure in the corresponding pressure region [123] is well confirmed by the calculations. In terms of the competition of the two
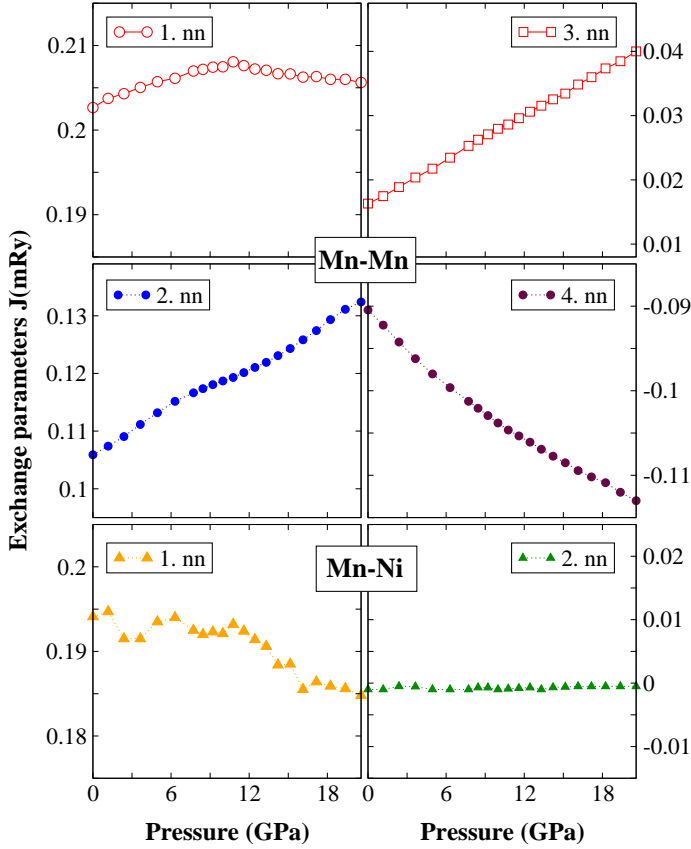
Figure 7.3: Pressure dependence of the first four nearest neighbor Mn-Mn exchange parameters and two Mn-Ni exchange parameters.

opposite trends discussed above this result means a stronger effect of the increasing hopping compared with the effect of decreasing atomic moments. Such a behavior is expected for large inter-atomic distances.

Note that in the interval from 9 GPa to 16 GPa we obtain a flat feature in the pressure dependence of the Curie temperature. This behavior is in a correlation with the recent experiment of Kyuji *et al.* [125] who obtained the Curie temperature increase from 338K at the ambient pressure to 395K at 12 GPa. At ∼7 GPa they obtained a decrease of the pressure gradient that can be put into correspondence to the theoretical flat feature.

Both measured and calculated Curie temperatures are in good agreement with the empirical interaction curve for the corresponding region of the Mn-Mn distances (Fig. 7.6).

### 7.2.2 High pressure region: Metamagnetic behavior

To verify the non-monotonous pressure dependence of $T_c$ predicted by the interaction curve we extended the calculation to smaller Mn-Mn distances down to $3.09\mathring{A}$. The calculated magnetic moments are presented in Fig. 7.4. The Mn moment decreases with the reduction of Mn-Mn distance. An interesting feature is obtained at $d_{Mn-Mn} = 3.416\mathring{A}$ where the value of the magnetic moment changes discontinuously. To study the origin of the discontinuity we employed the fixed-spin-moment method [126, 127, 128] that allows the calculation of the total energy as a function of the spin moment for a given lattice parameter. The corresponding
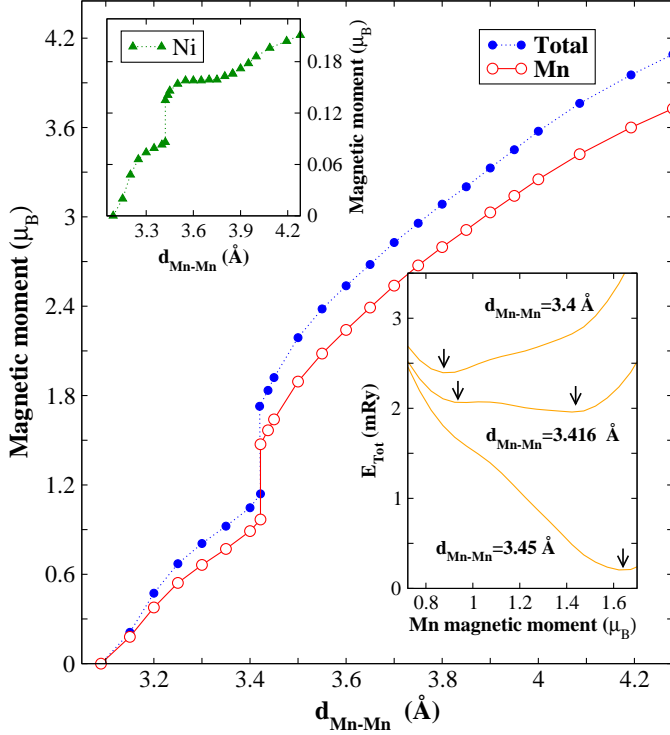
Figure 7.4: Mn and total magnetic moments as a function of the Mn-Mn distance. Upper inset shows the variation of induced Ni moment with Mn-Mn distance. Lower inset shows $E_{Tot}$ as a function of Mn magnetic moment for selected Mn-Mn interatomic distances. Arrows indicate the energy minima.

curves are presented in the inset in Fig. 7.4. For large Mn-Mn distance the curve has one minimum corresponding to a high-spin state. In the region of the discontinuity the curve has two local minima revealing the presence of a metastable state. At the point of discontinuity the minimum corresponding to the low-spin state becomes lower. With further decrease of the lattice volume the minimum corresponding to the high-spin state disappears. At $d_{Mn-Mn} = 3.09\mathring{A}$ the magnetic moment vanishes and the ground state of the system becomes a Pauli-paramagnet.

In Fig. 7.5, the first four nearest neighbor Mn-Mn exchange interactions are presented for the broad interval of the Mn–Mn interatomic distance. The pressure region discussed in the preceding section corresponds to the last three points in the plot. Three of the four leading parameters show nonmonotonous behavior that is reflected in the nonmonotonous behavior of the Curie temperature (Fig. 7.6). The absolute values of the 2nd, 3rd and 4th neighbor Mn-Mn parameters first increase with pressure, reach their maxima at the Mn-Mn distances in the region from about $4.0\mathring{A}$ to about $3.6\mathring{A}$ and decrease strongly with further decrease of the Mn-Mn distance. There are some weak peculiarities in the behavior of the exchange parameters at the region after the discontinues transition such as additional local extreme in the 1st, 3th and 4th neighbor parameters. They, however, compensate each other and the Curie temperature has only one maximum at the Mn-Mn distance of about 3.8 $\mathring{A}$ (Fig.7.6).

The non-monotonous behavior of the exchange parameters and $T_C$ can be interpreted as a result of the competition of two opposite monotonous trends appearing with the variation of the Mn-Mn distances discussed in the previous section. In the low–pressure region the influence of the increasing hopping prevails while in the high-pressure region the influence of
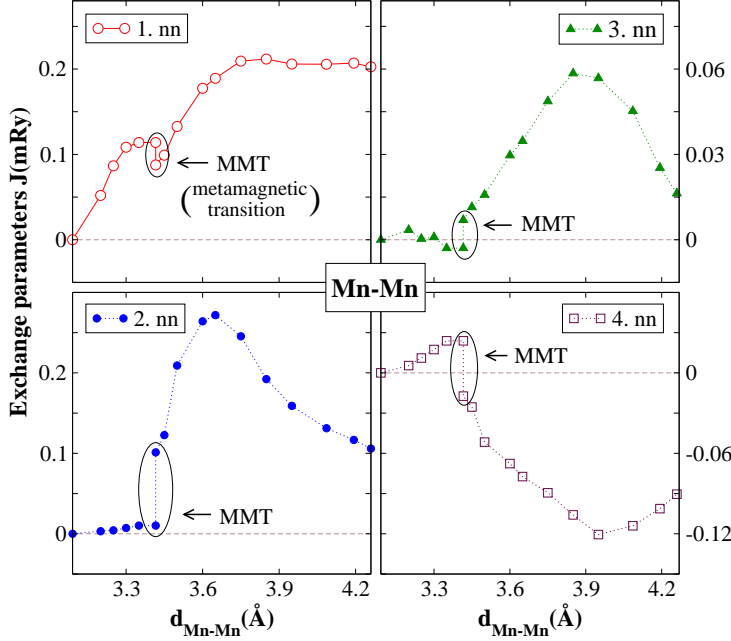
Figure 7.5: The first four nearest neighbor Mn-Mn exchange interactions in Ni$_2$MnSn as function of Mn-Mn interatomic distance. The ellipses show the region of the metamagnetic transition.

decreasing magnetic moments becomes more important.

Qualitatively, the calculated pressure dependence of $T_C$ in the broad pressure interval is in agreement with the Kanomata's empirical interaction curve. Indeed, we obtained non-monotonous pressure dependence characterized by one maximum separating the regions of positive and negative pressure gradients. The low-pressure part of the calculated dependence is in reasonable quantitative agreement with the Kanomata's interaction curve. For smaller lattice volumes the calculated Curie temperature decreases faster than it is prognosticated by the interaction curve. The calculations predict the discontinuity in the pressure dependence of the Curie temperature of Ni$_2$MnSn which is absent in the empirical interaction curve. The extension of the measurements to higher pressures is desirable to verify the predictions of the calculations.

## 7.3 Effect of the Mn-Ni swap on Curie temperature of Ni$_2$MnSn

The calculations of the Curie temperature of Ni$_2$MnSn discussed in the preceding sections are in good correlation with measured $T_c$ values for the range of pressures studied experimentally. A detailed numerical comparison shows, however, that the theoretical pressure derivative, $dT_c/dP$, estimated as 3.22 K/GPa is substantially smaller than the experimental estimation of 7.44K/GPa obtained by Gavriliuk *et al.* To verify the role of the atomic interchange between Ni and Mn sublattices observed experimentally [123] we performed calculation for a model system where the atoms of the Mn sublattice are interchanged with the atoms of one of the Ni sublattices. Although this model is a strong simplification of the experimental situation it allows the investigation of the trends resulting from the Mn-Ni interchange.

With Mn-Ni interchange we obtain a substantial difference in the electron structure of the
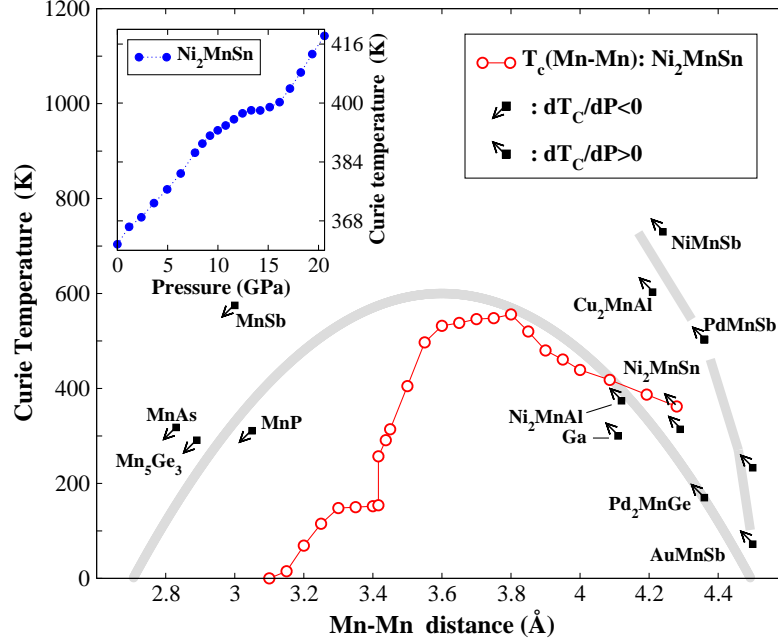
Figure 7.6: Schematic representation of Kanomata's empirical interaction curve and the calculated Curie temperature as a function of the interatomic Mn-Mn distance in Ni$_2$MnSn. Inset shows pressure variation of $T_C$ in the low pressure region. Small rectangles present the Curie temperatures of the corresponding compounds at ambient pressure. The attached arrows show the sign of $dT_C/dP$. (The experimental information is taken from Ref.[50]).

system. The corresponding DOS and magnetic moments for ambient and applied pressure of 16 GPa are presented in Fig.7.1(a) and table 7.1. In this case the Mn states hybridize differently with the states of two Ni atoms. As a result the magnetic moments of the Ni atoms assume different values. The total magnetic moment per formula unit decreases from 3.50$\mu_B$ at ambient pressure to the 3.09$\mu_B$ at the applied pressure of 16 GPa. The decrease of the total magnetic moment is mostly the result of the reduction of the Mn moment. Note that at the pressure of 16 GPa the relative variation of the total magnetic moment is two times larger than in Ni$_2$MnSn without Mn-Ni interchange. The change in the shape of the 3d peaks and broadening of the bands are similar to those for the system without swapping.

At zero pressure the pattern of exchange parameters (Fig. 7.1(b)) and resulting Curie temperature (Table 7.1) are very similar to the case without Mn-Ni interchange. However, the situation is different at applied pressure of 16 GPa. Both Mn-Mn and Mn-Ni[1] nearest-neighbor exchange parameters increase substantially. The remaining exchange parameters show small pressure dependencies. The interaction of the Mn moment with the moment of the second Ni atom is slightly reduced. The substantial increase of the leading exchange parameters with pressure results in considerable change of the Curie temperature from 400 K at ambient pressure to 562 K at 16 GPa. Assuming a linear variation of $T_C$ with pressure we estimate the pressure derivative, $dT_C/dP$, as 12.5 K/GPa. This value of $dT_c/dP$ exceeds strongly the corresponding value for the system without Mn–Ni atomic interchange. Since

the number of the swaped Mn and Ni atoms in our model is much larger than in the samples measured the calculated $dT_C/dP$ cannot be directly compared with the experimental pressure derivative. Important, however, that the Mn-Ni atomic interchange increases the pressure derivative of $T_C$ that gives an explanation for the low value of the theoretical pressure derivative in the case of the system without swapping. A detailed study of the influence of the inter-sublattice atomic interchange on the electron properties of the Heusler systems is an interesting extension of the present study.

# Chapter 8

# Summary and Conclusions

In this thesis, a systematic study of the exchange interactions and Curie temperature for various Heusler alloys are presented. The calculations are done within the parameter-free density-functional theory with the state-of-the-art ASW-method. We use the frozen-magnon approach to calculate interatomic exchange parameters. The Curie temperature is estimated within MF and RPA approaches.

The main focus is on the microscopic mechanisms of the formation of the long range magnetic order. In the choice of the compounds for the investigations, priority was given to the experimentally well-established systems. For Ni-based compounds $Ni_2MnZ$ (Z = Ga, In, Sn, Sb) we found that, despite closeness of the experimental Curie temperatures for all four systems, the exchange interactions vary widely depending on the Z constituent ($sp$-atom) and show RKKY-type oscillations. In particular, the intersublattice interactions change strongly from system to system. We show that, in agreement with experiment, different patterns of exchange interactions lead to similar values of the Curie temperatures. The role of the $sp$-electrons in mediating exchange interactions between Mn atoms is further emphasized by studying non-stoichiometric compositions of Pd- and Cu-based semi and full Heusler alloys. In this case we found that an important factor strongly influencing the electronic properties of the Heusler alloys was the spin polarization of the $sp$-electrons. We obtained a clear relationship between the strength of the exchange interactions and the $sp$-electron spin polarization. The larger the $sp$-electron polarization, the stronger the exchange interactions and, as a result the higher the Curie temperature. In particular the systems with vanishing $sp$-electron spin polarization are characterized by the value of the Curie temperature that is also very close to zero. This property reveals the decisive role of the $sp$-electrons of the X and Z atoms in mediating the exchange interaction between the Mn spin moments.

Half-metallic Heusler compounds form one of the most promising classes of materials for spintronics applications. A detailed investigation of magnetism in these systems is reported. We study the exchange interactions and Curie temperature in both ferromagnetic and ferrimagnetic compounds. The role of the inter-sublattice exchange interactions in formation of the very high Curie temperature in some full Heusler compounds (i.e., $Co_2MnSi$ and $Mn_2VAl$)

is revealed. We investigate the effect of the half-metallic gap on the stability of exchange interactions and Curie temperature. We study spin wave spectra and temperature dependence of the magnetization employing multi-sublattice Green function technique within Tyablikov decoupling scheme. We predict new semi Heusler compounds with very high $T_C$ values.

The pressure dependence of the Curie temperature in ferromagnetic systems provides an important information on the nature of magnetism. Our detailed study of the pressure dependence of exchange interactions and Curie temperature of the full Heusler alloy $Ni_2MnSn$ shows that the character of the pressure dependence of the exchange interactions is a consequence of a complex interplay of competing trends in the electronic properties of the system. In agreement with experiment, the Curie temperature increases with increasing pressure in the pressure region studied experimentally. Extending our theoretical study to a larger pressure interval, we obtained non-monotonic $T_C$ dependence and the presence of a metamagnetic transition. The $T_C$ behavior in the whole pressure interval is in qualitative correlation with Kanomatas empirical interaction curve. In the low-pressure region there is good quantitative agreement between the calculated values and the prediction of the empirical rule. Mn-Ni atomic interchange is shown to increase the pressure derivative of the Curie temperature which suggests a physical mechanism for the improved agreement between the experimental and theoretical estimations of this parameter.

# Zusammenfassung

Gegenstand dieser Arbeit waren theoretische Untersuchungen der Austauschinteraktionen und der Curie-Temperatur in verschiedenen Heusler-Legierungen. Die Berechnungen wurden im Rahmen der parameterfreien Dichtefunktionaltheorie mit Hilfe der ASW-Methode durchgeführt. Die Berechnung der Austauschwechselwirkungsparameter basiert auf der *frozen-magnon*- Näherung. Die Curie-Temperatur wurde innerhalb des *mean-field* (MF) und der *random-phase-approximation* (RPA) geschätzt.

Wir führten systematische Untersuchungen der *intra*- und *inter-sublattice* Austauschwechselwirkungen sowie der Curie-Temperatur von experimentell untersuchten Heusler-Legierungen durch. Wir behandelten besonders die mikroskopischen Mechanismen, welche zur Bildung der langreichweitigen magnetischen Ordnung führten. Bei den auf Ni basierenden Verbindungen $Ni_2MnZ$ (Z = Ga, In, Sn, Sb) war eine starke Abhängigkeit der Austauschwechselwirkungen von Z (dem *sp*-Atom) festzustellen, obwohl die berechnete und experimentelle Curie-Temperatur aller vier Verbindungen sehr ähnlich war. Untersucht man die nichtstöchiometrischen Verbindungen der auf Pd und Cu basierenden *semi* und *full* Heusler-Legierungen, wurde auch deutlich, welche Rolle die *sp*-Elektronen bei den Austauschwechselwirkungen zwischen den Mn-Atomen spielten. Es wurde festgestellt, dass die Spinpolarisation der *sp*-Elektronen die elektronischen Eigenschaften der Heusler-Legierungen stark beeinflussten. Es konnte ein klarer Zusammenhang zwischen der Stärke der Austauschwechselwirkung und der *sp*-Elektronen-Spinpolarisation festgestellt werden. In allen untersuchten Systemen war die Mn-Mn-Austauschwechselwirkung langreichweitig und es gab RKKY Oszillationen.

Desweiteren wurden ausführliche Untersuchungen zum Magnetismus von halbmetallischen Heusler-Verbindungen, die ein hohes Anwendungspotential im Bereich Magnetoelektronik besitzen, durchgeführt. Es wurden ferro- und ferrimagnetische Verbindungen untersucht. Die Rolle der *inter-sublattice* Austauschwechselwirkungen in der Anordnung der sehr hohen Curie-Temperatur wurde aufgedeckt. Weiterhin wurden die Auswirkungen der halbmetallischen Lücke auf die Stabilität der Austauschwechselwirkungen und der Curie-Temperatur untersucht. Außerdem wurden Spinwellenspektren und die Temperaturabhängigkeit der Magnetisierung unter Verwendung der *multisublattice*-Greenfunktion innerhalb des Entkopplungsschemas nach Tyablikov untersucht. Schließlich berechneten wir neue *semi* Heusler-Verbindungen mit sehr hohen $T_C$-Werten voraus.

Zuletzt befassten wir uns mit der Druckabhängigkeit von elektronischen Struktur, Austauschwechselwirkungen und der Curie-Temperatur in der ferromagnetischen Heusler-Legierung $Ni_2MnSn$. Wir bekamen einen Anstieg der Curie-Temperatur von 362 K bei Umgebungsdruck auf 396 K bei 12 GPa. Dies wurde auch experimentell bestätigt. Legte man die Gitterparamenter außerhalb des bereits experimentell untersuchten Grenzbereichs, gab es eine nicht-monotonische Druckabhängigkeit der Curie-Temperatur und einen metamagnetischen Übergang. Wir brachten die berechnete Abhängigkeit der $T_C$ von Gitterkonstante in Verbindung mit der entsprechenden Abhängigkeit, die durch die empirische Wechselwirkungskurve vorausgesagt wurde. Es wurde die bei Experimenten festgestellte atomische Mn-Ni Austausch simuliert, um den Einfluss auf die Curie-Temperatur zu untersuchen.

# Bibliography

[1] L.H. Thomas, Proc. Camb. Phil. Soc. 23, 542(1927).

[2] P. Hohenberg and W. Kohn, Phys. Rev. **136** 3864 (1964).

[3] W. Kohn and L. J. Sham, Phys. Rev. **140** A1133 (1965).

[4] F. Bloch Z. Physik, **57** 549 (1929).

[5] U. von Barth, L. Hedin, J. Phys. C **5** 1629 (1972).

[6] L. M. Sandratskii, Advances in Physics **47** 91 (1998).

[7] J. Kübler, K.-H. Höck, J. Sticht and A. R. Williams, J. Phys. F **18** 469 (1988).

[8] J. Kübler, *Theory of Itinerant Electron Magnetism*, Oxford (2000).

[9] C. Herring, in *Magnetism*, edited by G. T. Rado and H. Suhl, Vol. 4, Academic Press (1966).

[10] L. M. Sandratskii, Phys. Stat. Sol. (b) **135** 167 (1986).

[11] L. M. Sandratskii, J. Phys. F: Metal Phys. **16** L43 (1986).

[12] A. R. Williams, J. Kübler, and C. D. Gelatt, Phys. Rev. B **19** 6094 (1979).

[13] V. Eyert, *Entwicklung und Implementation eines Full-Potential-ASW-Verfahrens*, Ph.D. thesis, Technische Hochschule Darmstadt, 1991.

[14] V. Eyert, Int. J. Quant. Chem. **77** 1007 (2000)

[15] http://www.physik.uni-augsburg.de/ eyert/aswhome.shtml

[16] T. Moriya, *Spin Fluctuations in Itinerant Electron Magnetism*, Springer, Berlin (1985).

[17] P. Langewin, J. Phys. (Paris) **4** 678 (1905).

[18] P. Weiss, J. Phys.Radium **6** 661 (1907).

[19] W. Heisenberg, Z. Phys. **49** 619 (1928).

[20] F. Bloch, Z. Phys. **57** 545 (1929).

[21] E. Wigner, Phys. Rev. **46** 1002 (1934).

[22] E. C. Stoner, Proc. R. Soc. A **165** 372 (1938).

[23] P. Mohn, *Magnetism in the Solid State*, Springer, Berlin (2002).

[24] A. Aharoni, *Introduction to the theory of ferromagnetism*, Oxford (2001).

[25] P. Grünberg, R. Schreiber, Y. Pang, M. B. Brodsky, and H. Sowers, Phys. Rev. Lett. **57** 2442 (1986).

[26] P. Bruno and C. Chappert, Phys. Rev. Lett. **67** 1602 (1991).

[27] N.W. Ashcroft, N.D. Mermin, *Solid State Physics*, Thomson Learning (1976).

[28] F. Duan and J. Guojun, *Introduction to condensed matter physics*, volume 1, World Scientific (2005).

[29] V. A. Gubanov, A. I. Liechtenstein and A. V. Postnikov, *Magnetism and the electronic structure of crystals*, Springer, Berlin (1992).

[30] A. I. Liechtenstein, M. I. Katsnelson, V. P. Antropov, and V. A. Gubanov, J. Magn. Magn. Mater. **67** 65 (1987).

[31] N. M. Rosengaard and B. Johansson, Phys. Rev. B **55** 14975 (1997); S. V. Halilov, H. Eschrig, A. Y. Perlov, and P. M. Oppeneer, Phys. Rev. B **58** 293 (1998); L. M. Sandratskii and P. Bruno, Phys. Rev. B **67**, 214402 (2003).

[32] M. Pajda, J. Kudrnovsky, I. Turek, V. Drchal, and P. Bruno, Phys. Rev. B **64**, 174402 (2001).

[33] F. J. Himpsel, J. E. Ortega, G. J. Mankey and R. F. Willis, Advances in Physics **47** 511 (1998)

[34] P. W. Anderson, *Theory of magnetic exchange interactions: Exchange in insulators and semiconductors*, in *Solid State Physics*, edited by F. Seitz and D. Turnbull (Academic Press, New York), Vol. 14 pp. 99-214.

[35] S. V. Tyablikov, *Methods of Quantum Theory of Magnetism*, Plenum Press, New York (1967).

[36] H. B. Callen, Phys. Rev. **130** 890 (1963).

[37] F. Heusler, Verh. Dtsch. Phys. Ges. **5** 219 (1903).

[38] H. H. Potter, Proc. Phys. Soc., **41** 135 (1929).

[39] A. J. Bradley and J. W. Rodgers, Proc. R. Soc. London Ser. A **144** 340 (1934).

[40] H. Itoh, T. Nakamichi, Y. Yamaguchi, and N. Kazama, Trans. Jpn. Inst. Met. **24** 265 (1983).

[41] K. H. J. Buschow and P. G. van Engen, J. Mag. Magn. Mater. **25** 90 (1981).

[42] G. B. Johnston and E. O. Hall, J. Phys. Chem. Solids **29** 193 (1968).

[43] Z. Nishiyama, *Martensitic transformation*, Academic Press, New York, 1978.

[44] S. Fujii, S. Ishida and S. Asano, J. Phys. Soc. Jpn. **58** 3657 (1989).

[45] P. J. Brown, A. Y. Bargawi, J. Crangle, K-U Neumann and K. R. A. Ziebeck, J. Phys.: Condens. Matter **11** 4715 (1999)

[46] V. V. Khovailo, T. Takagi, J. Tani, R. Z. Levitin, A. A. Cherechukin, M. Matsumoto, and R. Note, Phys. Rev. B **65**, 092410 (2002).

[47] S. J. Murray, M. Marioni, S.M. Allen, R.C. O'Handley, and T.A. Lograsso, Appl. Phys. Lett. **77** 886 (2000).

[48] A. Sozinov, A.A. Likhachev, N. Lanska, and K. Ullakko, Appl. Phys. Lett. **80** 1746 (2002).

[49] H. Funakubo (Ed.),*Shape Memory Alloys*, Gordon and Breach Science Publishers, London, 1987.

[50] P. J. Webster and K. R. A. Ziebeck, in *Alloys and Compounds of d-Elements with Main Group Elements*, Part 2, edited by H. P. J. Wijn, Landolt-Börnstein, New Series, Group III, Vol. 19/c (Springer, Berlin, 1988), pp. 75-184.

[51] P. J. Webster, K. R. A. Ziebeck, and K.-U. Neumann in *Magnetic Properties of Metals*, Landolt-Börnstein, New Series, Group III, Vol. 32/c, ed by H. P. J. Wijn, (Springer, Berlin 2001) pp 64414

[52] J. Pierre, R. V. Skolozdra, J. Tobola, S. Kaprzyk, C. Hordequin, M. A. Kouacou, I. Karla, R. Currat and E. Leliévre-Berna, J. Alloys Comp. **262-263** 101 (1997).

[53] J. Tobola, J. Pierre, S. Kaprzyk, R.V. Skolozdra, and M.A. Kouacou, J. Phys.: Condens. Matter **10** 1013 (1998); J. Tobola and J. Pierre: J. Alloys Comp. **296** 243 (2000); J. Tobola, S. Kaprzyk, and P. Pecheur: Phys. St. Sol. (b) **236** 531 (2003).

[54] Y. Noda and Y Ishikawa, J. Phys. Soc. Jpn. **40** 690 (1976).

[55] P. J. Webster and K. R. A. Ziebeck, J. Mag. Magn. Mater. **50** 7 (1985).

[56] S. Ishida, Y. Kubo, J. Ishida, and S. Asano, J. Phys. Soc. Jpn. **48** 814 (1980).

[57] S. Ishida, J. Ishida, S. Asano, and J. Yamashita, J. Phys. Soc. Jpn. **45** 1239 (1978).

[58] J. Kübler, A. R. Williams, and C. B. Sommers, Phys. Rev. B **28**, 1745(1983).

[59] R. A. de Groot, F. M. Mueller, P. G. van Engen and K. H. J. Buschow, Phys. Rev. Lett. **50**, 2024 (1983).

[60] P. J. Webster and M. R. I. Ramadan, J. Mag. Magn. Mater. **13** 301 (1979).

[61] P. J. Webster and M. R. I. Ramadan, J. Mag. Magn. Mater. **20** 271 (1980).

[62] S. Ishida, S. Akazawa, Y. Kubo, and J. Ishida, J. Phys. F: Met. Phys. **12**, 1111 (1982); S. Ishida, S. Fujii, S. Kashiwagi, and S. Asano, J. Phys. Soc. Jpn. **64**, 2152 (1995).

[63] R. J. Soulen Jr., J. M. Byers, M. S. Osofsky, B. Nadgorny, T. Ambrose, S. F. Cheng, P. R. Broussard, C. T. Tanaka, J. Nowak, J. S. Moodera, A. Barry, and J. M. D. Coey, Science **282** 85 (1998).

[64] A. Stroppa , S. Picozzi, A. Continenza, and A. J. Freeman, Phys. Rev. B **68**, 155203 (2003).

[65] H. Akai, Phys. Rev. Lett. **81**, 3002 (1998).

[66] H. Akinaga, T. Manago, and M. Shirai, Jpn. J. Appl. Phys. **39**, L1118 (2000).

[67] I. Galanakis, P. H. Dederichs, and N. Papanikolaou, Phys. Rev. B **66**, 134428 (2002).

[68] I. Galanakis, P. H. Dederichs, and N. Papanikolaou, Phys. Rev. B **66**, 174429 (2002).

[69] J. Kübler, Physica B **127** 257 (1984).

[70] I. Galanakis, Phys. Rev. B **66** 012406 (2002); I. Galanakis and Ph. Mavropoulos, Phys. Rev. B **67**, 104417 (2003).

[71] D. C. Price, J. Phys. F, **8** 933 (1978).

[72] G. Malmström and D. J. W Geldart, J. Phys. F, **8** L17 (1978).

[73] J. R. Reitz and M. B. Stearns, J. Appl. Pyhs. **50** 2066 (1979).

[74] C. C. M. Campbell, J. Phys. F, **5** 1931 (1975).

[75] Le D. Khoi, P. Veillet and I. A. Campbell, J. Phys. F, **8** 1811 (1978).

[76] E. Zukowski, A. Andrejczuk, L. Dobrzyński, M. J. Cooper, M. A. G. Dixon, S. Gardelis, P. K. Lawson, T. Buslaps, S. Kaprzyk, K-U. Neumann and K. R. A. Ziebeck, J. Phys.: Condens. Matter **9** 10993 (1997).

[77] A. Deb, N. Hiraoka, M. Itou, Y. Sakurai, M. Onodera and N. Sakai, Phys. Rev. B **63**, 205115 (2001).

[78] J. Marcos, L. Mañosa, A. Planes, F. Casanova, X. Batlle, and A. Labarta, Phys. Rev. B **68** 094401 (2003).

[79] 3. O. Tegus, E. Brück, K. H. J. Buschow, and F. R. de Boer, Nature **415** 150 (2002).

[80] V. Provenzano, A. J. Shapiro, and R. D. Shull, Nature **429** 853 (2004).

[81] L. Pareti, M. Solzi, F. Albertini and A. Paoluzi, Eur. Phys. J. B **32** 303 (2003).

[82] T. Krenke, E. Duman, M. Acet, E. F. Wassermann, X. Moya, L. Manosa and A. Planes, Nature materials **4** 450 (2005).

[83] J. Enkovaara, A. Ayuela, J. Jalkanen, L. Nordström, and R.M. Nieminen, Phys. Rev. B **67**, 054417 (2003).

[84] E. Şaşıoğlu, L. M. Sandratskii and P. Bruno, Phys. Rev. B **70**, 024427 (2004).

[85] A. Ayuela, J. Enkovaara and R.M. Nieminen, J. Phys.: Condens. Matter **14**, 5325 (2002).

[86] J. Worgull, E. Petti, and J. Trivisonno, Phys. Rev. B **54**, 15695 (1996).

[87] A. Ayuela, J. Enkovaara,K. Ullakko and R.M. Nieminen, J. Phys.: Condens. Matter **11**, 2017 (1999).

[88] C. Walle, L. Offernes and A. Kjekshus, J. Alloys and Comp., **349** 105 (2003).

[89] S. K. Ren, W. Q. Zou, J. Gao, X. L. Jiang, F. M. Zhang and Y. W. Du, J. Mag. Magn. Mater., **288** 276 (2005).

[90] S. Kämmerer, A. Thomas, A. Hütten, and G. Reiss, Appl. Phys. Lett. **85** 79 (2004).

[91] S. Okamura, R. Goto, S. Sugimoto, N. Tezuka, and K. Inomata, J. Appl. Phys. **96** 6561 (2004).

[92] E. Girgis, P. Bach, C. Rüster, C. Gould, G. Schmidt, and L. W. Molenkamp, Appl. Phys. Lett. **86** 142503 (2005).

[93] T. Block, M. J. Carey, D. A. Gurney, and O. Jepsen, Phys. Rev. B **70** 205114 (2004).

[94] Ph. Mavropoulos, K. Sato, R. Zeller, P. H. Dederichs, V. Popescu, and H. Ebert, Phys. Rev. B **69** 054424 (2004); Ph. Mavropoulos, I. Galanakis, V. Popescu, and P. H. Dederichs, J. Phys.: Condens. Matter **16** S5759 (2004).

[95] I. Galanakis, Phys. Rev. B **71** 012413 (2005).

[96] P. Larson, S. D. Mahanti, and M. G. Kanatzidis, Phys. Rev. B **62** 12574 (2000).

[97] D. Orgassa, H. Fujiwara, T. C. Schulthess, and W. H. Butler, Phys. Rev. B **60** 13 237 (1999).

[98] S. Picozzi, A. Continenza, and A. J. Freeman, Phys. Rev. B **69** 094423 (2004).

[99] P. A. Dowben and R. Skomski, J. Appl. Phys. **93** 7948 (2003); *ibid.* **95** 7453 (2004).

[100] *Half-metallic Alloys: Fundamentals and Applications*, Lecture Notes in Physics, Vol. 676, I. Galanakis and P. H. Dederichs (eds), pp. 139, Springer-Berlin, Heidelberg (2005).

[101] J. Kübler, Phys. Rev. B **67** 220403(R) (2003).

[102] E. Şaşıoğlu, I. Galanakis, L. M. Sandratskii and P. Bruno, J. Phys.: Condens. Matter **17** 3915 (2005).

[103] R.A. de Groot, Physica B **172** 45 (1991); H. van Leuken and R.A. de Groot, Phys. Rev. Lett. **74** 1171 (1995).

[104] C. Jiang, M. Venkatesan and J. M. D. Coey, Solid State Commun. **118** 513 (2001).

[105] S. Ishida, S. Asano, and J. Ishida, J. Phys. Soc. Jpn. **53**, 2718 (1984)

[106] Ruben Weht and Warren E. Pickett, Phys. Rev. B **60**, 13006 (1999).

[107] E. Şaşıoğlu, L. M. Sandratskii and P. Bruno, J. Phys.: Condens. Matter **17** 995 (2005).

[108] K. H. J. Buschow and P. G. van Engen, J. Mag. Magn. Mater. **25** 90 (1981).

[109] G. Fuster, N. E. Brener, and J. Callaway, J. L. Fry, Y. Z. Zhao and D. A. Papaconstantopoulos, Phys. Rev. B **38** 423 (1988).

[110] D. Jiles, *Introduction to Magnetism and Magnetic Materials*, Chapman & Hall, London (1998).

[111] Ming Zhang, Xuefang Dai, Haining Hu, Guodong Liu, Yuting Cui, Zhuhong Liu, Jinglan Chen, Jianli Wang and Guangheng Wu, J. Phys.: Condens. Matter **15** 7891 (2003).

[112] Ming Zhang, Zhu-Hong Liu, Hai-Ning Hu, Guo-Dong Liu, Yu-Ting Cui, Guang-Heng Wu, Ekkes Brueck, Frank R.de Boer, and Yang-Xian Li, J. Appl. Phys. **95** 7219 (2004).

[113] A. Sakuma, J. Phys. Soc. Jpn. **71** 2534 (2002).

[114] B. Sanyal, L. Bergqvist, and O. Eriksson, Phys. Rev. B **68** 054417 (2003).

[115] L. Castellitz, Z. Metallkde. **46** 198 (1955).

[116] H. Ido, T. Suziki and T. Kaneko, J. Phys. Soc. Japan, **29** 1490 (1970).

[117] T. Kaneko, H. Yoshida, and K. Kamigaki, J. Appl. Phys. **52** 2046 (1981).

[118] N. Menyuk, J.A. Kafalas, K. Dwight and J. B. Goodenough, Phys. Rev. **177** 942 (1969).

[119] T. Kanomata, K. Shirakawa and T. Kaneko, J. Magn. Magn. Mater. **65** 76 (1987).

[120] T. Kaneko, K. Shirakawa, T. Kanomata, K. Watanabe and H. Masumoto, J. Magn. Magn. Mater. **54** 933 (1986).

[121] T. Kaneko, K. Watanabe, K. Shirakawa, and H. Masumoto, J. Magn. Magn. Mater. **31** 79 (1983).

[122] K. Shirakawa, T. Kanomata and T. Kaneko, J. Magn. Magn. Mater. **70** 421 (1987)

[123] A. G. Gavriliuk, G. N. Stepanov, V. A. Sidorov and S. M. Irkaev, J. Appl Phys. **79** 2609 (1995).

[124] Y. Kurtulus, R. Dronskowski, G. D. Samolyuk, and V. P. Antropov, Phys. Rev. B **71** 014425 (2005).

[125] S. Kyuji, S. Endo, T. Kanomata and F. Ono, Physica B **237** 523(1997).

[126] K. Schwarz and P. Mohn, J. Phys. F: Met. Phys. **14** L129 (1984).

[127] P. H. Dederichs, S. Blügel, R. Zeller, and H. Akai, Phys. Rev. Lett., **53** 2512 (1983).

[128] L. M. Sandratskii and E. N. Kuvaldin, J. Phys.: Condens. Matter **3** 7663 (1991).

# Erklärung

Hiermit erkläre ich, da ich keine anderen als die von mir angegebenen Quellen und Hilfsmittel zur Erstellung meiner Dissertation verwendet habe. Den benutzten Werken wörtlich oder inhaltlich entnommene Stellen sind als solche gekennzeichnet. Die Dissertation wurde bisher an keiner anderen Universität oder Hochschule vorgelegt.

Halle (Saale), den 23. Dezember 2005

Ersoy Şaşıoğlu

# Curriculum Vitae

**Personal data:**

Name Surname: Ersoy Şaşıoğlu
Date of Birth: 15 December 1975
Place of Birth: Kaş, Antalya, Turkey
Nationality: Turkish
Marital Status: Married

**Education:**

1992-1996: BS in Department of Astronomy-Physics, Faculty of Science, Ege University, Izmir, Turkey.
1997-1999: MS in Department of Physics, Fatih University, Istanbul, Turkey. Thesis: "Effect of electron-electron correlation on density of states in disordered systems". Supervisor: Prof. Dr. E. P. Nakhmedov.
2003 - 2006: PhD in Max-Planck-Institut für Mikrostrukturphysik, Halle, Germany. Thesis: "First-principles study of the exchange interactions and Curie temperature in Heusler alloys". Supervisor: PD Dr. L. M. Sandratskii.

**Work experience:**

1997-2001: Research assistant in physics department at Fatih University, Istanbul, Turkey.
August - October, 2001: Visiting scientist (2 Months) Max-Planck-Institute for the Physics of Complex Systems, Dresden, Germany.
2001-2003: Teaching assistant in physics department at Fatih University, Istanbul, Turkey.

**Languages:**

Turkish (native)
English
German (beginner)